

GROWTH MECHANISM OF GRAPHENE SYNTHESIZED ON NI/CU ALLOY
THROUGH CVD METHOD AND USE GRAPHENE AS
A DIFFUSION BARRIER FOR
THERMOELECTRIC DEVICE

by

Jiachen Xue, M.S

A dissertation submitted to the Graduate Council of
Texas State University in partial fulfillment
of the requirements for the degree of
Doctor of Philosophy
with a Major in Materials Science, Engineering and Commercialization
August 2016

Committee Members:

Qingkai Yu

Gary Beall

Nikoleta Theodoropoulou

Yihong Chen

Dongsheng Mao

COPYRIGHT

by

Jiachen Xue

2016

FAIR USE AND AUTHOR'S PERMISSION STATEMENT

Fair Use

This work is protected by the Copyright Laws of the United States (Public Law 94-553, section 107). Consistent with fair use as defined in the Copyright Laws, brief quotations from this material are allowed with proper acknowledgment. Use of this material for financial gain without the author's express written permission is not allowed.

Duplication Permission

As the copyright holder of this work I, Jiachen Xue, authorize duplication of this work, in whole or in part, for educational or scholarly purposes only.

DEDICATION

To my beloved parents

ACKNOWLEDGEMENTS

I would like to express my deep appreciation to my supervisor, Dr. Qingkai Yu, for his guidance and support during my graduate studies. He also helped me to develop my interest in CVD technology and establish the ability to do independent research. Likewise, I appreciate my committee members, Dr. Gary Beall, Dr. Nikoleta Theodoropoulou, Dr. Yihong Chen and Dr. Dongsheng Mao for their valuable advice and suggestions on my research work. I would also take this opportunity to express my gratitude to Dr. Casey Smith and Dr. Eric Schires for their help in the Analysis Research Service Center. Special thanks also go to the Materials Science, Engineering and Commercialization program at Texas State University for providing me the opportunity to pursue my PhD. I also would like to thank my friends and fellow at txstate Zhihong Liu and Joel Warner from MicroPower Global for providing their support and encouragement throughout this period of my life. Finally, I express my special thanks to my parents for their support and unwavering faith in me.

TABLE OF CONTENTS

	Page
ACKNOWLEDGEMENTS.....	v
LIST OF TABLES.....	viii
LIST OF FIGURES	ix
ABSTRACT.....	xii
CHAPTER	
1 SECTION ONE GROWTH MECHANISM OF GRAPHENE SYNTHESIZED ON NI/CU ALLOY THROUGH CVD METHOD.....	1
1.1 Introduction.....	1
1.1.1 Graphene.....	1
1.1.2 Graphene synthesis methods	3
1.1.2.1 Mechanical exfoliation to synthesis Graphene.....	4
1.1.2.2 Chemical exfoliation to synthesis Graphene	5
1.1.2.3 Chemical exfoliation graphene oxide to synthesis Graphene.....	9
1.1.2.4 SiC precipitation to synthesis Graphene.....	11
1.1.2.5 CVD method to synthesis Graphene	12
1.1.3 Raman spectroscopy in Graphene.....	15
1.1.4 Raman spectroscopy for isotope labeled Graphene	21
1.1.5 Scanning electron microscope (SEM) for Graphene.....	23

1.2	Methods	26
1.2.1	Single crystal Graphene growth	26
1.2.2	Isotope labeled graphene.....	27
1.2.3	Characterization.....	29
1.2.3.1	Scanning electron microscope.....	29
1.2.3.2	Raman spectrum and mapping	30
1.3	Results and discussion.....	32
1.3.1	Nucleation density.....	32
1.3.2	Large single crystal graphene	36
1.3.3	Raman spectrum for isotope labeled graphene	38
1.3.4	Raman mapping for isotope labeled Graphene.....	41
1.3.5	Competition between body participation and surface adsorption for graphene growth	49
1.4	Conclusion	52
2	GRAPHENE AS DIFFUSION BARRIER FOR THERMOELECTRIC DEVICE	54
2.1	Introduction.....	54
2.1.1	Thermoelectric materials.....	54
2.1.2	Diffusion in thermoelectric device	58
2.1.3	Impermeability of Graphene.....	59

2.2	Methods	62
2.2.1	Diffusion of Ni/G/Cu and Ni/Cu test.....	62
2.2.2	Ni/PbTe and Ni/G/PbTe Devices.....	63
2.2.3	InTe/PbTe and InTe/mG/PbTe Devices	63
2.2.4	SEM and EDS.....	64
2.3	Results and Discussion	68
2.3.1	Diffusion test of Ni/G/Cu and Ni /Cu.....	69
2.3.2	Diffusion and efficiency test for Ni/G/PbTe and Ni/PbTe.....	71
2.3.3	Diffusion test for InTe/mG/PbTe and InTe/PbTe	73
2.3.4	Power conversion efficiency test for InTe/mG/PbTe and InTe/PbTe	79
2.4	Conclusion	81
APPENDIX SECTION		83
REFERENCES		97

LIST OF TABLES

Table	Page
1. Methods for prepare Graphene and their properties and applications.....	3
2. Growth condition and time for graphene on Ni/Cu alloy with different content.....	31

LIST OF FIGURES

Figure	Page
1.1	Graphene is a 2D material for carbon materials of all other dimensionalities2
1.2	Scheme for mechanical exfoliation graphene. 5
1.3	Chemical exfoliation to synthesis Graphene. 7
1.4	Chemical exfoliation via graphene oxide to synthesis Graphene. 10
1.5	SiC precipitation to synthesis Graphene. 11
1.6	Scheme of growing Graphene on Ni (left) ⁹ and Cu (right)..... 12
1.7	Optical micrograph of a monolayer graphene transferred onto a 285 nm SiO ₂ /Si substrate. 14
1.8	Rayleigh (elastic) scattering and Raman (Stokes) scattering..... 17
1.9	Phonon-displacement pattern for graphene and graphite. 19
1.10	Raman spectra of pristine (top) and defected (bottom) graphene. The main peaks are labeled. 20
1.11	Schematic diagrams of the possible distribution of C isotopes in Graphene films based on different growth mechanisms for sequential input of C isotopes.. 23
1.12	SEM and SEM image of Graphene on Cu. 25
1.13	Growth condition for pure ¹² C Graphene..... 27
1.14	Growing isotope labeled Graphene with 2 switches..... 28
1.15	Growing isotope labeled Graphene with 1 switch. 29
1.16	SEM of Graphene flakes on Cu. 30
1.17	SEM of Graphene seeding on Ni/Cu alloy (10%, 15% and 20%) and on Cu. 34
1.18	Nucleation density vs Ni content (atom %)..... 35
1.19	Large single crystal Graphene flakes up to 400 μm with good hexagonal shape can be easily obtained on Ni/Cu alloy. 36
1.20	SEM of single crystal flakes of Graphene grown on Ni/Cu alloy (10%, 15% and 20%) and small Graphene flakes on Cu. 37
1.21	Raman spectrum of pure ¹² C graphene (top) and pure ¹³ C graphene (bottom)..... 39

1.22	Raman spectrum of graphene with resolvable ^{12}C and ^{13}C region and graphene composed by randomly mixed ^{12}C and ^{13}C	40
1.23	Raman mapping of isotope labeled Graphene.....	42
1.24	Extracted peak position and distance from Figure 1.19.	43
1.25	Calculated C13 content vs distance from Figure 1.20.....	43
1.26a.	Raman mapping of isotope labeled Graphene grew on Ni/Cu with 20%Ni.	45
1.26b.	Raman mapping of isotope labeled Graphene grew on Ni/Cu with 15%Ni.	46
1.26c.	Raman mapping of isotope labeled Graphene grew on Ni/Cu with 10%Ni.	47
1.27	Calculated ^{13}C content vs distance from center in Figure1.22.	48
1.28a	Optical image of large single crystal flake.	50
1.28b	Optical image of large single crystal flake and Raman mapping (competition between body participation and surface adsorption). ...	51
2.1	Scheme of thermoelectric device working principal	55
2.2	Structure of PbTe crystal.....	57
2.3	Merit zT for different TE materials.....	58
2.4	Graphene lattice structure and geometric pore.....	60
2.5	Backscatter coefficient as a function of atomic number of specimen atoms.	65
2.6	Excitation of a characteristic X-ray a auger electron or photon by a high energy electron or photon.	66
2.7	EDS spectrum of glass with Si, O, Ca, Al, Fe and Ba.	67
2.8	Schematic of devices manufacture.	68
2.9	Ni/Cu before and after annealing for 30mins, Ni/G/Cu after annealing for 30mins, 120mins and 240mins	70
2.10	EDAX of Ni/PbTe and Ni/G/PbTe after annealing at 500C for 12hrs.....	71
2.11	Top, Normalized output power efficiency of Ni/G/PbTe (red) and Ni/PbTe (blue).....	72
2.12	EDAX image of device before anneal	74
2.13	Line EDS for InTe/PbTe (left) and InTe/mG/PbTe (right) after annealing at 500C	74

2.14	Device with (left, scale bar 10 μm) and without (right, scale bar 10 μm) Graphene barrier after annealing at 500C for 3hrs (Green, lead; Silver, Indium; Blue, Tellurium) ,.....	75
2.15	Device with (left, scale bar 5 μm) and without (right, scale bar 10 μm) Graphene barrier after annealing at 500C for 8hrs (Green, lead; Silver, Indium; Blue, Tellurium).	76
2.16	Device with (left, scale bar 5 μm) and without (right, scale bar 10 μm) Graphene barrier after annealing at 500C for 13hrs (Green, lead; Silver, Indium; Blue, Tellurium).	77
2.17	Device with (left, scale bar 5 μm) and without (right, scale bar 5 μm) Graphene barrier after annealing at 500C for 18hrs (Green, lead; Silver, Indium; Blue, Tellurium)	77
2.18	Device with (left, scale bar 10 μm) and without (right, scale bar 5 μm) Graphene barrier after annealing at 500C for 24hrs (Green, lead; Silver, Indium; Blue, Tellurium).	78
2.19	Device with (left, scale bar 5 μm) and without (right, scale bar 20 μm) Graphene barrier after annealing at 500C for 36hrs (Green, lead; Silver, Indium; Blue, Tellurium), nearly no Te was detected in a large portion of area for device without Graphene.	78
2.20	Normalized power output at $\Delta T = 420\text{C}$ for InTe/mG/PbTe and InTe/PbTe after annealing at 500C for 0, 3, 13, 18, 24 and 36hrs. ..	80
2.21	Normalized power output of devices with (solid) and without (hollow) graphene after annealing at 500C for different times.	81

ABSTRACT

Graphene is the first two-dimensional (2D) atomic crystal available to the world. It is a two-dimensional sheet of sp^2 -hybridized carbon. Its extended honeycomb network is the basic building block of other important allotropes; it can be wrapped to form 0 dimension fullerenes, rolled to form 1 dimension nanotubes and stacked to form 3 dimensions graphite. Long-range π -conjugation in Graphene yields extraordinary thermal, mechanical, and electrical properties, which have long been the interest for many theoretical studies and more recently became an exciting area for experimentalists.

Large single crystal Graphene is preferred for applications such as electronic devices and diffusion barriers. Also to deliver unique performance, single crystal Graphene is desired.

Here we studied the growth mechanism behind the world's first inch size single crystal Graphene with a fast growth rate on Ni/Cu alloy substrate through chemical vapor deposition method. Our observation indicated that body participation and surface adsorption both contributed to the fast growth of Graphene on Ni/Cu alloy and the present of Ni element suppressed nucleation of Graphene seed much more efficiently than methods reported by other groups.

We further researched the effect of Ni content on graphene growth rate and nucleation density.

We also used Graphene as diffusion barrier to prevent Ni metal solder diffusing into PbTe thermoelectric material at high operation temperature (500C). Our preliminary results showed single layer Graphene is a promised high temperature diffusion barrier for thermoelectric device. Only less than 10% of Ni was found diffused into PbTe while device without Graphene has nearly 40% of Ni in PbTe. InTe/mG/PbTe (multilayer graphene barrier) device showed a ~40% more power output than InTe/PbTe device.

We propose that multilayer Graphene transferred on PbTe device would prevent metal diffusing into PbTe and improve the power output of PbTe devices.

1 SECTION ONE GROWTH MECHANISM OF GRAPHENE SYNTHESIZED ON NI/CU ALLOY THROUGH CVD METHOD

1.1 Introduction

1.1.1 Graphene

Graphene is the first two-dimensional (2D) atomic crystal available to the world. It is a two-dimensional sheet of sp^2 -hybridized carbon. Its extended honeycomb network is the basic building block of other important allotropes; it can be wrapped to form 0dimension fullerenes, rolled to form 1dimension nanotubes and stacked to form 3dimension graphite (Figure 1.1)^{1, 1b}. Long-range π -conjugation in Graphene yields extraordinary thermal, mechanical, and electrical properties, which have long been the interest for many theoretical studies and more recently became an exciting area for experimentalists².

The material properties of Graphene (such as amazing mechanical stiffness, strength and elasticity, very high electrical and thermal conductivity³, and many others^{4, 1a} are supreme^{5, 5b}. These properties suggest that Graphene could take the place of other materials in existing applications and deliver better performance. Also, since all these extreme properties are combined in one material, Graphene could also enable some disruptive technologies.

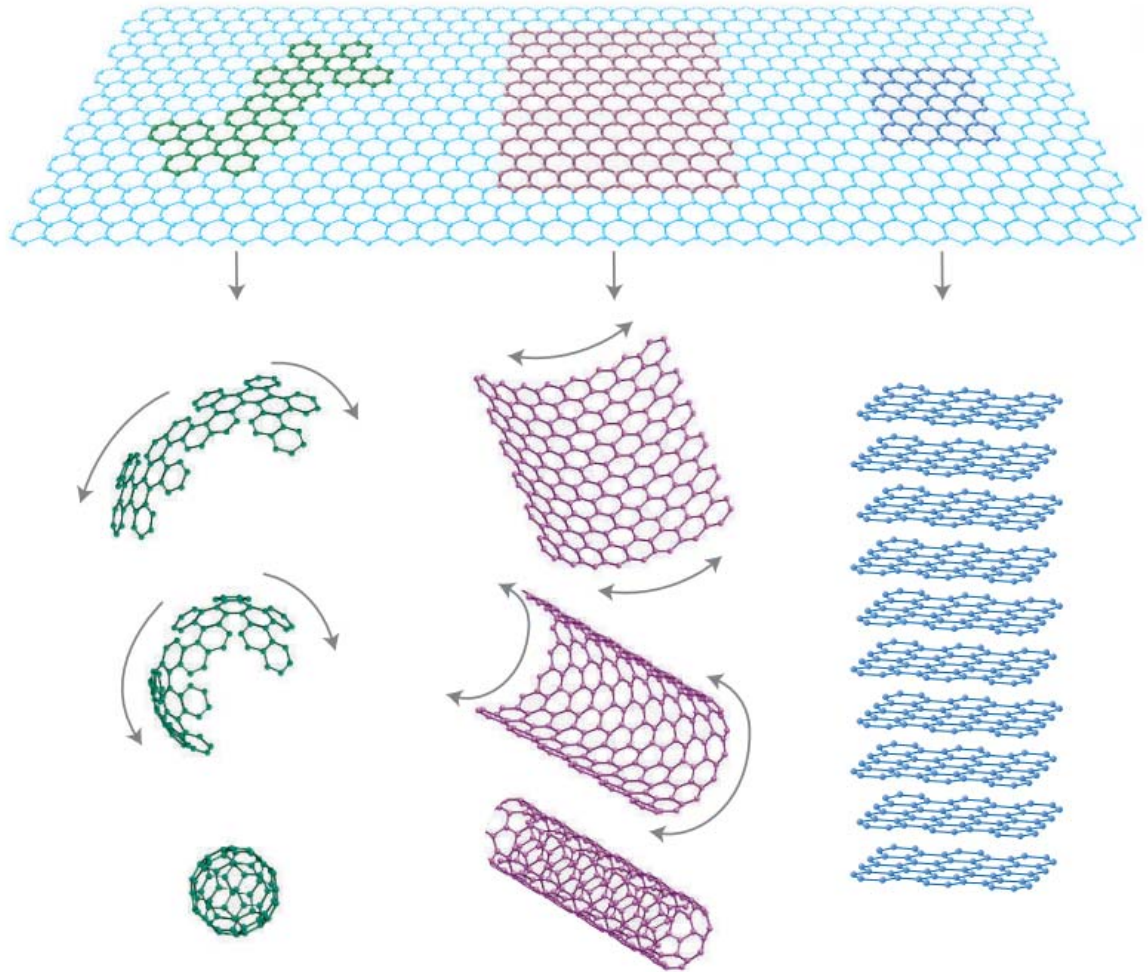


Figure1.1 Graphene is a 2D material for carbon materials of all other dimensionalities. It can be wrapped up into 0D bucky balls, rolled into 1D nanotubes or stacked into 3D graphite.^{1a}

The properties of high conductivity, good transparency and elasticity will find use in flexible electronics^{5a}, whereas transparency, impermeability and conductivity will find application in transparent protective coatings and barrier films^{3, 6}; and the potential use of these types' combinations is continuously expanding.

1.1.2 Graphene synthesis methods

Graphene is promising material for nanoscale electronics and flexible nanometers devices^{5a} because of their novel properties such as quantum transport and optical transmittance. Thus, it is important to prepare high-quality Graphene over large areas. Large-scale synthesis methods such as chemical vapor deposition (CVD)⁷ and epitaxial growth on metal substrates (e.g., Ni, Cu, Co, Ag, Ir) have been developed^{8,9,10}.

Table 1 Methods for prepare Graphene and their properties and applications.

Method	Crystallite size (μm)	Sample size (mm)	Charge carrier mobility (at ambient temperature) ($\text{cm}^2 \text{V}^{-1} \text{s}^{-1}$)	Applications
Mechanical exfoliation	>1,000	>1	$>10^6$	Research
Chemical exfoliation	<0.1	Infinite as a layer of overlapping flakes	100 (for a layer of overlapping flakes)	Coatings, paint/ink, composites, transparent conductive layers, energy storage, bioapplications
Chemical exfoliation via graphene oxide ¹¹	100	Infinite as a layer of overlapping flakes	1 (for a layer of overlapping flakes)	Coatings, paint/ink, composites, transparent conductive layers, energy storage, bioapplications
CVD (Chemical vapor deposition)	1,000	1,000	10,000	Photonics, nanoelectronics, transparent conductive layers, sensors,

Table 1
continued

bioapplications

SiC ¹²	50	100	10,000	High-frequency transistors and other electronic devices
-------------------	----	-----	--------	---

1.1.2.1 Mechanical exfoliation to synthesis Graphene

Mechanical exfoliation is the first method that successfully obtained high quality single layer Graphene. The method was reported by Dr Geim's group using a thermo release tape to peel Graphene from HOPG (Highly Ordered Pyrolytic Graphite) in 2004. The general idea of this method is the cleavage of graphene layers from the bulk HOPG surface. There are two kinds of mechanical routes to exfoliate graphite into graphene flakes, i.e. normal force and shear force. One can apply normal force to overcome the van der Waals attraction when peeling two graphite layers apart, such as micromechanical cleavage by thermo release tape. As the exfoliation might peel off more than one layer, repeat the process would finally result in a single layer graphene flake.

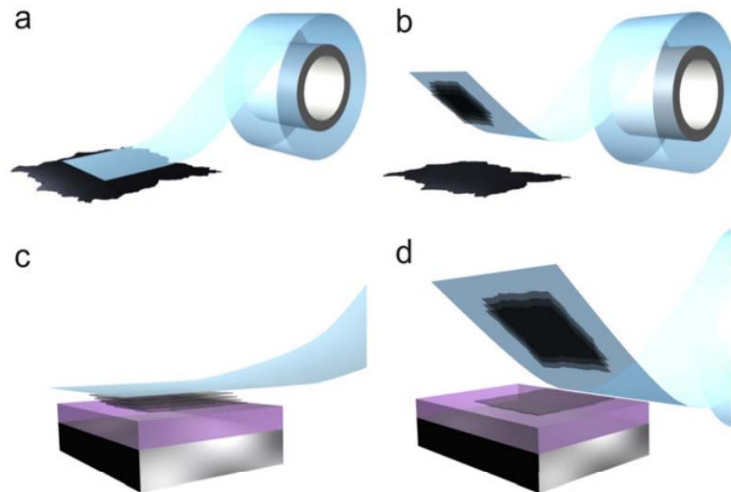


Figure 1.2 Scheme for mechanical exfoliation graphene.

This method can be used to prepare high-quality and large-area graphene flakes. Based on the graphene samples prepared by mechanical exfoliation, many outstanding properties of graphene have been observed. But, this method is extremely labour-intensive, time consuming and has a very low production rate. It is limited to laboratory research and seems impossible to scale up for massive industrial production. To date, the best performance graphene is still obtained from mechanical exfoliation method.

1.1.2.2 Chemical exfoliation to synthesis Graphene

The electrochemistry of graphite has a long history. Many interests are displayed in the electrochemical intercalation, deintercalation and functionalization of graphite to obtain functionalized exfoliated graphite and GICs, which have potential applications in electrochemical energy systems.

The various intercalation chemistry of graphite is useful to obtain single-layer graphene sheets based on the preferred expanding interlayer space which facilitates long-range exfoliation. However, previous research in the past two decades had shown that although graphite intercalation compounds are excellent precursors for exfoliated graphite, intercalation–exfoliation of graphite via thermal shock, acid treatment and intercalation all yielded only thin graphite nanoplatelets instead of single or few layers graphene sheets. After generate expanded graphite by acid treatments and thermal shocks, intercalants must be added to further expand the interlayer distance. Sonication of the resultant GIC in stabilizers (or surfactants) results in stable colloidal suspension of graphene monolayer sheets in organic or aqueous solutions, as demonstrated by Dai and co-workers.¹³ They sonicated expanded graphite in a long-chain aromatic polymer called poly(m-phenylenevinylene-co-2,5-dioctoxy-p-phenylenevinylene) (PmPV) dissolved in dichloroethane to produce a stable dispersion of chemically modified graphene (CMG) sheets and semiconducting graphene nanoribbons.

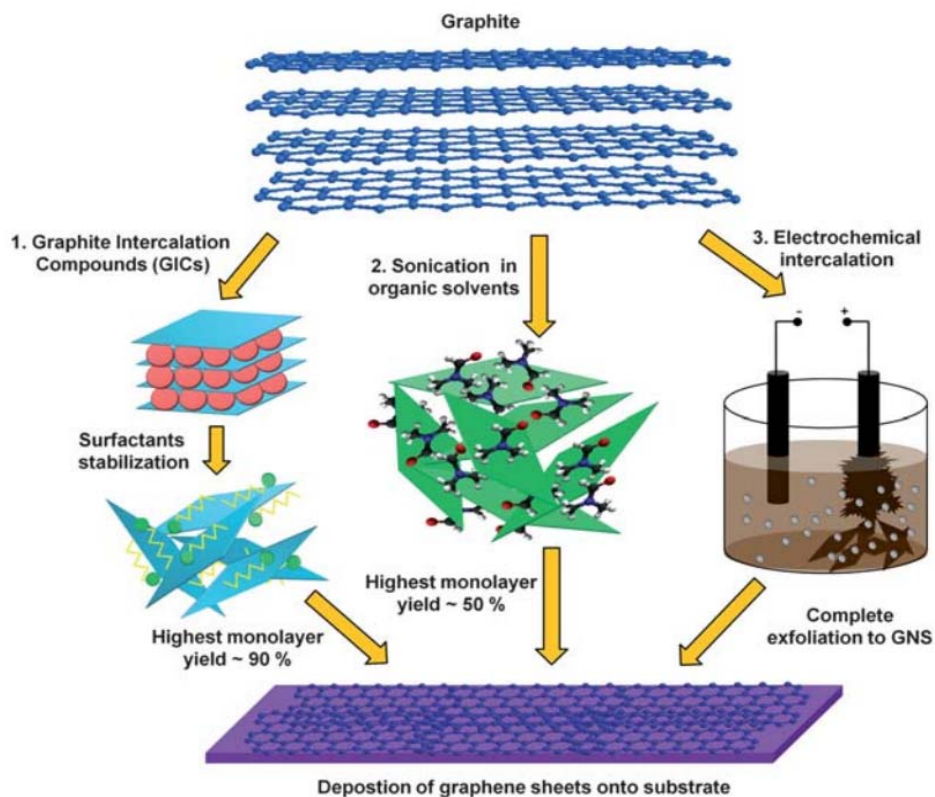


Figure 1.3 Chemical exfoliation to synthesis Graphene.⁷

Liquid phase exfoliation of graphite and graphite derivatives are common methods to obtain stable colloidal suspension of graphene sheets. The quality of these graphene sheets are undoubtedly higher than those derived from graphite oxide due to the absence of oxygen functionalities which disrupt electrical conductivity and carrier mobility. Without the aid of intercalants (such as Li ions), this method is only possible if the right solvent or solvent mixtures produce an adequate graphene–solvent interaction which can overcome the graphene–graphene interlayer van der Waals interaction. The enthalpy of mixing of graphene in solvents should be close to zero. This can occur when the solvent

surface energy (or surface tension) is close to that of graphene surface energy. In most cases, the net energetic penalty for long-range exfoliation is small and can be overcome by mechanical agitation such as sonication. However, prolonged sonication leads to undesirable fragmentation of exfoliated graphene sheets which results in small sized graphene sheets of lateral dimension 1 μm . Colloidal suspension of graphene sheets in organic solvents such as DMF, NMP and chloroform have been reported. Novoselov and co-workers reported that sonicating graphite in DMF returned a high yield of monolayer flakes up to 50%.¹⁴ DMF sufficiently prevents exfoliated graphene sheets from agglomerating due to its good wetting of individual graphene sheets.

Luo and co-workers reported an electrochemical approach to obtain imidazolium-based ionic-liquid-functionalized graphene sheets.¹⁵ Exfoliation of ILs functionalized graphene sheets readily formed a stable colloidal suspension in DMF, DMSO and NMP. Loh and co-workers demonstrated a facile one-pot ionic-liquid assisted electrochemical exfoliation approach to obtain fluorescent carbon nanoribbons, nanoparticles and graphene from graphite. The mechanism of the exfoliation is due to a complex interplay of anodic oxidation of water and anionic intercalation from the ionic liquid. Using ILs with high water content (>10% water) as the electrolyte, water-soluble, oxidized carbon nanomaterials were generated. In the case of electrolyte using concentrated ILs, IL-functionalized carbon nanomaterials were generated instead. The chemical composition and surface passivation of the exfoliated carbon nanoparticles can be controlled by changing the water/IL ratio in the electrolyte, thus allowing the fluorescence from

the exfoliated nanoparticles to be tuned from the ultraviolet to visible regions. The marriage between ILs and graphene can form a gel-like composite called “bucky gel” and these designer materials show great versatility for applications as electrodes, capacitors, sensors and actuators.

1.1.2.3 Chemical exfoliation via graphene oxide to synthesis

Graphene

Despite the relative novelty of graphene as a material of broad interest and potential raised in the 21 century, GO has a history that extends back many decades to some of the earliest studies involving the chemistry of graphite. The first, well-known example came in n 1859 when British chemist B. C. Brodie was exploring the structure of graphite by investigating the reactivity of flake graphite.¹⁶ One of the reactions he performed involved adding potassium chlorate ($KClO_3$) to slurry of graphite in fuming nitric acid (HNO_3). Brodie determined that the resulting material was composed of carbon, hydrogen, and oxygen, resulting in an increase in the overall mass of the flake graphite.

There is several different methods to obtain oxidize graphene from oxidized graphite, thermal reduction at 1050C, electrical reduction and chemical reduction.

The Hummers method is one of the most accepted methods. One could obtain graphene at low-cost by reducing graphene oxides (GO). The basic method was developed by Hummers et al. in the 1950's.¹⁷ The GO, which is oxidized chemically from a graphite crystal and is dissolved in aqueous solution,

can be easily deposited on an arbitrary substrate in monolayer or few-layer form.¹⁸ The monolayer GO can be reduced into graphene, but it contains many defects and functional groups due to the oxidation process. Recent efforts have produced the high-quality graphene with a carrier mobility exceeding $1000 \text{ (cm}^2 \text{ V}^{-1} \text{ s}^{-1}\text{)}$, although the yield at present is not high enough.¹⁹ This reduced GO is based on the solution technique, and so is most suitable for printed electronics and chemical applications.

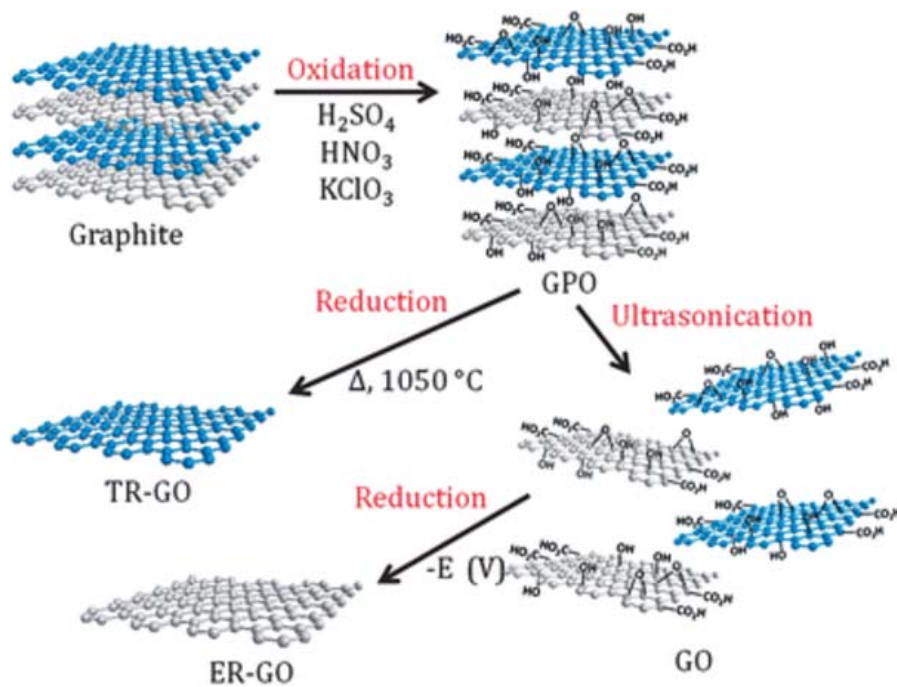


Figure 1.4 Chemical exfoliation via graphene oxide to synthesis Graphene.¹¹

1.1.2.4 SiC precipitation to synthesis Graphene

The phenomenon of graphitized carbon at the surface of a SiC single crystal was first reported by Badami in 1965.²⁰ He studied graphite formed on decomposed silicon carbide at 2180 C, by X-ray diffraction and revealed that the c-axis of graphite is along the c-axis of the hexagonal SiC crystal. In the decade following this discovery, van Bommel and coworkers discovered the crystallographic orientation relation between graphite and SiC by a low-energy electron diffraction (LEED) experiment.²¹ They demonstrated that the (1120) graphite and (0002) graphite planes are parallel to the (1100) SiC and (0001) SiC planes, respectively, and that the graphitization process proceeded via the surface reconstruction phase.

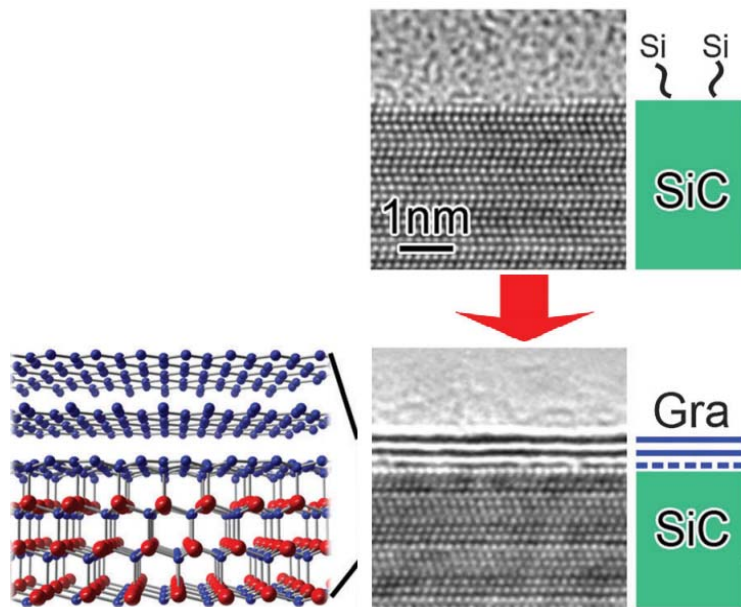


Figure1.5 SiC precipitation to synthesis Graphene.¹²

1.1.2.5 CVD method to synthesis Graphene

Two main different CVD growth mechanisms have been revealed²²(Figure 1.6), growth of graphene on Ni occurs by a so called carbon segregation or precipitation process⁹ while graphene on Cu grows through the surface adsorption process¹⁰. It is believed that the segregation of Graphene on Ni foil is mainly taking place during cooling when carbon solubility of Ni decreasing dramatically thus forms multilayer Graphene islands instead of uniform Graphene films as latter is preferred for most applications. On the other hand, Graphene starts growing on copper at high temperature with Carbon source from splitting hydrocarbon gas. Cu has a very low carbon solubility, thus the carbon consumed during growth are mostly came from environment gas, once Graphene covered Cu surface will not be no catalyst cooper exposed to feeding gas, this so called self-limited effect result in a uniform single layer Graphene.¹⁰

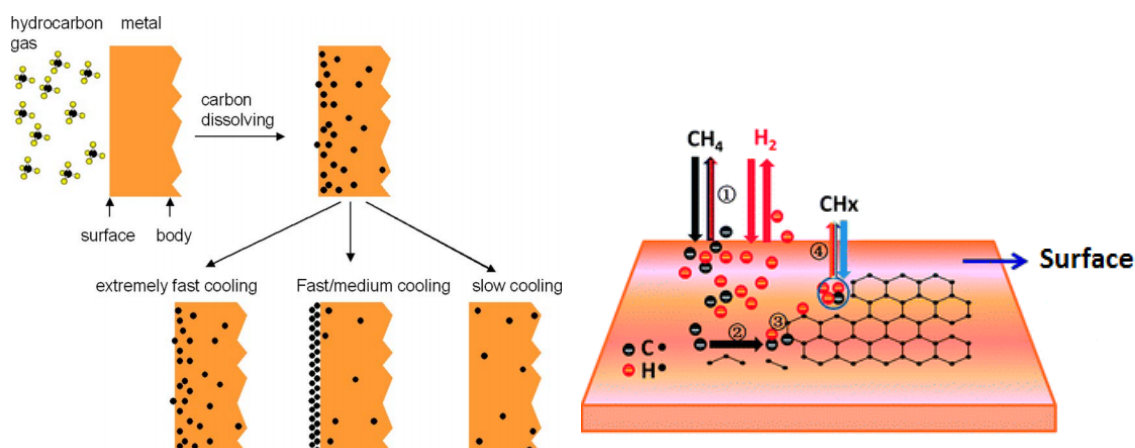


Figure1.6 Scheme of grow Graphene on Ni and Cu .²³

Though the single layer Graphene obtained from Cu substrate has stunning material properties, due to the small grain size and large amount of grain boundaries it is still not as good as exfoliated Graphene.^{1a, 4, 1b} While recent theoretical studies suggest that the grain boundaries themselves may not have a strong intrinsic effect on carrier transport, they are the sites of preferable adsorption of external species, which can cause appreciable scattering of charge carriers; it is also a weak spot and will decrease Graphene's mechanical strength.²⁴

In a general crystallization process, two steps take place in sequence: nucleation and growth. For the case of Graphene grew on Cu^{22, 25}, carbon concentration have great impact on both steps: higher carbon partial pressure will increase growth rate but at same time it will also increase number of nucleus.²⁶ Thus one can hardly find a sweet spot to achieve both less nucleus and faster growth rate to grow Graphene on Cu substrate by simply tuning feeding gas. There is successful case where large size single crystal Graphene has been grown on Cu by CVD method by using oxidized Cu substrate to suppress nuclear,²⁷ the method is complicated and takes way too long to grow.²⁷ A centimeter size single crystal graphene would take 12 hours to grow under high vacuum.²⁸

The use of an alloy substrate^{3, 4} to improve Graphene synthesis has attracted much attention recently. It has been found that an alloy catalyst can dramatically increase the quality of Graphene films even at low CVD temperatures. Some experimental studies have found that a rationally designed binary alloy metal can

effectively overcome the shortcomings of pure metals and activate the self-limited growth of homogeneous monolayer graphene. Monolayer and bilayer graphene films have been prepared by changing only the atomic percentage of Ni and Cu in Cu–Ni alloy (Figure 1.7). In short, substrate alloying provides a new way of thinking about the optimization of CVD-produced high-quality Graphene films and rationalizes the catalyst design during growth, in addition to the control of the growth temperature and the amount of reactants.²⁹

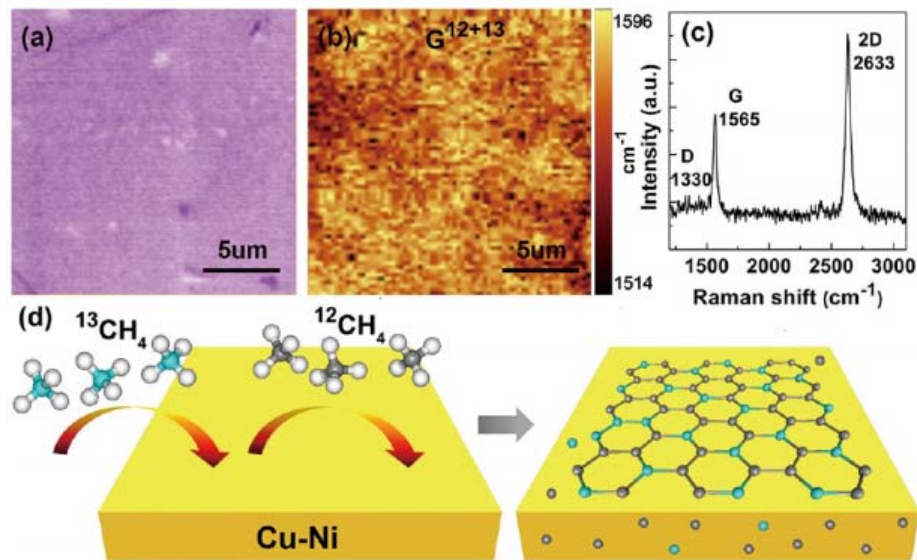


Figure 1.7 (a) Optical micrograph of a monolayer graphene transferred onto a 285 nm SiO₂/Si substrate. (b) The corresponding Raman map generated by the position of the G band (G¹²⁺¹³, 1500-1650 cm⁻¹). (c) A Raman spectrum acquired from panel b. Schematic diagrams of the growth process of carbon isotope labeled graphene, and the possible distribution of ¹²C and ¹³C atoms in Graphene films and inside the Cu/Ni alloy. ¹²C (gray) and ¹³C (blue) atoms.

A recent study by Dr. Xiaoming Xie's group shows that they are able to grow large single crystal Graphene on Cu/Ni alloy. It only takes 2.5 hrs to grow this 2.25cm single crystal Graphene at a rapid growth rate of 170 $\mu\text{m}/\text{min}$, which is about ten times faster than report on large single crystal Graphene grew on Cu (14-17 $\mu\text{m}/\text{min}$).²⁸

This finding of super fast single crystal Graphene growth rate is undoubtedly crucial to better and faster production of single crystal graphene growth, but the growth mechanism behind it is still unknown. In our work, taking the same Cu–Ni alloy substrate used by Dr Xie, we will use carbon isotope labeling in conjunction with Raman spectroscopic mapping to determine the carbon trace during the growth process.

1.1.3 *Raman spectroscopy in Graphene*

Since the discovery of the Raman effect in 1928 by C.V. Raman and K.S. Krishnan, Raman spectroscopy has become an established as well as a practical method of chemical analysis & characterization applicable to many different chemical species.

It provides information about molecular vibrations that can be used for sample identification and quantization.³⁰

Raman spectroscopy is a form of vibrational spectroscopy, much like infrared (IR) spectroscopy.³⁰ However, IR bands arise from a change in the dipole moment of a molecule due to an interaction of light with the molecule, Raman bands arise from a change in the polarizability of the molecule due to the same

interaction. This means that these observed bands (corresponding to specific energy transitions) arise from specific molecular vibrations. When the energies of these transitions are plotted as a spectrum, they can be used to identify the molecule as they provide a “molecular fingerprint” of the molecule being observed. Certain vibrations that are allowed in Raman are forbidden in IR, whereas other vibrations may be observed by both techniques although at significantly different intensities thus these techniques can be thought of as complementary.

The technique involves shining a monochromatic light source (i.e. laser) on a sample and detecting the scattered light. The majority of the scattered light is of the same frequency as the excitation source; this is known as Rayleigh or elastic scattering. A very small amount of the scattered light (ca. $10^{-5}\%$ of the incident light intensity) is shifted in energy from the laser frequency due to interactions between the incident electromagnetic waves and the vibrational energy levels of the molecules in the sample. Plotting the intensity of this "shifted" light versus frequency results in a Raman spectrum of the sample as Figure 1.4. Generally, Raman spectra are plotted with respect to the laser frequency such that the Rayleigh band lies at 0 cm^{-1} . On this scale, the band positions will lie at frequencies that correspond to the energy levels of different functional group vibrations. The Raman spectrum can thus be interpreted similar to the infrared absorption spectrum.

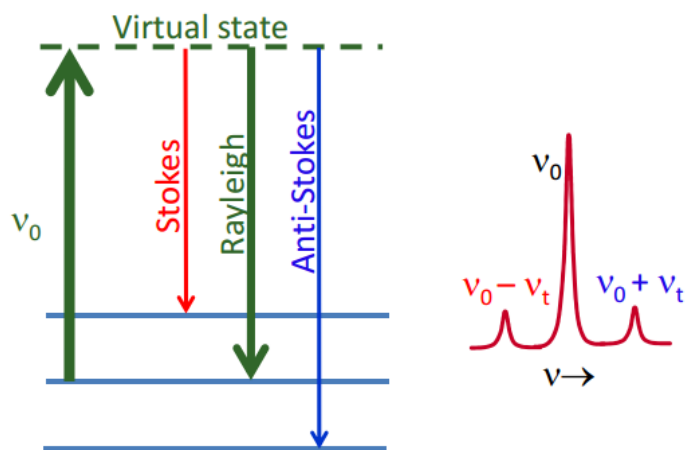


Figure 1.8 Rayleigh (elastic) scattering and Raman (Stokes) scattering.

Raman spectroscopy had become one of the most popular techniques for the characterization of disordered and amorphous carbons, fullerenes, nanotubes, diamonds, carbon chains and polyconjugated molecules. Raman techniques are particularly useful for Graphene because the absence of a band gap makes all wavelengths of incident radiation resonant, thus the Raman spectrum contains information about both atomic structure and electronic properties. Resonance could also be reached by ultraviolet excitation.³¹

In 1970, Tuinstra and Koenig (TK) first reported the work of using Raman to test graphite and assigned the mode at $\sim 1580\text{cm}^{-1}$ to the high frequency E_{2g} Raman allowed optical phonon.²³ They also measured in defected and nanocrystalline graphite a second peak at $\sim 1350\text{cm}^{-1}$. They did not give any names to these Raman peaks.^{32, 33, 34} The first nomenclature was proposed by Vidano and Fishbach in 1977.³⁵ Since they observed strong lines at ~ 1580

and $\sim 2700\text{cm}^{-1}$ in pristine graphite, while other bands at ~ 1350 and $\sim 1620\text{cm}^{-1}$ only appeared in defected graphite, they called the former G, G' (from Graphite) and the latter D, D' (from Disorder). Nemanich and Solin detected a sharp band at $\sim 3250\text{cm}^{-1}$ in pristine graphite, as well as a weaker one at $\sim 2450\text{cm}^{-1}$.³⁶ They also noted a further peak at $\sim 2950\text{cm}^{-1}$ in defected samples, later named D'' by Vidano et al.³⁷ In 1979 Nemanich and Solin, by polarization dependent measurements, assigned all peaks between 2300 and 3250cm^{-1} in pristine graphite as overtones. In 1981 Vidano et al. studied the excitation energy dependence, and confirmed G' to be the D overtone, and the $\sim 3250\text{cm}^{-1}$ peak the D' overtone, since these shifted at twice the rate of their fundamentals. They stressed those bands behaved differently from G, that did not move with excitation energy. Thus, by 1981 it was clear that, while the Raman allowed first-order G peak did not shift with excitation energy, the "defect-related" bands D, D', their overtones and combinations did.³⁸

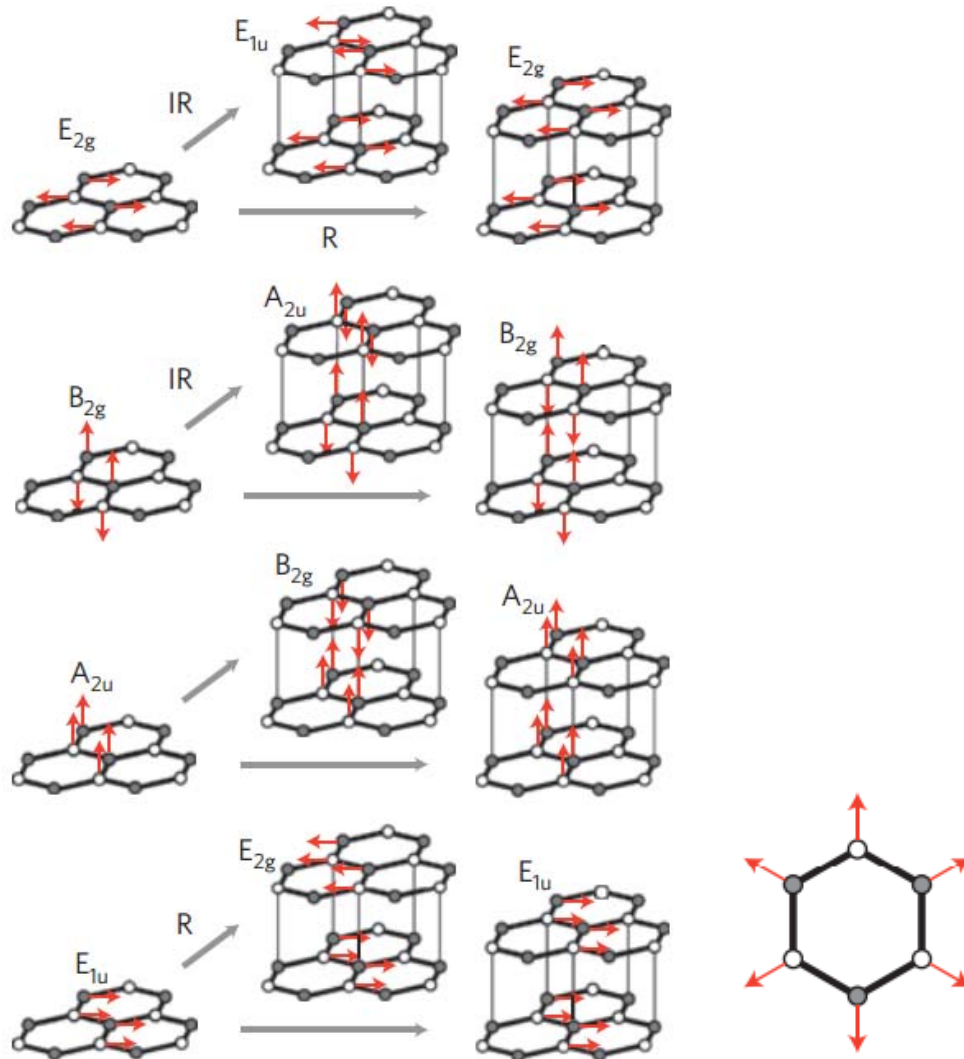


Figure 1.9 Phonon-displacement pattern for graphene and graphite. Empty and filled circles represent inequivalent carbon atoms. Red arrows show atom displacements. Grey arrows show how each phonon mode in graphene gives rise to two phonon modes of graphite. Their labelling shows Raman-active (R), infrared-active (IR) and inactive (unlabelled) modes; Breathing (A_{1g}) mode.³¹

There is two degenerate optical modes, one in-plane E_{2g} optical mode, and one out-of-plane optical mode B_{2g} . The E_{2g} phonons are Raman active, whereas the B_{2g} phonon is neither Raman nor infrared active (Figure 1.9).

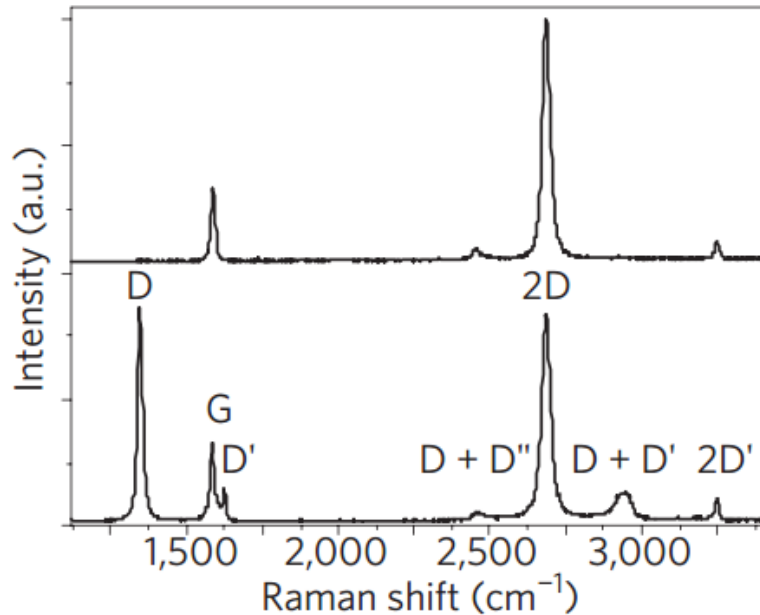


Figure 1.10 Raman spectra of pristine (top) and defected (bottom) graphene. The main peaks are labeled.

In a general Raman spectrum (Figure 1.10, Raman spectra of pristine and defected graphene), the G peak corresponds to the high-frequency E_{2g} phonon. The D peak is due to the breathing modes of six-atom rings and requires a defect for its activation. Because the 2D and 2D' peaks originate from a process where momentum conservation is satisfied by two phonons with opposite wave vectors, no defects are required for their activation, and are thus always present.^{1b}

1.1.4 Raman spectroscopy for isotope labeled Graphene

Since Raman scattering is related to the energy of molecular, the Raman frequency modes are inversely proportional to the square root of the atomic mass, the relation of frequencies of the carbon mixed Graphene (ω_i) can be derived as

$$\omega_i = \omega_{i,12} \sqrt{\frac{m_{12}}{n_{12}m_{12} + n_{13}m_{13}}} \quad (1)$$

where $\omega_{i,12}$ is the Raman shift of band i of ^{12}C -graphene, m_{12} and m_{13} are the atomic masses, and n_{12} and n_{13} are the atomic fractions of ^{12}C and ^{13}C , respectively. Thus one can trace the carbon migration and study how Graphene grows by Raman spectrum mapping.

Ruoff's group reported their discovery through the Raman mapping method on isotope carbon labeled Graphene to uncover growth mechanism of Graphene on Cu and Ni. They revealed the different mechanisms of Graphene grew on these two metal substrates. By purging $^{13}\text{CH}_4$ and $^{12}\text{CH}_4$ carbon source in sequence, Graphene precipitate from Ni and surface adsorbed on Cu has different Raman pattern of carbon isotope.

Graphene grew on Cu mainly involves two steps, nucleation and crystal growing. After the initial seed forming, carbon atom from decomposed methane will attach to its edge and growing concentrically. While for Graphene on Ni, carbon atom first dissolved in Ni foil since Ni has high carbon solubility (1-2% in Ni at 1000-1000C compare to virtually zero in Cu³⁹). During cooling, carbon atom

participates out and forms multi layer Graphene islands as carbon solubility decreased with decreasing temperature.

Isotope carbon source was purged in sequence at growth condition, ^{13}C core formed on Cu substrate but dissolved in Ni substrate (Figure 1.11). As they switch the feeding ^{13}C methane into ^{12}C methane, for Cu substrate, ^{12}C continuously grow on edge of ^{13}C Graphene seed and surround the ^{13}C region. While for Ni substrate, ^{12}C also dissolved in Ni substrate and participate out together with ^{13}C formed Graphene composed by mixed ^{13}C and ^{12}C . Since the ^{13}C and ^{12}C are randomly mixed at atomic level for Graphene grew on Ni, the Raman frequency of Graphene grew on Ni has only one well defined peak as described by equation 1. For Graphene grew on Cu, isotope carbon formed different isotope region and Raman frequency only have peaks at pure ^{13}C and ^{12}C position.

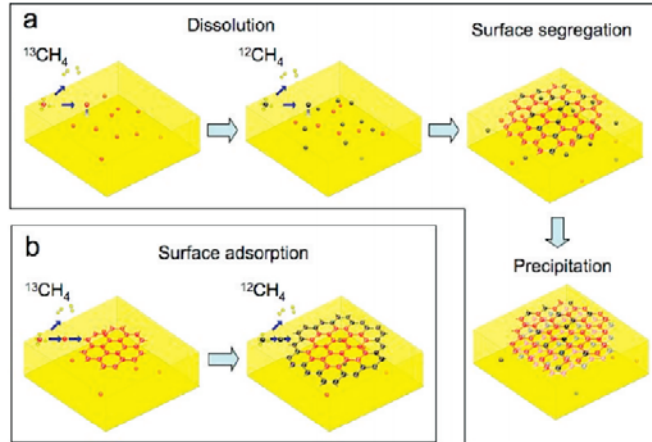


Figure 1.11 Schematic diagrams of the possible distribution of C isotopes in Graphene films based on different growth mechanisms for sequential input of C isotopes. (a) Graphene with randomly mixed isotopes such as might occur from surface segregation and/ or precipitation. (b) Graphene with separated isotopes such as might occur by surface adsorption.

1.1.5 Scanning electron microscope (SEM) for Graphene

Another important method for Graphene characterization is Scanning electron microscope (SEM). SEM is the most widely accepted method of electron microscope. It examines microscopic structure of specimen by scanning the surface of materials. SEM image is obtained by a focused electron beam that scans over the surface area of a sample. Electron beam is condensed by 3 electromagnetic condensers to reduce its diameter into the nanometer scale.

The electron beam probe scanning is operated by a beam deflection system. The deflection system controls the probe to move over the sample surface line by line. Signal electrons emitted from the sample are collected by a detector, amplified and used to form the image.

There are two different types of electron signal detected in a SEM: secondary electrons and backscattered electrons. When high energy electrons strike at sample, they generate inelastic and elastic scattering. Inelastic scattering produces secondary electrons which are electrons ejected from atoms in the sample, they are usually deflected at small angles and show considerably high energy loss. Elastic scattering produces backscattered electrons which are incident electrons scattered by sample atoms, they are normally scattered at large angles and have very less energy loss compare to secondary electrons. Secondary electrons are the primary signals for achieving topographic contrast, while backscattered electrons are useful for formation of elemental composition contrast (section 2).

As Graphene is composed by sp^2 carbon, it has a universal $\pi-\pi$ electron cloud with abundant electrons. When a high energy electron beam strike at sample surface, electrons will cumulate if the sample has a poor conductivity, and scatter more secondary electrons. For case of Graphene, it has very high conductivity and $\pi-\pi$ electron cloud will adsorb quite amount of strike energy, result in uniform low electrons scattering area (Fgiure 1.12).

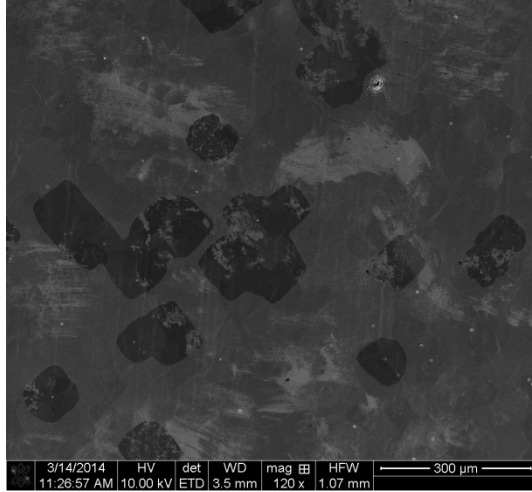


Figure1.12 SEM and SEM image of Graphene on Cu.

1.2 Methods

1.2.1 *Single crystal Graphene growth*

Ni/Cu alloy with different Ni contents (10%, 15%, 20% Ni) were used as substrates to grow single crystal Graphene. The Ni/Cu alloys with different Ni content were obtained from Dr Wu without further treatment and will be directly used.

Ni/Cu alloy substrate is placed in a 2in quartz chamber and ramp to 900C at 15C/min, then continuously ramping to 1050C at 10C/min. A mixed gas flow of 200sccm Ar and 20sccm H₂ is used as protective gas and provide a reduction environment. The alloy substrate will be annealed at 1050C for 2hrs for Ni and Cu to be thoroughly mixed, followed by decreasing chamber pressure to 100Torr until stable. Then change gas feeding as: 100sccm H₂, 20sccm Ar and 0.1sccm methane flow (total 0.5% methane in Ar) for Graphene growth for certain time and cool down and stop methane flow as illustrated in Figure 1.13. This growth recipe may subject to change for optimizing the best result (hexagonal single flake Graphene) for substrates with different Ni content. Different growth time (5 - 30mins) will be tested to obtain the suitable size of Graphene for Raman mapping (seed size 20-50 μm, flake size 100-200μm).

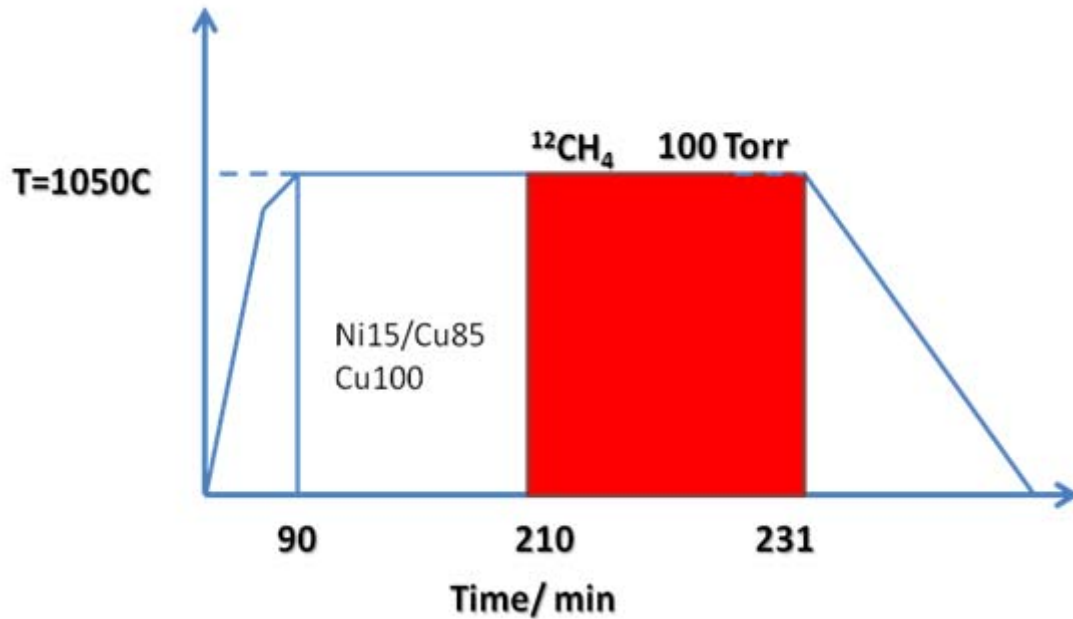


Figure1.13 Growth condition for pure ^{12}C Graphene.

1.2.2 Isotope labeled graphene

After finding the best growth recipe, alternative of $^{13}\text{CH}_4$ and $^{12}\text{CH}_4$ methane flow will be used as carbon source to grow single Graphene flakes on Ni/Cu (15/85) alloy as illustrated in Figure 1.10. The growth condition for isotope labeled Graphene is 0.5% $^{12}\text{CH}_4$ in 20sccm Ar and 100sccm H_2 for 7mins then change the methane carbon source to 0.5% $^{13}\text{CH}_4$ in 20sccm Ar and 100sccm H_2 for another 7 mins, followed by a second 7mins 0.5% $^{12}\text{CH}_4$ purge. Then stop methane and hydrogen gas purge, resume 200sccm Ar & 20sccm H_2 and start to cool down. This growth recipe may subject to small changes for optimizing the best result for substrates with different Ni contents. The Graphene formed on Ni/Cu alloy could be studied.

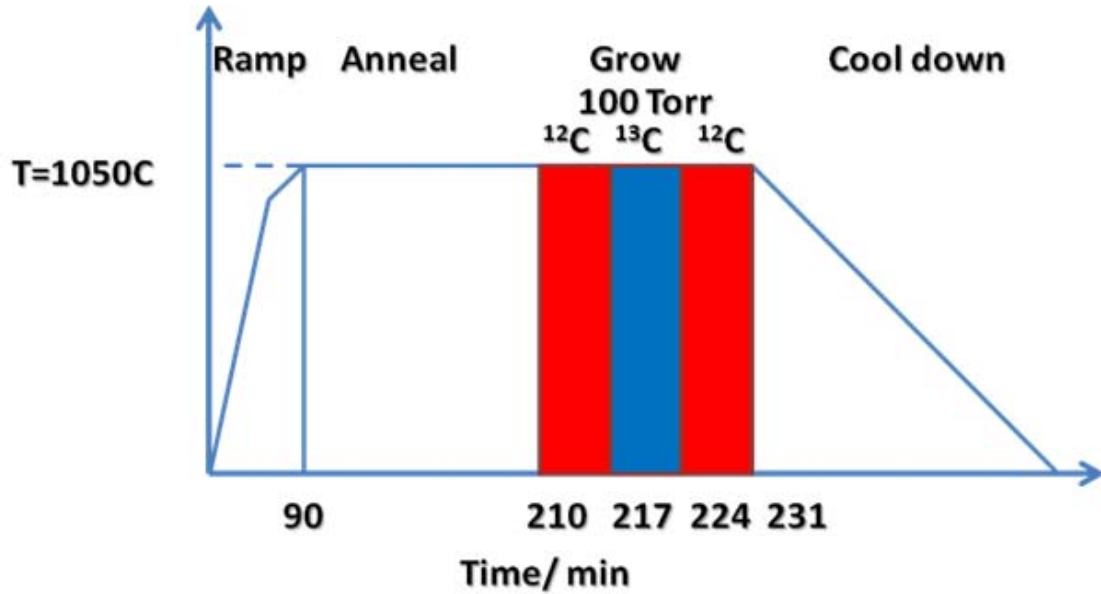


Figure 1.14 Growing isotope labeled Graphene with 2 switches.

To further study the mechanism of Graphene growing on Ni/Cu alloy, one switch purge is used instead of two switches as Figure 1.15. At growth condition, 0.5% $^{13}\text{CH}_4$ in 20sccm Ar and 100sccm H_2 was purged in for 10mins then change the methane carbon source to 0.5% $^{12}\text{CH}_4$ in 20sccm Ar and 100sccm H_2 for another 10 mins. After growth, stop methane and keep Ar and H_2 flow to ambient pressure and cool down.

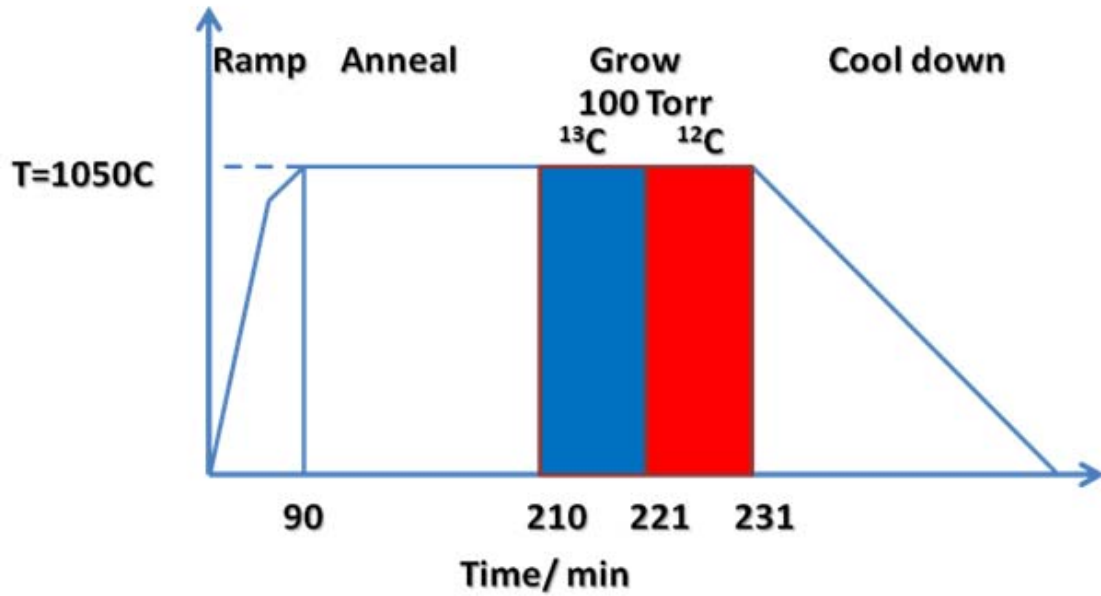


Figure 1.15 Growing isotope labeled Graphene with 1 switch.

1.2.3 Characterization

1.2.3.1 Scanning electron microscope

Scanning electron microscope (SEM) will be used to determine the size and shape of Graphene flakes grown on Ni/Cu alloy.

Due to its high conductivity, Graphene flakes could be easily identified under electron beam as uniform dark area. Graphene seeds will also be studied as an important aspect.

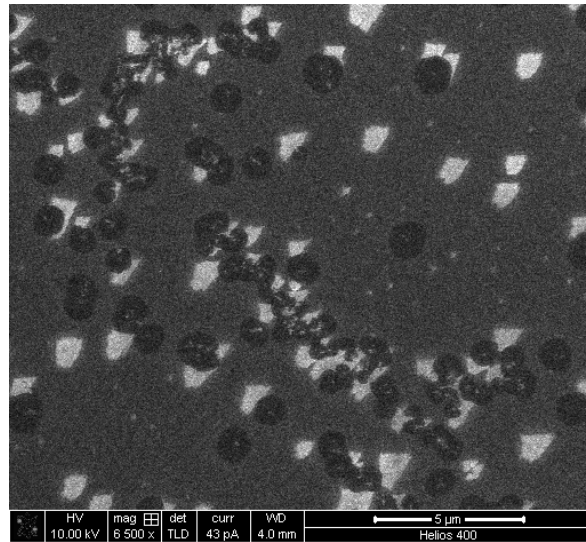


Figure1.16 SEM of Graphene flakes on Cu.

Graphene sample will be transferred onto silicon wafer with 300nm SiO₂ layer for Raman spectroscopic mapping to determine the carbon migration for Graphene grew on Ni/Cu alloy. We use PMMA as transfer support, 3% PMMA in chloroform is spun coated on Graphene/Alloy foil and dried. Then put the sample upside down in oxygen plasma chamber to etch Graphene on back side. After 1min oxygen plasma etching, place sample on 10 wt% ammonium persulfate solution to etch the alloy foil. Sample film will then be transferred to silicon wafer and dry overnight. The final step is to wash out PMMA with acetone.

1.2.3.2 Raman spectrum and mapping

Thermo Scientific DXR Raman microscope (excitation laser is 532nm) will be used to image the carbon map and exam quality of Graphene grew on Ni/Cu alloy. The DXR Raman microscope has a resolution down to 500nm, which is good for identify small C¹³ and C¹² clusters and their boundaries. Since Raman

frequency modes are inversely proportional to the square root of the atomic mass, the relation of frequencies of the carbon mixed Graphene (ω_i) can be derived as

$$\omega_i = \omega_{i,12} \sqrt{\frac{m_{12}}{n_{12}m_{12} + n_{13}m_{13}}} \quad (1)$$

where ω_{i12} is the Raman shift of band i of ^{12}C -graphene, m_{12} and m_{13} are the atomic masses, and n_{12} and n_{13} are the atomic fractions of ^{12}C and ^{13}C , respectively. Thus one can calculate content of each isotope and track carbon migration base on the Raman frequency.

1.3 Results and discussion

1.3.1 Nucleation density

Different gas feeding rate during growth and cooling has been studied to find out the best experiment condition for hexagonal Graphene flakes. Summary of growth condition and graphene flakes are list in table 2.

The nucleation density of Graphene was shown as Figure 1.17, growth condition is 20sccm 0.5% CH₄ in Ar and 100sccm H₂ for 10mins at 100 Torr for all Ni/Cu alloy while for Cu foil, we have to increase the carbon source to 2% CH₄ to nuclei at analog condition.

Table 2. Growth condition and time for graphene on Ni/Cu alloy with different Ni content.

	H ₂ (sccm)	Ar(sccm)	CH ₄ (sccm)	Time(mins)	Size/shape
Ni/Cu 10%Ni	100	20	0.05(0.25%)	5	-
				10	-
				15	-
				20	-
	100	20	0.1(0.5%)	5	seed/hexagonal
				10	~40μm/hexagonal
				15	~60μm/hexagonal
				20	~90μm/hexagonal
	100	20	0.15(0.75%)	5	seed/round
				10	~100μm/hexagonal
				15	~150μm/hexagonal
				20	full covered
Ni/Cu 15%Ni	100	20	0.05(0.25%)	5	-
				10	-
				15	-
				20	-
	100	20	0.1(0.5%)	5	seed/hexagonal
				10	~100μm/hexagonal
				15	~150μm/hexagonal
				20	~250μm/hexagonal
	100	20	0.15(0.75%)	5	~50μm/round
				10	~250μm/round

Table2 Continued	100	20	0.05(0.25%)	15	nearly full covered
				20	full covered
				5	-
				10	-
				15	-
Ni/Cu 20%Ni	100	20	0.1(0.5%)	20	-
				5	seed/round
				10	~50 μ m/hexagonal
				15	~150 μ m/hexagonal
				20	~400 μ m/hexagonal
	100	20	0.15(0.75%)	5	~100 μ m/round
				10	nearly full coverd
				15	full covered
				15	full covered
				20	full covered

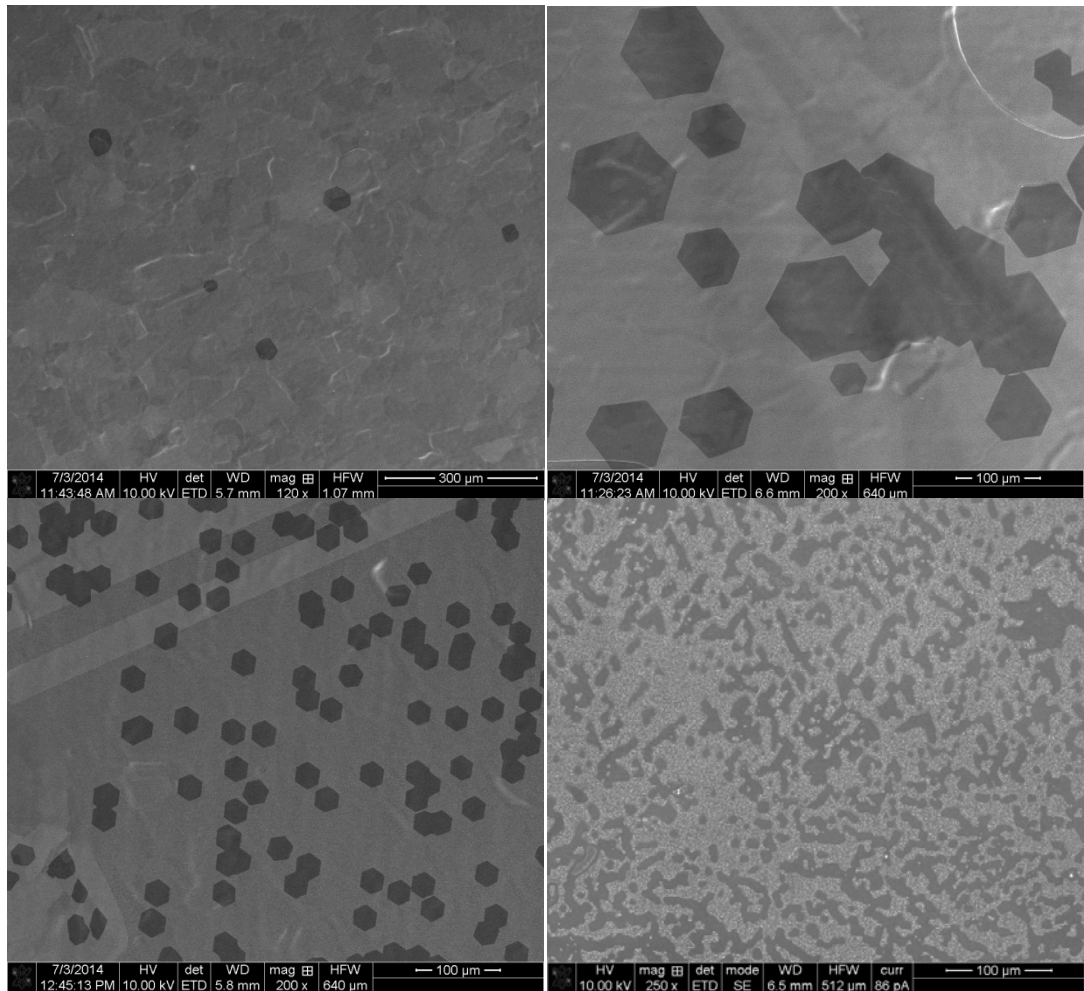


Figure 1.17 SEM of Graphene seeding on Ni/Cu alloy (10%, 15% and 20%) and on Cu.

Result shown in Figure 1.17 indicating Graphene seeding on Ni/Cu alloy have much lower nucleus compare to pure Cu from SEM image though the carbon feeding concentration for Cu substrate is 3 times higher than that for Ni/Cu alloy. For Ni/Cu alloy with 3 different Ni contents, the nucleation density is different, too. Ni/Cu alloy with 20% Ni has the lowest nucleation density as $5/ (1\text{mm})^2$, while for Ni/Cu alloy with 15% Ni, nucleation density is about $100/ (1\text{mm})^2$. Decrease Ni content to 10%, nucleation density increases to about $1000/ (1\text{mm})^2$. More

detailed work was done by Dr Xie's group as Figure 1.18, consistent with our result that with an increasing Ni content nucleation density decreased. Since they are using the local feeding method where there's a decreased carbon concentration from local feeding probe (nucleus) towards Graphene growing front, nucleation density from their result is much lower than what we have here using an environmental feeding method.

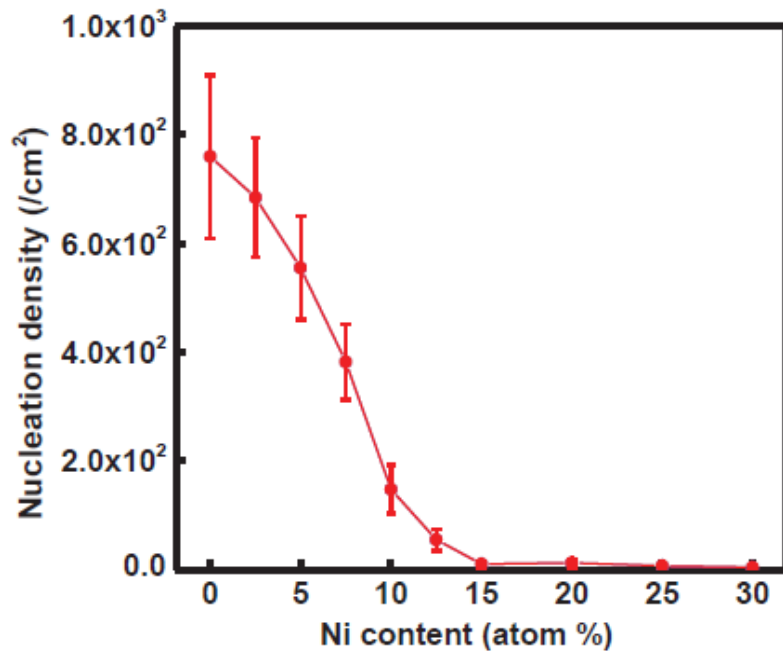


Figure1.18 Nucleation density vs Ni content (atom %).

Above results shows increasing Ni content would decrease nucleation density; our hypothesis is increasing Ni content would increase the energy required for nucleation.

1.3.2 Large single crystal graphene

Single crystal flakes as large as 400 μm with a good hexagonal shape could be easily grown on Ni/Cu alloy using environmental feeding as indicated in Figure 1.19. To grow single crystal hexagonal Graphene flakes for Raman mapping ($\sim 100\mu\text{m}$), total growth time is set to be around 14 mins with 20sccm 0.5% CH_4 in Ar and 100sccm H_2 . This is to control the growth rate so one can monitor the effects of gas change on isotope content in graphene. Since we are expecting a cooperated behavior of Ni body participation and Cu surface adsorption.

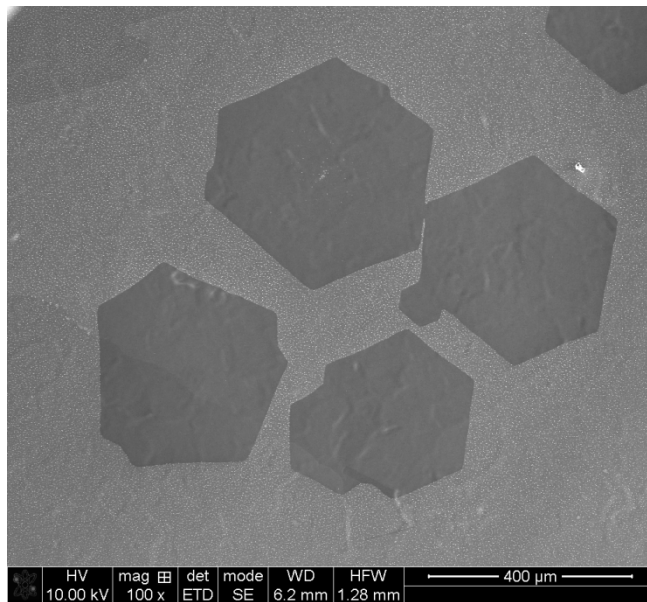


Figure1.19 Large single crystal Graphene flakes up to 400 μm with good hexagonal shape can be easily obtained on Ni/Cu alloy.

Single crystal Graphene flakes grown on Ni/Cu alloy and Cu substrate are shown in Figure 1.20, Graphene flakes grew on Ni/Cu alloy with 20% Ni content

has the largest size about 200 μm , Graphene grew on alloy with 15% Ni are about 150 μm . On Ni/Cu alloy substrate with only 10% Ni, Graphene flakes are much smaller, about 50 μm . Similar to seeding experiment, carbon feeding for pure Cu substrate is much higher (2% CH_4) but has a smaller flake size.

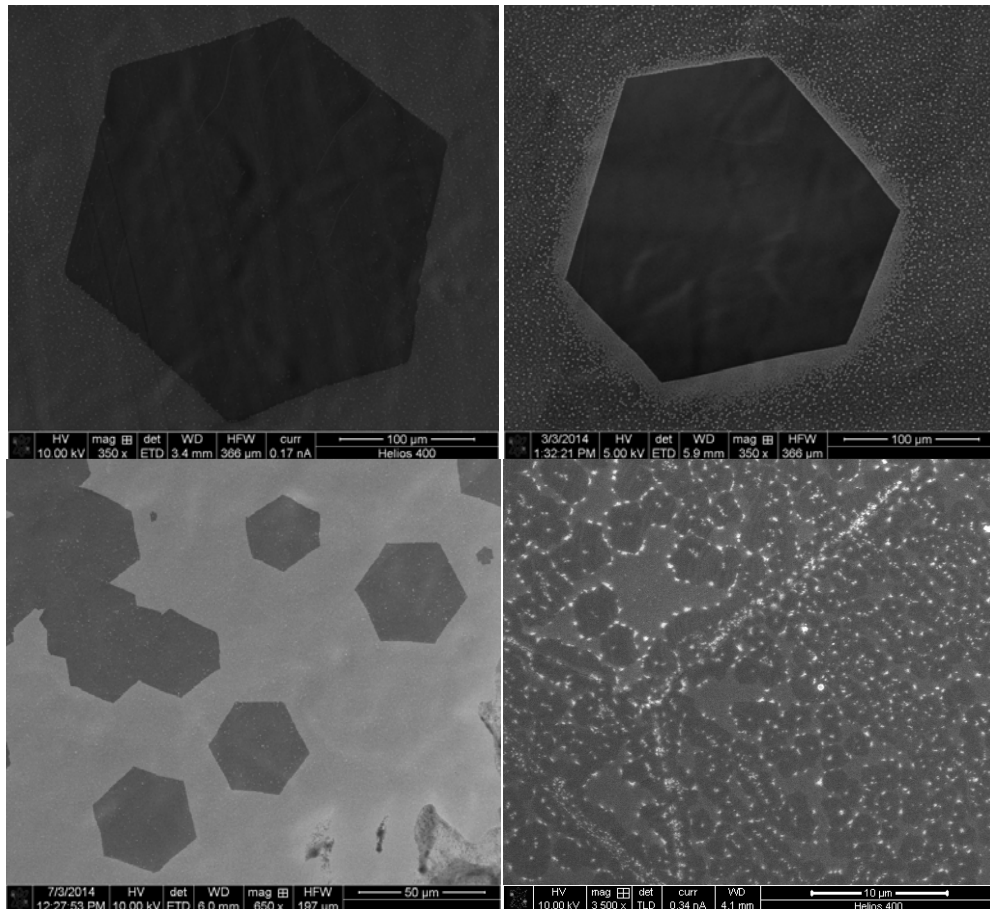


Figure1.20 SEM of single crystal flakes of Graphene grown on Ni/Cu alloy (10%, 15% and 20%) and small Graphene flakes on Cu.

1.3.3 Raman spectrum for isotope labeled graphene

Raman spectrum for pure ^{12}C Graphene, pure ^{13}C Graphene on silicon wafer are shown as follow. Graphene composed by pure ^{12}C has 2D band at 2660cm^{-1} , while pure ^{13}C Graphene has 2D band at 2580cm^{-1} . This result does not follow equation 1 precisely, which is due to inner stress from different thermal expansion rate between alloy and Graphene. This peak position difference has also been seen in Raman spectrum for Graphene grew on Ni/Cu alloy with different Ni contents.

For none atomic level carbon isotope mixture (surface adsorption on Cu like substrate), at switch boundary, we found the Raman spectrum has two individual peaks for each band (G band or 2D band), consistent with Graphene spectrum obtained from each isotope region solely. While for the case of participation, carbon isotope connected to Graphene growth front randomly, and only one peak for each band can be detected (for 2D band it is between 2580cm^{-1} and 2660cm^{-1}).

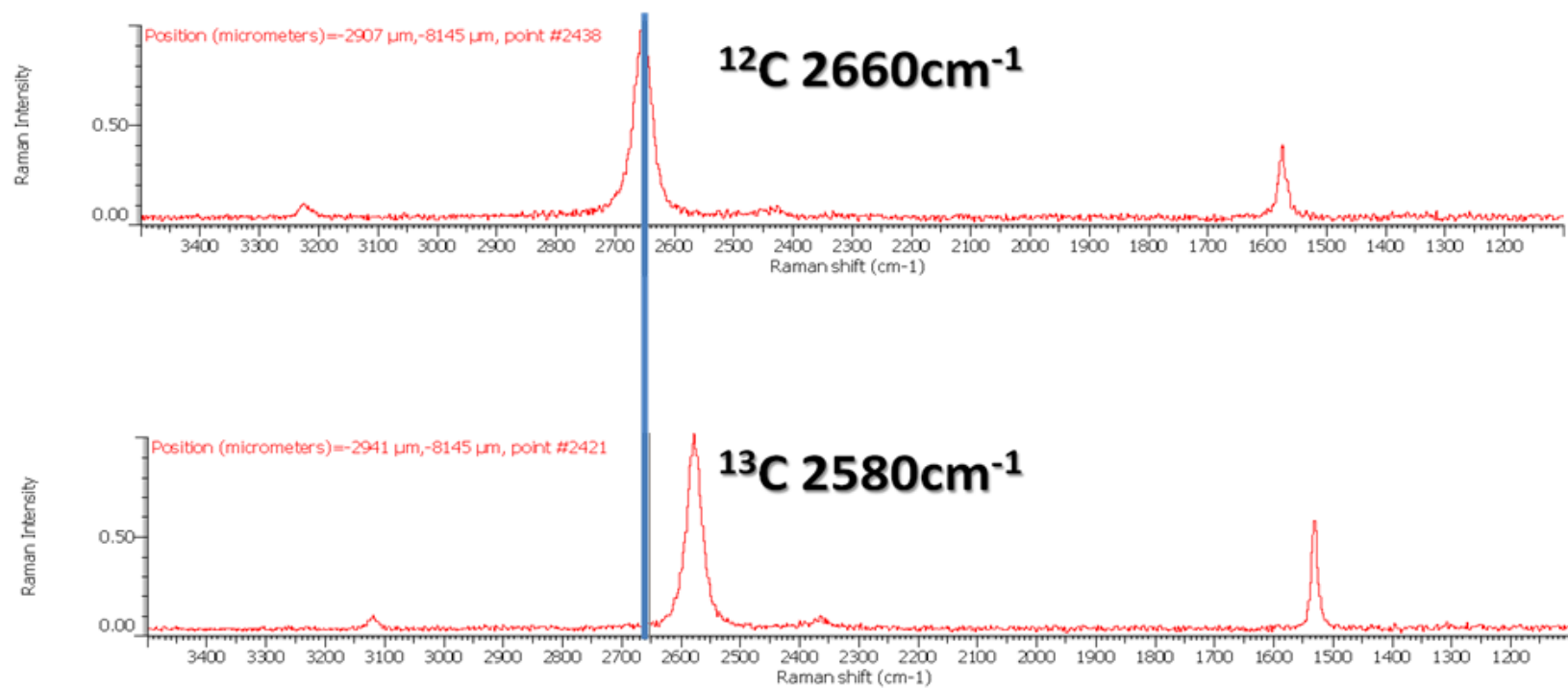


Figure 1.21 Raman spectrum of pure ^{12}C graphene (top) and pure ^{13}C graphene (bottom).

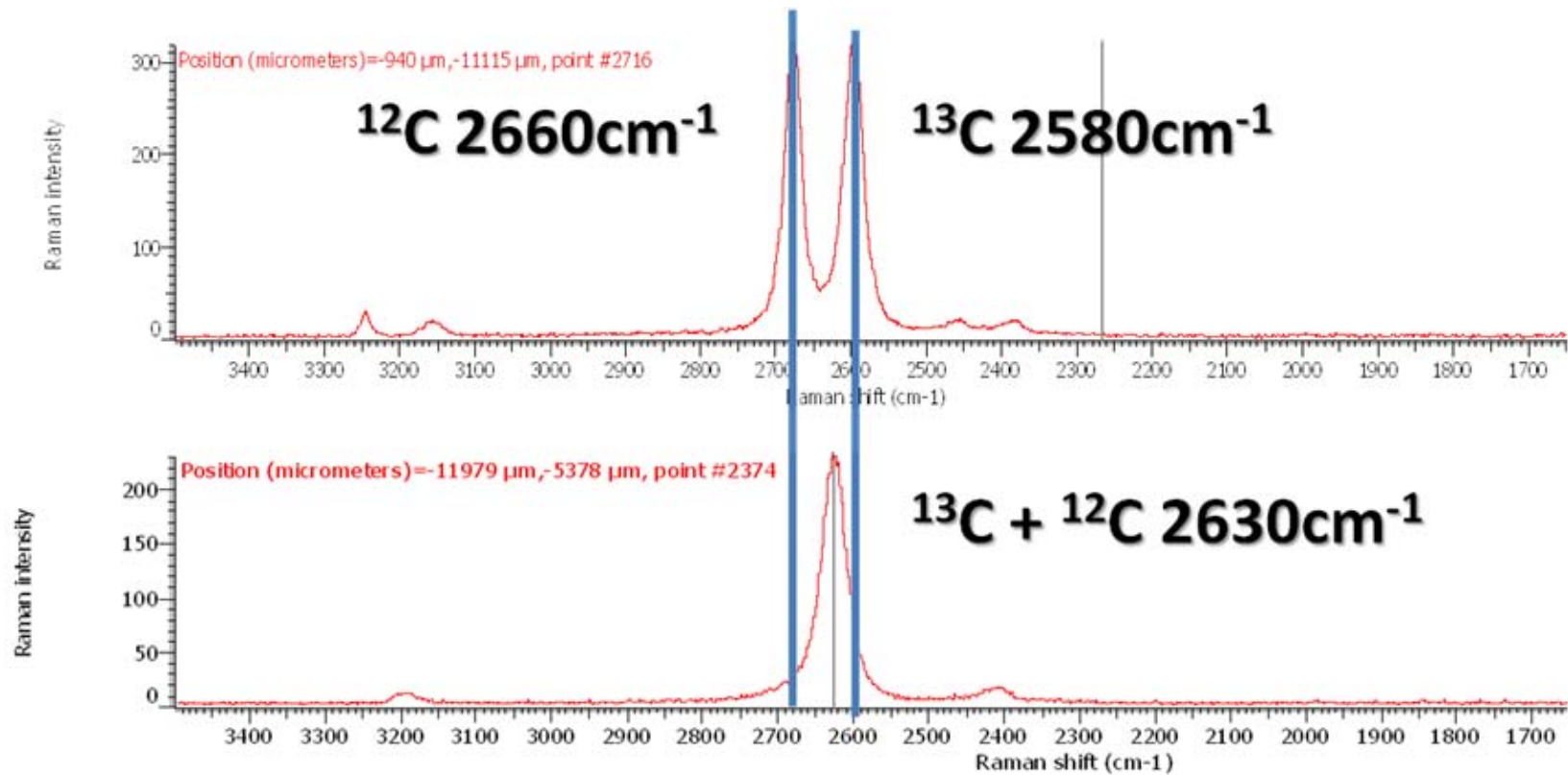


Figure 1.22 Raman spectrum of graphene with resolvable ^{12}C and ^{13}C region (top) and graphene composed by randomly mixed ^{12}C and ^{13}C (bottom).

1.3.4 Raman mapping for isotope labeled Graphene

Raman mapping for isotope labeled Graphene grown on Ni/Cu (15%) alloy is shown in Figure 1.23, center seed is composed by pure C^{12} indicated the nucleation initiated during the first 7mins before introducing $^{13}CH_4$. Blue shift of frequency is observed as a yellow region when $^{13}CH_4$ was purged into the chamber, peak position experienced a sharp blue shift from 2671 cm^{-1} (red) to 2625 cm^{-1} (yellow) and then gently shift to 2591 cm^{-1} (blue) at the end of $^{13}CH_4$ purge. When a second $^{12}CH_4$ feeding was introduced, rapid red shift indicates ^{12}C was added to Graphene growth front edge again. Peak position continuously red shifted to 2660 cm^{-1} as more ^{12}C bonded to Graphene growth front.

This result is different from any previous reports on CVD growth mechanism of Graphene since they are either body segregation (peak position gently shifts as Ni) or surface adsorption (peak position sharply shifts as Cu). Raman mapping for body segregation would result in a homogeneous distribution of ^{13}C and ^{12}C while surface adsorption lead to concentric pattern of pure ^{12}C or ^{13}C . Base on flow rate (120 sccm/min mass based flow rate), pressure (100Torr) and chamber volume ($\sim 300\text{ cm}^3$), we calculated the approximate time required to completely change carbon source from ^{12}C to ^{13}C in chamber is less than 1min. Thus the effect of isotope gas mixture would be negligible.

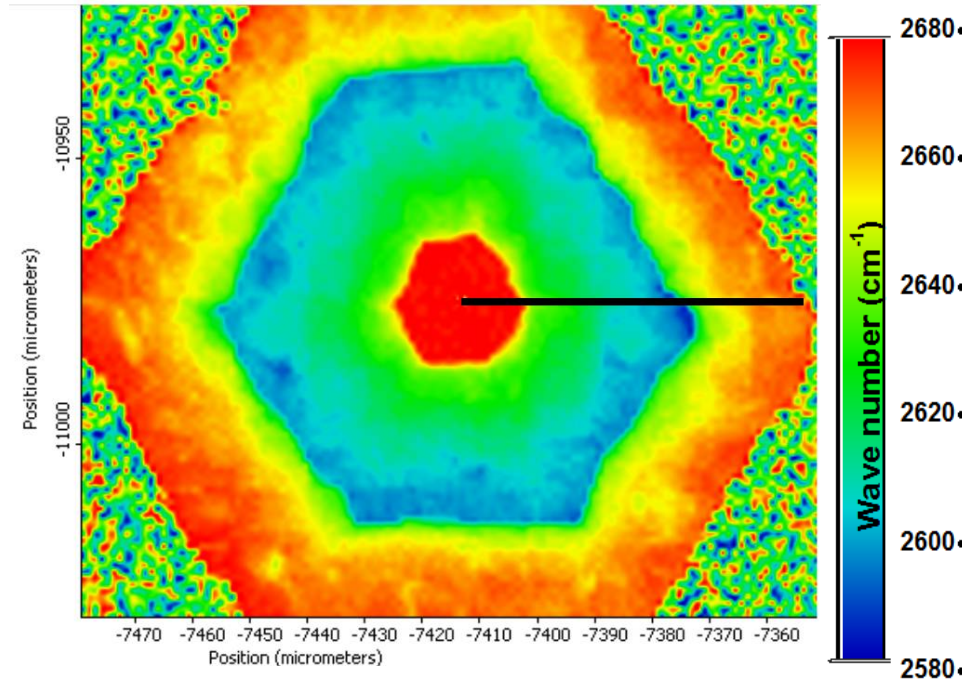


Figure 1.23 Raman mapping of isotope labeled Graphene.

To further study how carbon migrates during Graphene growth, we used equation 1 to determine isotope content profile from Figure 1.23 to explain how carbon is attached to Graphene growth front edge. Extracted peak position profile is the average of 3 consecutive lines along the black line and corresponding to content calculated are shown in Figure 1.24 and Figure 1.25. Graphene core is formed by pure ^{12}C to $10\mu\text{m}$ when carbon source was switch to ^{13}C . After ^{13}C was introduced, content decreases dramatically confirmed a surface adsorption behavior of Cu while the lateral gentle change indicates body participation of ^{12}C from Ni. This result is not surprising since Cu and Ni would not form compound and they are both good substrate for Graphene growth thus they shall both contribute to the growth of Graphene. We need to point out that no ^{12}C or ^{13}C cluster other than the ^{12}C core was detected, indicated no preference

of carbon segregation or adsorption during CVD growing Graphene on Ni/Cu (15/85) alloy at 1050C.

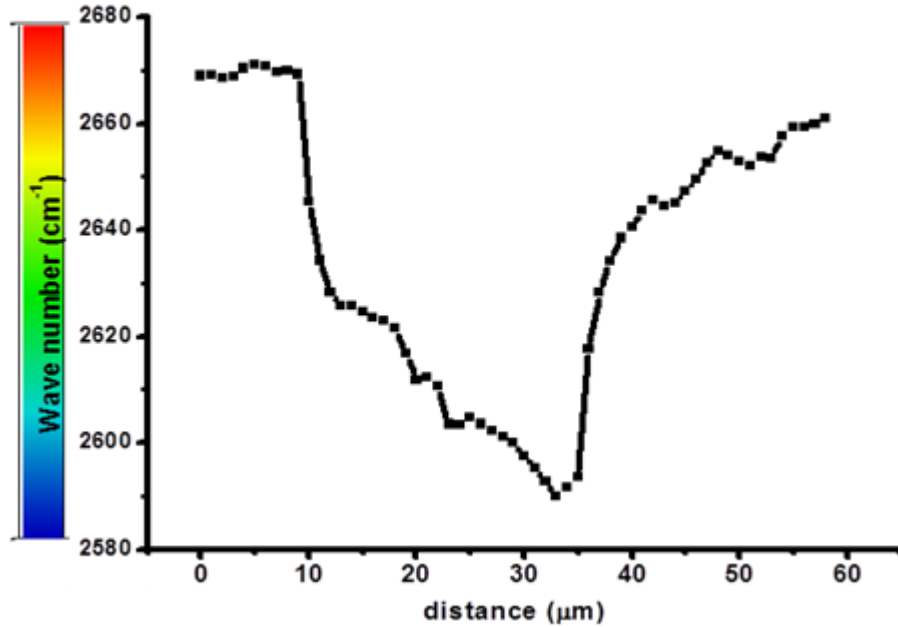


Figure1.24 Extracted peak position and distance from Figure 1.19.

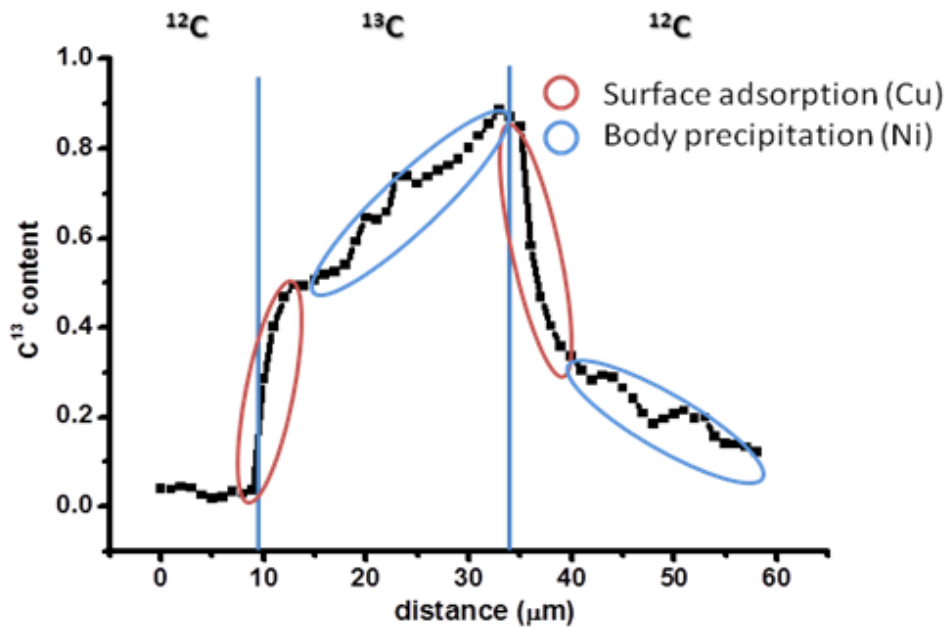


Figure1.25 Calculated C13 content vs distance from Figure 1.20.

This result clearly shows that at high temperature sequentially introduced isotopic carbon would diffuse into the Ni/Cu (15/85), segregation and surface absorption of carbon take place at same time with no preference at atomic level. Nucleus is significantly decreased by using Ni/Cu (15/85) alloy compare to pure Cu. Cu foil placed in chamber with Ni/Cu (15/85) showed no seeds or Graphene flake at the same growth condition indicated that though adding Ni content suspending nucleus, it does not increase the energy required to form seed, on the contrary it helps seeding at early stage and suppress forming of new nucleus. Further study will be conducted on how different Ni contents would affect the carbon behavior on nuclear, segregation and adsorption. This would help us to look insight what is the main role of Ni and Cu in Graphene growth via CVD method.

Three Ni/Cu alloy substrates were studied with one switch method: 10% Ni, 15% Ni and 20% Ni. Raman mapping of isotope labeled Graphene grew on these three substrates are shown in Figure 1.26. The false color scale bar indicates peak position of 2D band from 2580 cm^{-1} - 2670 cm^{-1} . All three hexagonal single crystal Graphene flakes are single layer and cored with pure ^{13}C nucleus.

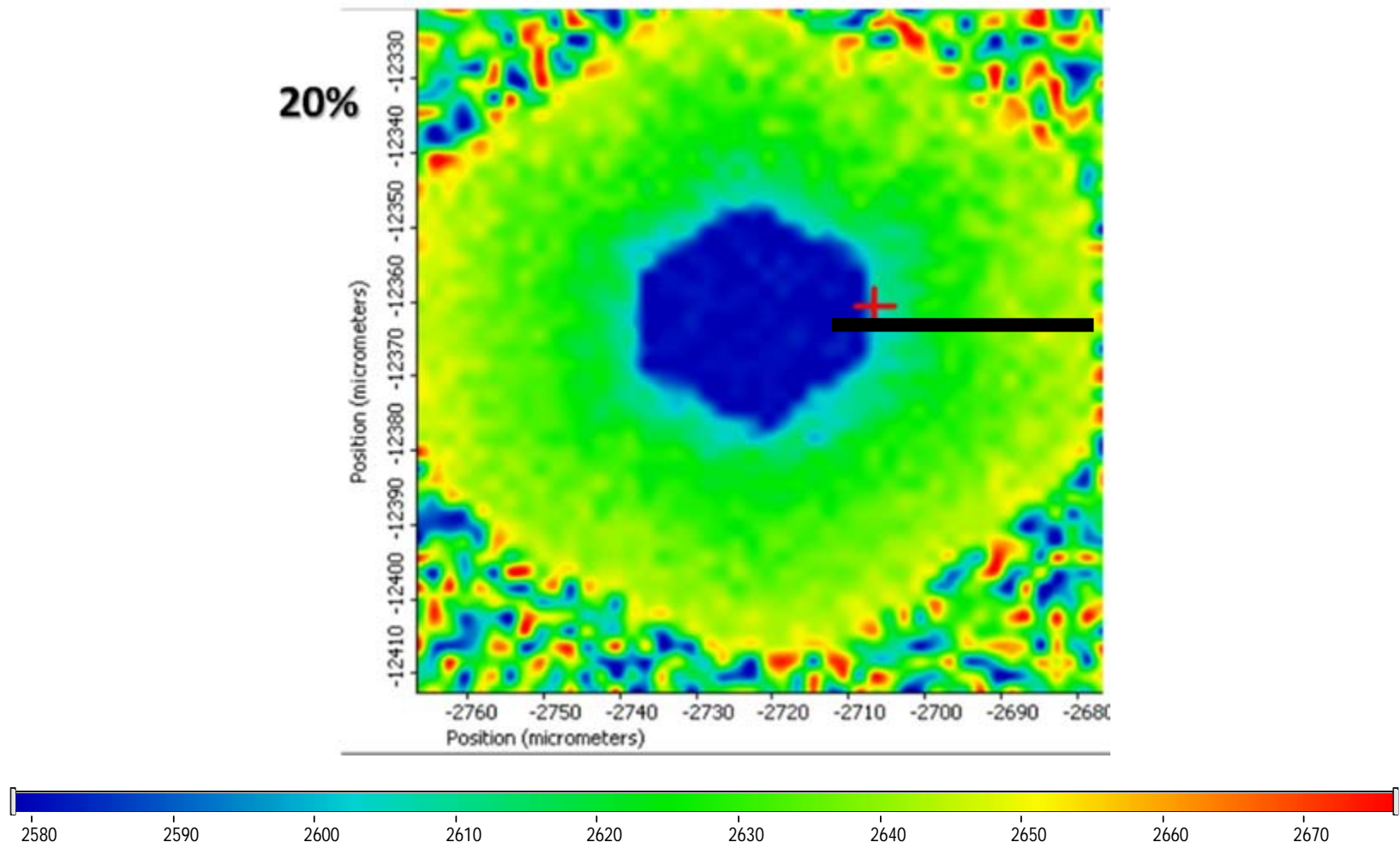


Figure 1.26a. Raman mapping of isotope labeled Graphene grown on Ni/Cu with 20%Ni.

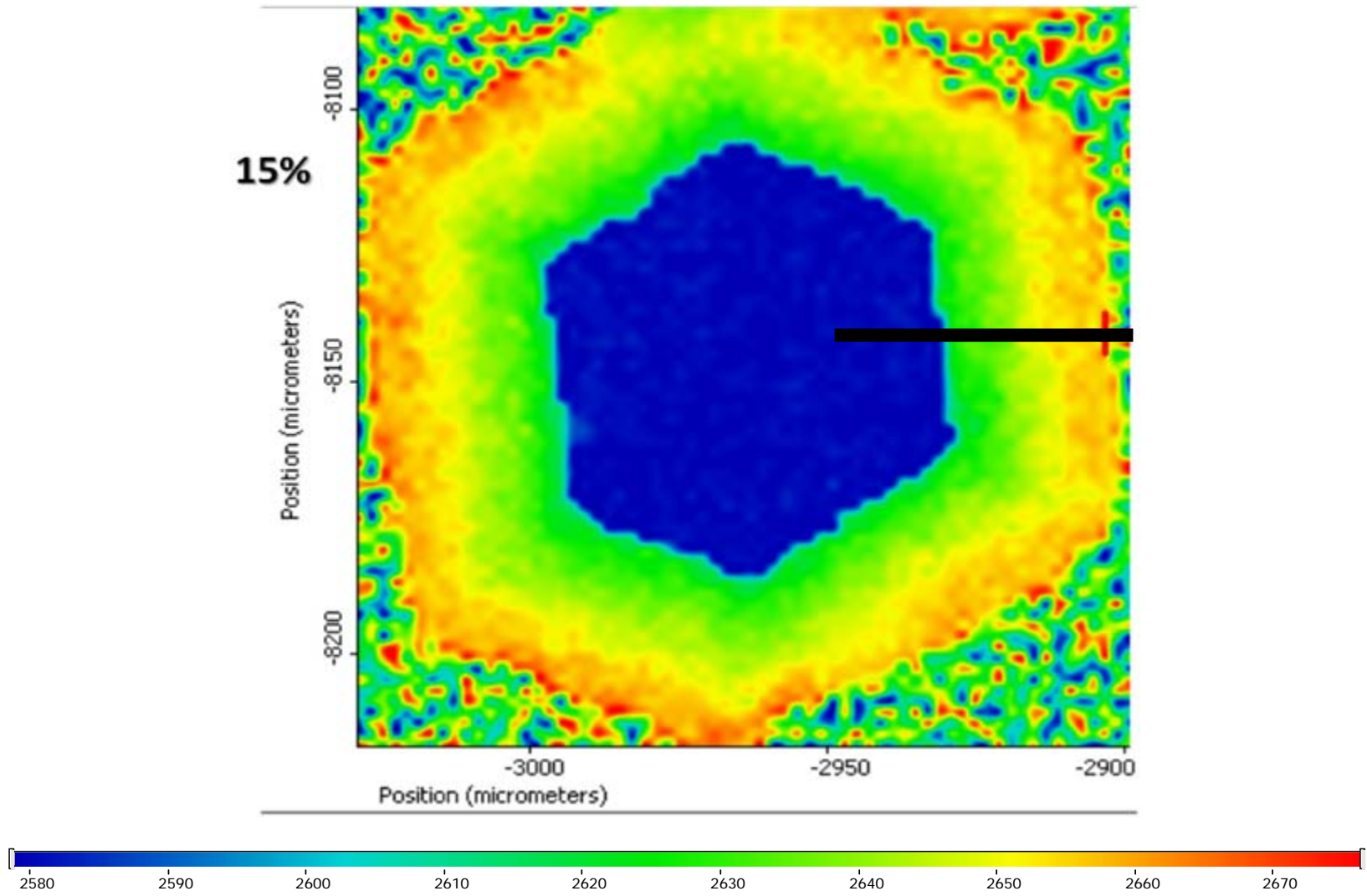


Figure 1.26b. Raman mapping of isotope labeled Graphene grew on Ni/Cu with 15%Ni.

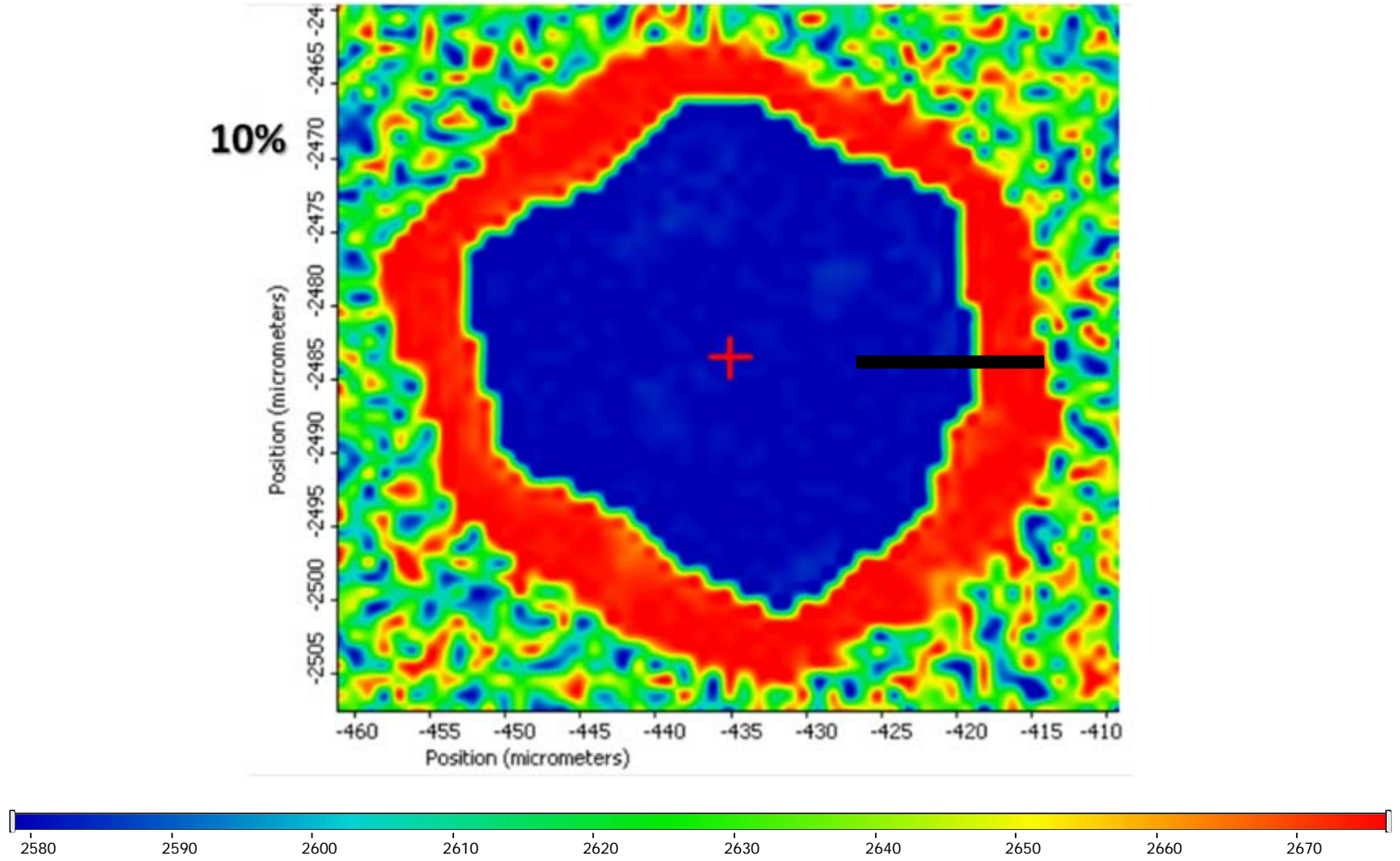


Figure1.26 C Raman mapping of isotope labeled Graphene grew on Ni/Cu with 10% Ni.

Extracted peak position profile is the average of 3 consecutive lines along the black line and corresponding content was calculated as Figure 1.27

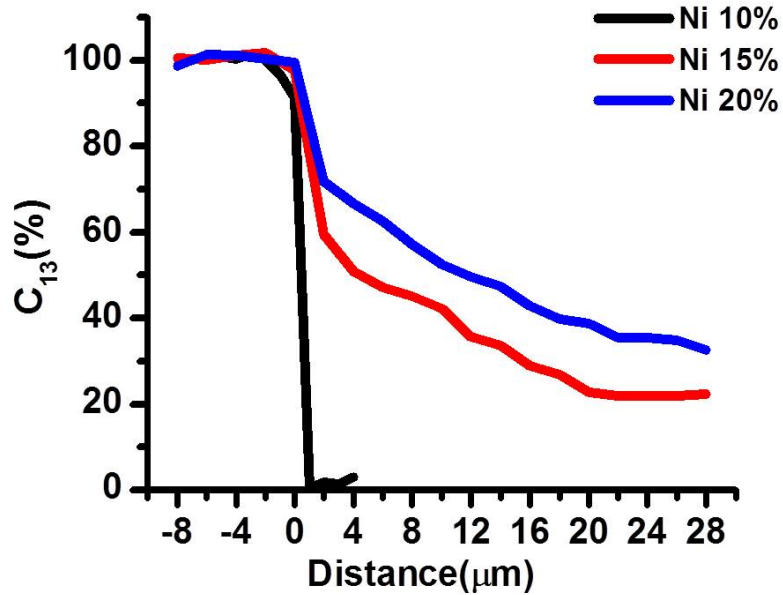


Figure1.27 Calculated ^{13}C content vs distance from center in Figure1.22.

All three isotope-labeled Graphene have pure ^{13}C core, switch point is noted as $0\mu\text{m}$. Among three Ni contents, Graphene grew on 10% Ni content has a very sharp change from pure ^{13}C to pure ^{12}C . A 100% ^{13}C to 100% ^{12}C change was observed, it also has nearly no transition region (might because low resolution of our instrument, as the smallest increment is $1\mu\text{m}$ which is still relative large). But still, this result indicates for Graphene grow on Ni/Cu alloy with 10% Ni, carbon atom added to Graphene growth front mostly came from gas environment.

On the other hand, for Graphene grew on alloy with 15% Ni and 20% Ni, a gentle transition was observed after the initial sharp change. ^{13}C content decrease to 60% after switch for Graphene on 15% Ni alloy, thus we could consider there is 40% carbon on Graphene came from gas environment. For

alloy with 20% Ni, the transition from ^{13}C to ^{12}C is gentler compare to Graphene grew on 15% Ni alloy, and the portion of ^{12}C from gas environment decrease to 25%. After the initial fast change, the transition from ^{13}C to ^{12}C slowed down and reached a plateau. This is because as new ^{12}C dissolved in substrate, the portion of carbon from body participation is a mixture of old ^{13}C and new ^{12}C instead of pure ^{13}C .

These observations confirmed our hypothesis that Graphene grew on Ni/Cu alloy involves both body participation and surface adsorption methods. With an increasing Ni content, more carbon atom connected to Graphene growth front through participating out from alloy substrate. And increase Ni content would also slightly increase growth rate of Graphene on alloy.

1.3.5 Competition between body participation and surface adsorption for graphene growth

Interestingly, for Ni/Cu alloy substrate with 20% Ni, at higher carbon feeding rate, (0.9% methane in Ar) hexagonal concentric pattern can be observed as Figure 1.28. These periodical patterns happened to match the in chamber pressure change (85-115 Torr) came from mechanically valve adjusting. Thereby we were able to see this competition between Graphene grew through body participation and surface adsorption. With the change of in chamber pressure, methane partial pressure ranged from 0.71Torr to 0.96Torr, while carbon concentration in alloy substrate remains the same. Thus, by increasing in chamber pressure from 85Torr to 115Torr, more carbon was connected to Graphene growth front through surface adsorption method.⁴⁰

This result again confirmed that at 1050C, ~100Torr, Ni and Cu both contribute to the formation of Graphene on Ni/Cu alloy, but there is a competition between these two methods based on in chamber pressure (differences between carbon concentration in substrate and in chamber environment).



Figure 1.28. (a) Optical image of large single crystal flake.

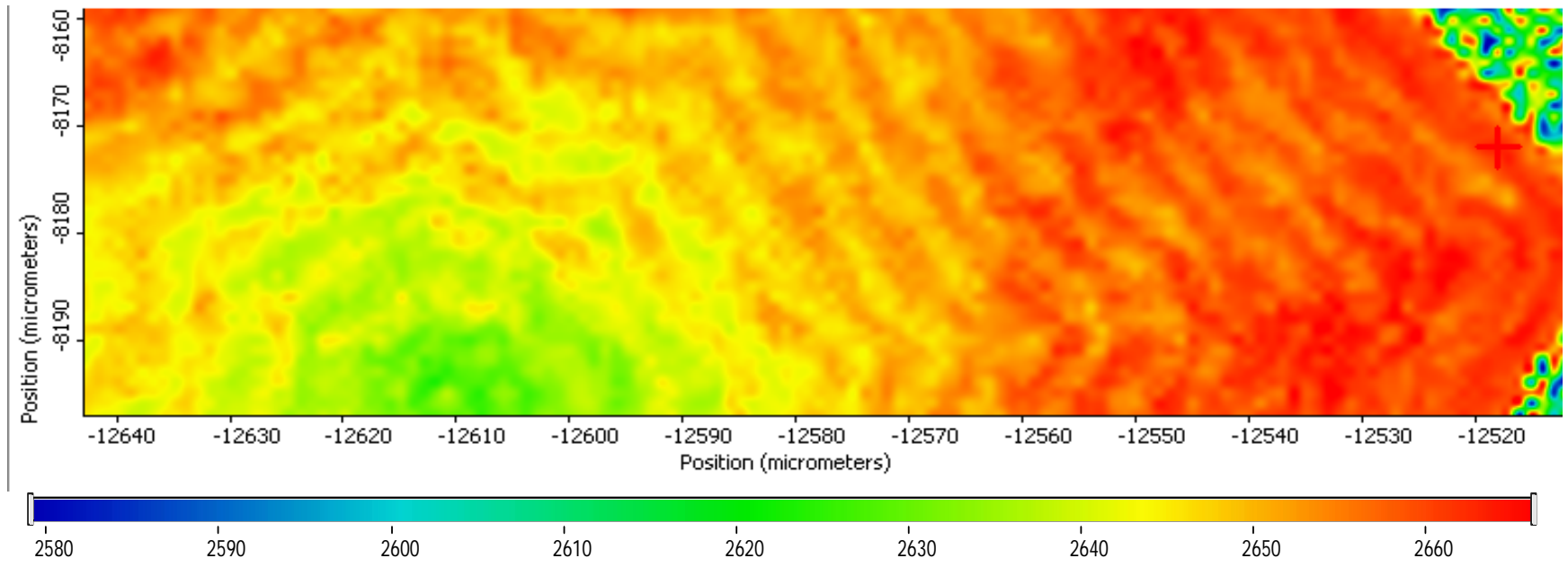


Figure1.28 Optical image of large single crystal flake and (b) Raman mapping (competition between body participation and surface adsorption).

1.4 Conclusion

We successfully obtained isotope labeled Graphene on Ni/Cu alloy with three different Ni contents. No Graphene was obtained on pure Cu substrate under same growth condition, large single crystal Graphene (400 μm) with perfect hexagonal shape can be obtained within 30mins.

Growth condition is designed to obtain single crystal Graphene flakes of 100 μm - 150 μm . Nucleation density and growth rate (flake size) are also studied for three substrates. Our results consist with Dr Xie's report that increase Ni content would dramatically decrease Graphene nucleation density on Ni/Cu alloy substrate. Though due to the local feeding method they used, nucleation density from their report is much lower than our result.

Among three substrates, Graphene grew on 10% Ni are much smaller than the others. With the help of isotope labeling, we could further studied growth mechanism of Graphene grew on Ni/Cu alloy substrate. One isotope methane switch was utilized to trace carbon migration during Graphene growth. The nucleuses were composed by pure ^{13}C about 50 μm large. Feeding carbon was then quickly switched to ^{12}C .

For Graphene grew on substrate with 10% Ni, the transition from ^{13}C to ^{12}C is very sharp indicating Graphene grew on this substrate mainly through surface adsorption method which is Graphene is mainly composed by environment carbon in the chamber. For Graphene grew on substrate with 15% and 20% Ni, the transition from ^{13}C to ^{12}C is much gentler than that on 10% Ni. As more Ni in substrate, carbon solubility increased and carbon dissolved in alloy has a higher

concentration that is able to support growth of Graphene. With an increasing Ni content to 20%, more carbon came from participation of alloy substrate. Thus, we confirmed that Graphene grew on Ni/Cu alloy is a combination of surface adsorption (Cu) and body participation (Ni) behavior.

With more carefully study on Graphene grew on Ni/Cu alloy (20% Ni), we observed the competition of Graphene grew through surface adsorption and body participation. As the in chamber pressure periodically changed between 85 Torr and 115 Torr, Graphene grew on 20% Ni alloy substrate have had a concentric pattern corresponding to Graphene growth competition between surface adsorption and body participation. As the in chamber pressure changed within 85 Torr to 115 Torr, carbon partial pressure inside chamber ranged from 0.71Torr to 0.96Torr, while carbon concentration in alloy substrate maintained same (retard from environmental change). At low carbon partial pressure, less carbon from environment connected to Graphene growth front, results in a low ^{12}C region. With carbon partial pressure increasing to 0.83 Torr, more carbon from environment connected to Graphene growth front leads to an increase of ^{12}C content.

In particular, carbon migration plays an important role in Graphene growth, our study implied that it can be controlled to some extent by changing the alloying ratio of Cu to Ni together with carbon source concentration. Our studies will provide a guide for improving Graphene synthesis and fast fabricating large single crystal Graphene films with high quality.

2 GRAPHENE AS DIFFUSION BARRIER FOR THERMOELECTRIC DEVICE

2.1 Introduction

2.1.1 *Thermoelectric materials*

Thermoelectric (TE) effects have long been known since the Seebeck effect and the Peltier effect were discovered in 1800s. The Seebeck effect describes the phenomenon that a voltage is generated in a conductor or semiconductor subjected to a temperature difference. Equilibrium is reached between the chemical potential for diffusion and the electrostatic repulsion due to the build-up of charge. In n-type thermoelectric materials, charge carriers are electrons. More electrons diffuse from cold surface to hot surface due to the temperature gradient and generated an electrostatic potential, similar for hole carriers for p-type thermoelectric materials shown Figure 2.1.^{38, 41}

This effect is the basis of thermocouples and can be applied to thermal to electrical energy conversion. The inverse process, in which an electrical current creates cooling or heat pumping at the junction between two dissimilar materials, is known as Peltier effect. Starting in late 20th century, interest in thermoelectric materials was renewed because of increased global energy demand and global warming caused by excessive CO₂ emissions.⁴²

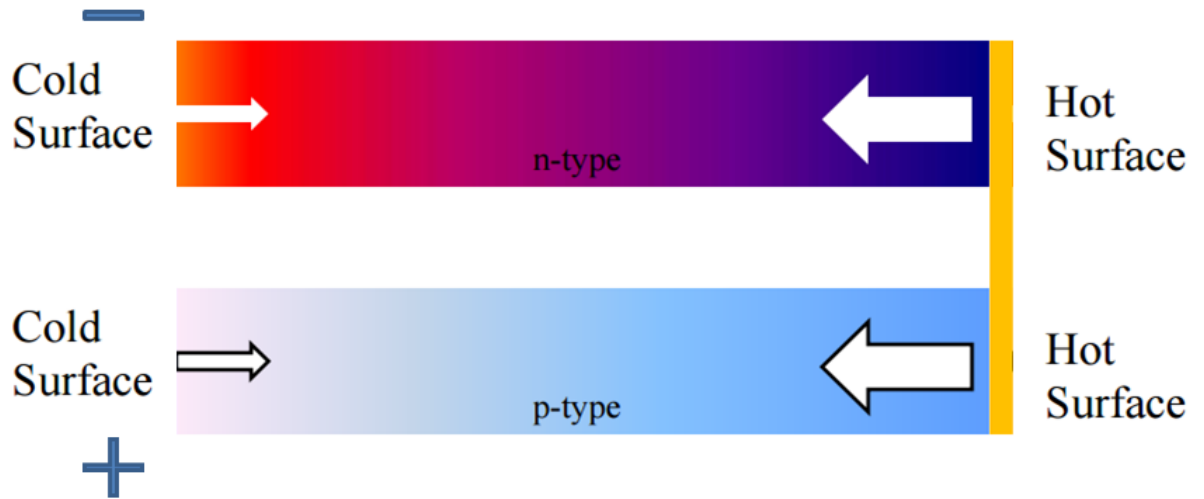


Figure 2.1 Scheme of thermoelectric device working principal

The maximum efficiency of a thermoelectric device for both thermoelectric power generation and cooling is determined by the dimensionless figure-of-merit, zT ,

$$ZT = \frac{S^2 \sigma}{\kappa} T$$

where S is the Seebeck coefficient (a measure of a material's ability to generate a voltage for a given change in temperature), σ is the electrical conductivity, σS^2 is the power factor, and $\kappa = \kappa_p + \kappa_e$ is the thermal conductivity which is composed of lattice (phononic) thermal conductivity κ_p and electronic thermal conductivity κ_e . T is the average temperature between source and sink.

Thermoelectric materials have been developed for decades; it is the major electricity supply for satellites deep into the space. Recently, more and more thermoelectric materials have been used in automotives and electricity generator

planets to collect and convert waste heat to electricity.⁴³ But there is still big challenge for thermoelectric materials being widely accepted due to its poor reliability of metalized contact layer which could easily diffuse into the semiconductor material and form compounds.⁴⁴

Lead telluride (PbTe Figure 2.2) is one of the earliest thermoelectric materials used in the world. The “world’s first atomic battery” was presented in the oval office of the White House in middle 20th century. This radioisotope thermoelectric generator (RTG) contained simple alloys of PbTe for both the n- and p-type elements. And NASA used this design for its first RTG powered spacecraft, the Transit 4A, and modified designs and materials based on PbTe in the Apollo missions and the 1975 launch of the Viking 2 mission to Mars. Research on PbTe fades out in laboratories because at that time the calculated theoretical zT limitation was only about 1.4 for pure n-type PbTe (even lower for p-type PbTe) which is too low to be used in real world applications. But recently, new methods as doping PbTe with other element such as Titanium, Iodine could improve the merit zT to 2.0 and a power conversion efficiency of higher than 10% can be achieved.⁴⁵

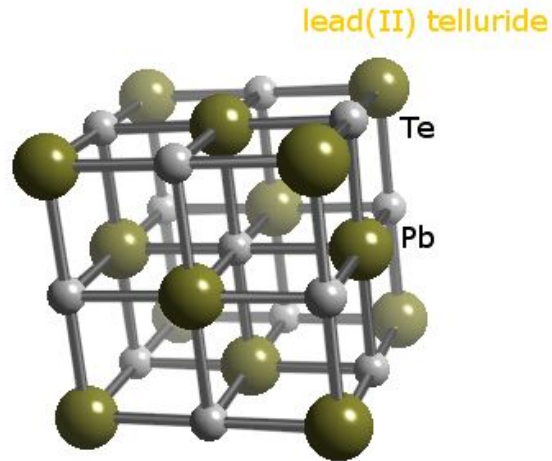


Figure 2.2 Structure of PbTe crystal.

Though merit zT is an important parameter for thermoelectric material, a TE device with high efficiency of energy conversion relies on not only a high figure of merit (zT) of TE materials but also good contacts between TE materials and electrodes. For a good contact, the following conditions must be met: (a) the joints should block the diffusion of the elements which may degrade the properties of TE elements in electrodes into TE materials, (b) the joints should be metallurgically bonded and mechanically stable will not cause any cracks or other defects, and (c) the electrical and thermal contact resistances of the joints are required to be low.⁴⁶

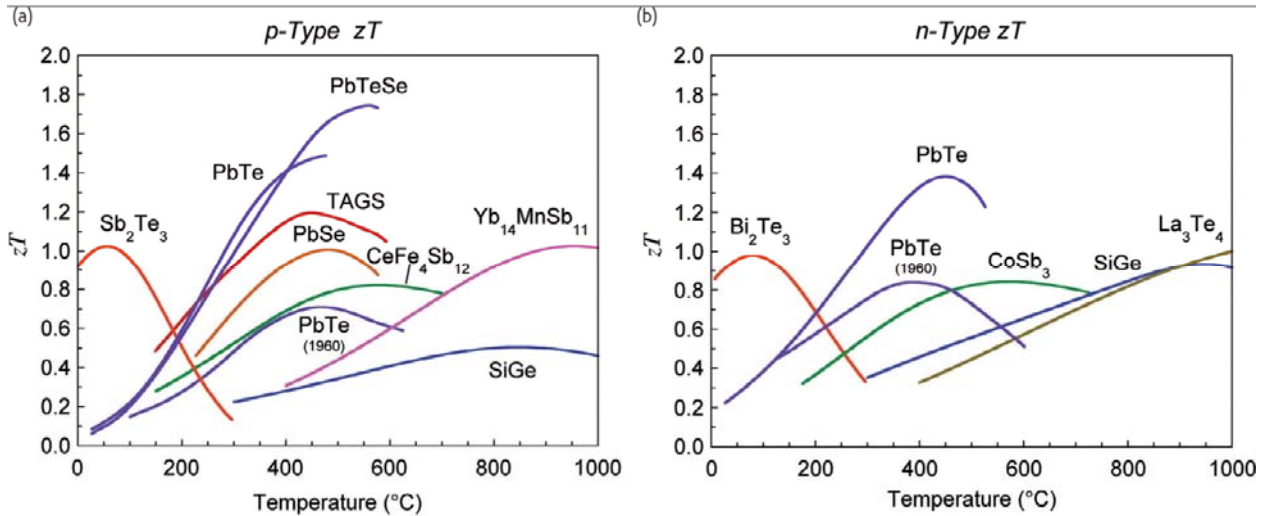


Figure 2.3 Merit zT for different TE materials

2.1.2 Diffusion in thermoelectric device

Preventing diffusion between semiconductor and metallic solder or buffer layer has always been a problem in semiconductor industry. The problem becomes even more severe for high temperature operated thermoelectric materials as increased degradation rate due to fast metal diffusion at high temperature. Metal solder is usually used to combine the heat pool (usually copper) and the thermoelectric device, it should form good contact with both sides and have both high electrical and thermal conductivity. Copper and many other metals are very poisonous to thermoelectric device, it will dramatically reduce the power efficiency of the thermoelectric device by destroy lattice structure (phonon vibration requires a perfect crystal structure) in the semiconductor material at high temperature. And copper also has an extremely fast diffusion rate. Thus the solder should be able to protect thermoelectric device from copper. Research on different diffusion barrier has been reported

such as Ni, Fe layers. Metal barriers normally requires a certain thickness (ie. 400 μ m for Fe).⁴⁷

2.1.3 Impermeability of Graphene

The impermeability of Graphene has gained tremendous interests in different fields from protection coating to diffusion barrier.^{48,49} Although it is only one atom thick, Graphene's π - π electron orbital forms a dense, delocalized electron cloud which blocks the gap within its aromatic rings (Figure 2.3).⁵⁰ The π - π electron orbital creates a repelling field, which does not allow even the smallest molecules, such as hydrogen and helium, to pass through even when an about 1–5 atm pressure difference is imposed across its atomic thickness at room temperature. The ability to withstand such pressure differences (6 atm) in graphene is a result of its high strength (breaking strength = 42 N/m) and Young's modulus (1 TPa), which retains the structural integrity of Graphene. While the theoretical studies have shown that there is no gap in electron-density around the aromatic rings to allow molecules to pass, it can be seen the geometric gap calculated from van der Waals (vdw) radius of carbon will be smaller than the size of He (Figure 2.3). The C–C bond length of 0.142 nm in graphene implies that considering the nuclei alone, the pore size would be 0.246 nm.⁵⁰ Now if we add the vdw radius of carbon of 0.11 nm, this geometric pore size would decrease to 0.064 nm. This geometric gap is smaller than the vdw diameter of small molecules like helium and hydrogen: 0.28 nm and 0.314 nm (bond-length (0.074 nm) + 2r (0.12 nm)), respectively. All these properties together with high conductivity make Graphene a perfect diffusion barrier for electronic devices. Hong et al utilized Graphene as

barrier to prevent Cu diffuse into Si, SLG and MLG Graphene could block Cu up to 700 and 900 °C, respectively. Kim et al also reported Graphene as a diffusion barrier in Al/Si are stable upon annealing up to 700 °C.

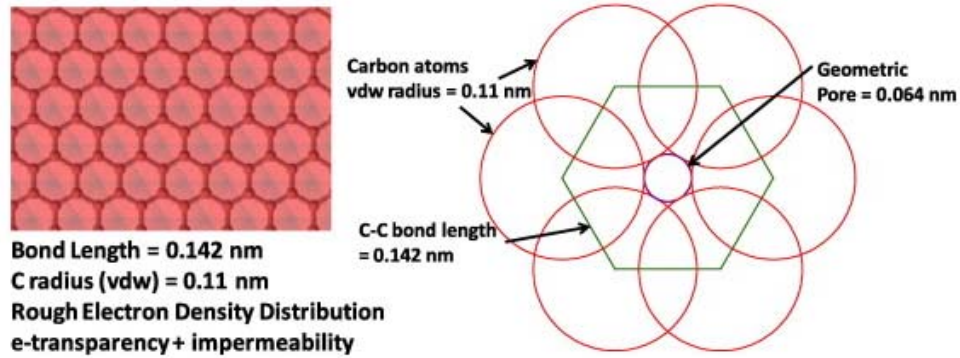


Figure 2.4 Graphene lattice structure and geometric pore.⁵⁰

Study on using transferred Graphene as a diffusion barrier showed good performance in preventing interdiffusion of semiconductor materials and metal. But not much effort addressed on preventing interdiffusion between metal and thermoelectric materials with Graphene. Moreover, Graphene has a high in plane thermal conductivity about $10^3 \text{ Wm}^{-1}\text{K}^{-1}$ while out of plane thermal conductivity is only $2 \text{ Wm}^{-1}\text{K}^{-1}$ at 500C, this low out of plane thermal conductivity would create a sharp temperature gradient between solder and PbTe device which is preferred for higher power conversion efficiency.⁵¹

Current study using Graphene as a diffusion barrier has mainly conducted on polycrystalline Graphene grown on Cu. Polycrystalline Graphene has a problem as too many grains. Those grain boundaries are weak points for both chemical attack and diffusion. Grain boundaries usually are more reactive and due to the

lattice mismatch, missing carbon atoms would leave vacuum as diffusion path way, thus large single crystal Graphene is preferred for applications like diffusion barrier.

2.2 Methods

2.2.1 *Diffusion of Ni/G/Cu and Ni/Cu test*

Single layer Graphene was grown on 25 μ m Cu foil (Alfa 99.5%) at 1050C under atmosphere pressure. The Cu foil was ultrasonic cleaned with DI water, IPA and Acetone in sequence for 3mins each. Cu substrate is placed in a 2in quartz chamber and ramp to 900C at 15C/min, then ramp to 1050C at 10C/min. A mixed gas flow of 200sccm Ar and 20sccm H₂ is used as protective and reduction environment. The substrate will be annealed at 1050C for 10mins, followed by 30mins 30sccm H₂ and 300sccm CH₄ (500ppm in Argon) for Graphene growing. After growing, sample was push out from hot chamber and cool down.

Graphene grew on Cu foil is examed by Raman Microscope and SEM to confirm a continuous single layer Graphene is obtained on Cu foil.

To electroplate thin Ni layer on Cu foil, Graphene covered Cu foil was placed in nickel sulfamate solution (Technic inc.) and electroplating at current 5A/ft² for 3mins, formed Ni/G/Cu sandwich structure. Ni was also electroplated on pure 25 μ m Cu foil using the same procedure. Then anneal both samples at 500C for 30mins, 120mins and 240mins in 150sccm Ar and 15sccm H₂ at atmosphere pressure. The cross section was monitored using EDAX element content analysis to study diffusion between Ni and Cu.

2.2.2 *Ni/PbTe and Ni/G/PbTe Devices*

The n-type PbTe wafer was obtained from Micropower Group and cut into 2 pieces, single layer Graphene was transferred on half wafer using PMMA as a support. Spin coat 3 wt% PMMA on Graphene on Cu foil and anneal at 80C for 5 mins to dry off the PMMA and use ozone etching Graphene on the back side to expose Cu foil. Place PMMA coated Graphene/Cu foil in 10wt% $(\text{NH}_4)_2\text{S}_2\text{O}_8$ to etch Cu without introducing any metal ions. Cu foil could float at surface of etchant due to hydrophobic PMMA film. After etching all Cu foil, carefully transfer PMMA coated Graphene on top of PbTe half wafer and dry overnight. PMMA film can then be removed by rinse in acetone.

Both half wafers were electroplated in nickel sulfurnate solution (Technic inc) at $5\text{A}/\text{ft}^2$ for 3mins. Followed annealing at 500C under 200sccm Ar and 20sccm H_2 for 12hrs, and cut by a diamond thaw to exam cross section element content with EDAX. Efficiency test was conducted by Micropower Group for both devices with/out Graphene.

2.2.3 *InTe/PbTe and InTe/mG/PbTe Devices*

n-type PbTe wafer was obtained from Micropower Group and cut into 2 pieces. Large single layer Graphene was utilized as previous described. A single layer PMMA method was used to transfer 4 layers Graphene on PbTe half wafer. In a typical practice, spin coat 3 wt% PMMA on Graphene on Cu foil and anneal at 80C for 5 mins and use plasma ozone etches Graphene on the back side. Place the PMMA coated Graphene/Cu foil in 10wt% $(\text{NH}_4)_2\text{S}_2\text{O}_8$ to etch Cu without introducing any metal ions. After etching all Cu foil, carefully transfer

PMMA coated Graphene on top of another Graphene/Cu foil and dry overnight. Then ozone etching the backside Graphene and repeats until four layers Graphene was attached to PMMA film. PMMA and 4 layers Graphene was then carefully transferred on top and bottom sides, dry overnight. PMMA film can be removed by merge in acetone.

Electroplating about 5 μm InTe layer around the half wafer (Micropower Global, 0.4A for 5min). Half wafers were then cut into 2mm^3 devices by a diamond saw and annealed at 500C under 200sccm Ar and 20sccm H₂ for different times (3, 13, 18, 24 and 36hr). Cross section was polished and examined by EDS and SEM to track Indium diffusion in PbTe wafer and power output efficiency of those wafers with/out Graphene was tested by Micropower Global.

2.2.4 SEM and EDS

Though secondary scattering is the primary scattering for SEM, backscattered electrons could also give out useful information. Compositional contrast is the variation of gray levels in an SEM image corresponds to variation in chemical composition of the sample. An image formed by back scattering electrons presents useful compositional contrast if the sample consists of more than one chemical element. Compositional contrast raised from the capability of backscattered electrons to escape from the specimen depends on the atomic numbers of the element.

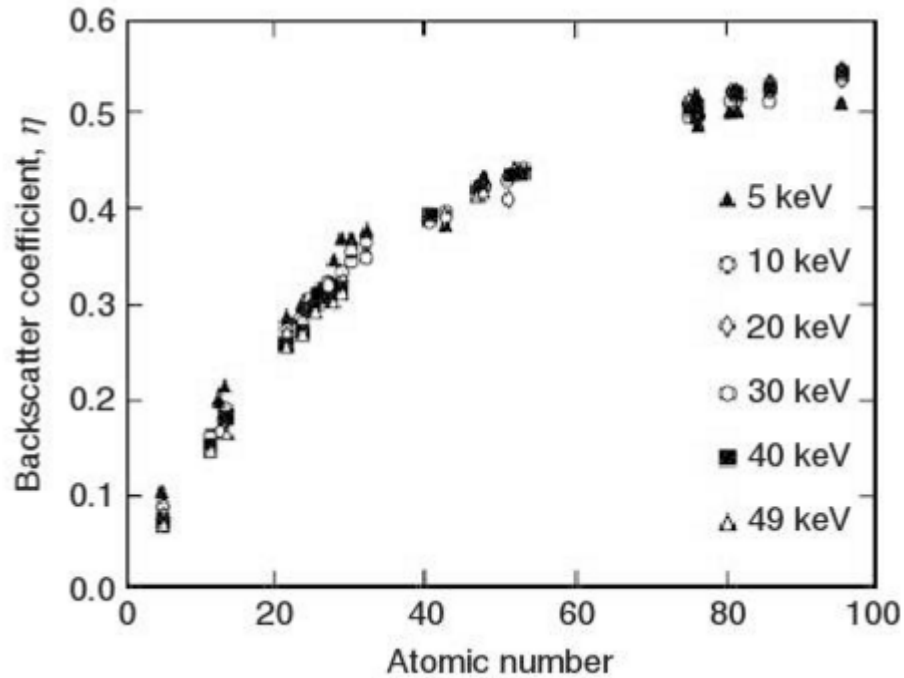


Figure 2.5 Backscatter coefficient as a function of atomic number of specimen atoms.

The back scattering capability of element is characterized by backscatter coefficient η :

$$\eta = \frac{n_{BSE}}{n_i}$$

η is the ratio of the number of backscattering electrons escaping from the sample to the number of the incident electrons. It increases with the atomic numbers as in Figure.2.5. Thus area in a sample composed by chemical elements with higher atomic number will generate more backscattered electrons. Detector will collect the number of backscattered electrons, the difference in number of backscattered electrons will appear in grey scale in the SEM image.

An area with higher atomic number elements will backscatter more electrons and appear brighter in the SEM image under backscattering mode.

Energy dispersive spectroscopy (EDS) and wavelength dispersive spectroscopy are both family members of X-ray fluorescence spectrometry. X-ray fluorescence spectrometry analyzes the chemical elements of samples by detecting the characteristic X-ray emitted from the samples after radiation by high energy primary X-rays. The emitted characteristic X-Ray can be analyzed by either energy (EDS) or wavelength (WDS).

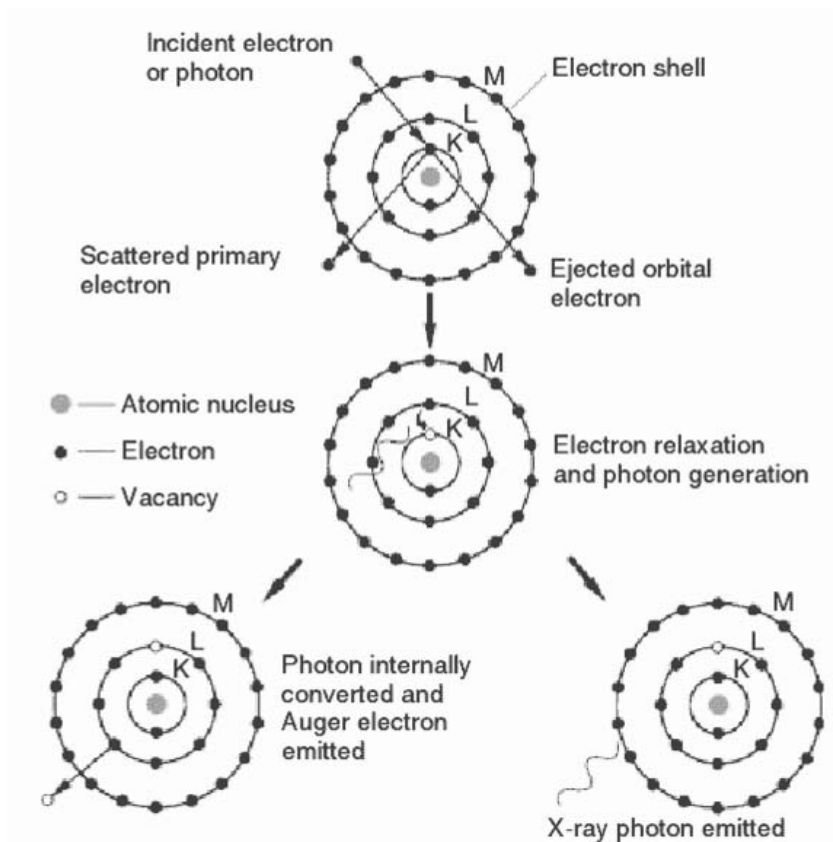


Figure 2.6 Excitation of a characteristic X-ray a auger electron or photon by a high energy electron or photon.

EDS became a commercial product in the early 1970s and rapidly overtook WDS. It is structurally simpler and relatively faster compare to WDS system. EDS

detector collects the signals of characteristic X-rays energies from a whole range of elements in a sample at the same time. The resolution of energy dispersion is about 150-200 eV, not as good as the corresponding resolution of WDS, the lightest element that can be detected by EDS is O (Z=8) compare to C (Z=6) for WDS.

The energy dispersive spectrum is presented as the relative intensity of characteristic X-ray lines across the X-ray energy range. A spectrum in a range from 0.1 (100eV) to about 10-20 keV can resolve both heavy and light elements as both M or L lines of heavy elements and K lines of light elements can be detected in this range. As indicated in Figure 2.7

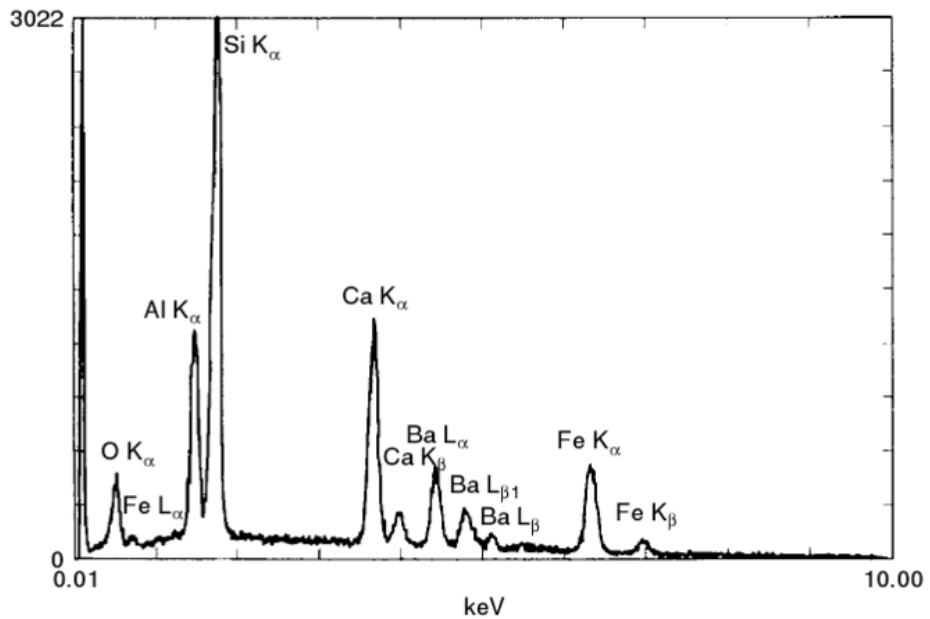


Figure 2.7 EDS spectrum of glass with Si, O, Ca, Al, Fe and Ba.

2.3 Results and Discussion

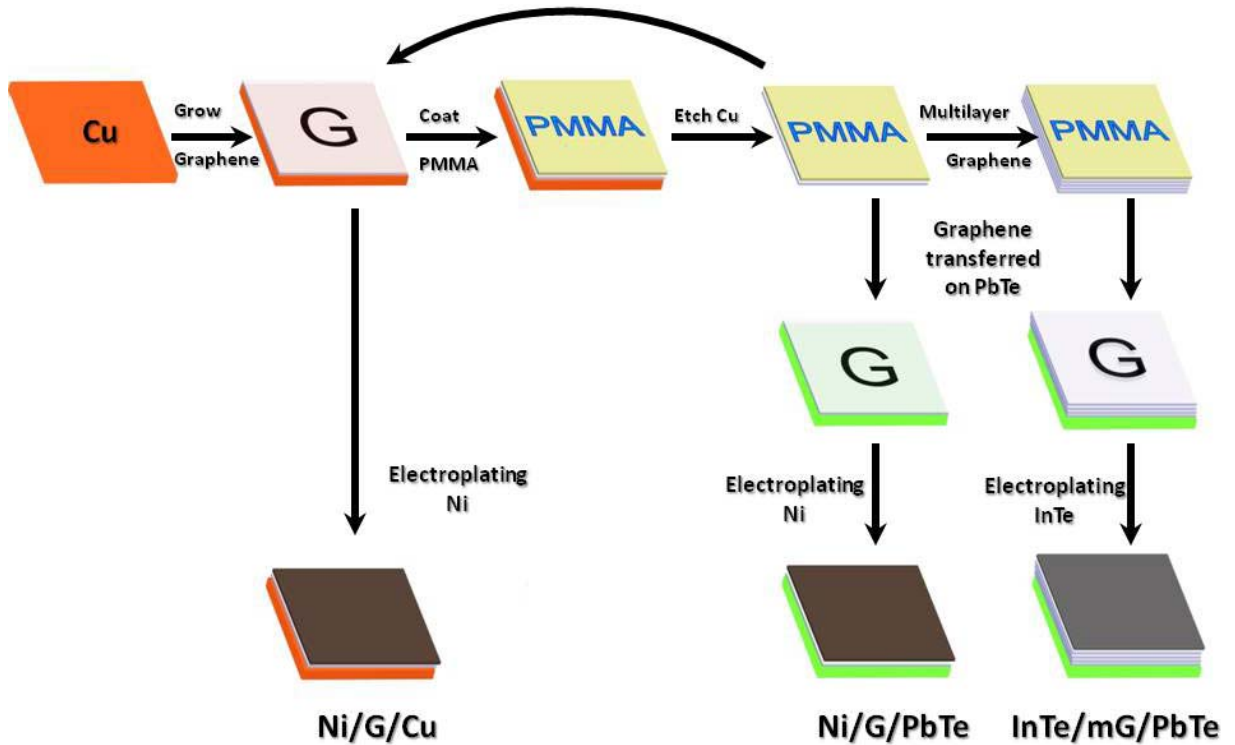
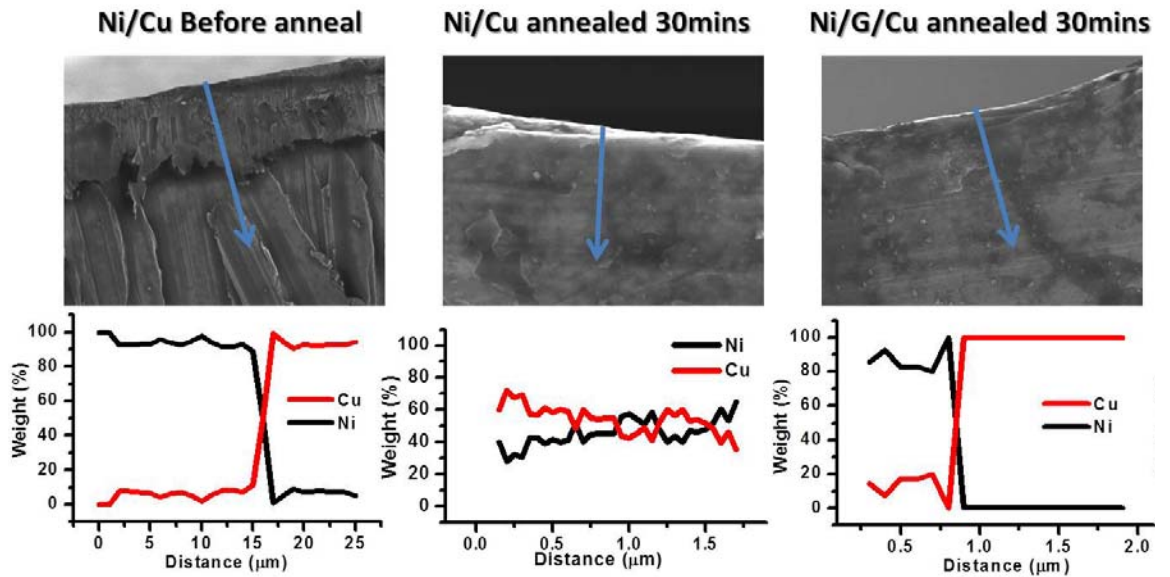


Figure 2.8 Schematic of devices manufacture.

A scheme of devices fabricated and tested is illustrated in Figure 2.8. Single layer was obtained from Cu foil substrate through a CVD method. Thin Ni metal layer was directly deposited on Graphene covered copper foil for diffusion test. Ni/G/PbTe device was obtained by transfer a single layer graphene with PMMA supportive film and electroplated thin Ni layer. Single PMMA layer transfer method was used to fabricate thermoelectric device with multi layer graphene barrier. Multi-layer graphene coated PbTe device was then electroplated with thin InTe layer as solder.

2.3.1 Diffusion test of Ni/G/Cu and Ni /Cu

SEM and EDAX data for diffusion test of Ni/G/Cu and Ni /Cu are shown in Figure 2.9, as made sample had a sharp boundary between Ni and Cu. After annealing at 500C for 30 mins, sample without Graphene became an alloy of Ni and Cu, while sample has a Graphene barrier maintained the sharp boundary (Figure 2.9).



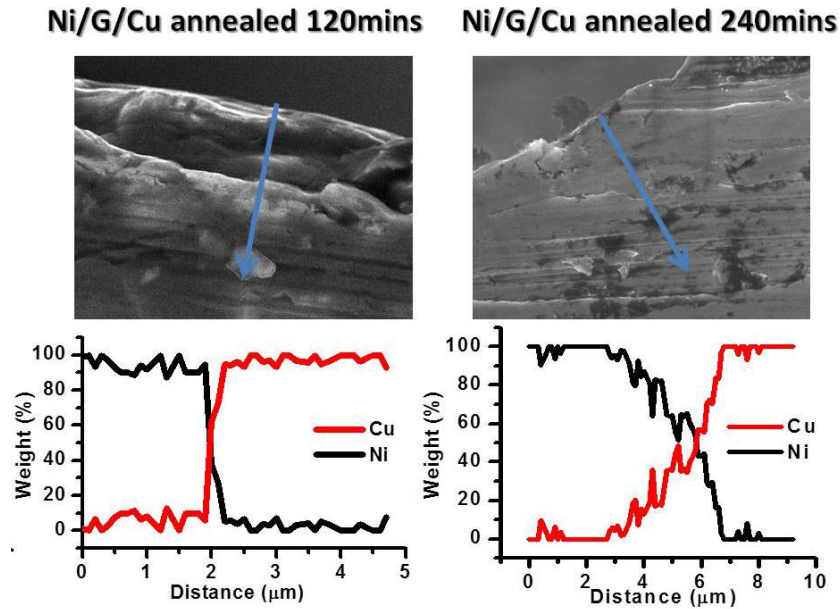


Figure 2.9 Ni/Cu before and after annealing for 30mins, Ni/G/Cu after annealing for 30mins, 120mins and 240mins

When increase annealing time to 120mins (Figure 2.9), the Ni and Cu component fluctuated but sharp boundary between of Ni and Cu remained. EDAX for Ni/G/Cu annealed for 240mins (Figure 2.9) showed even more atoms diffused through the Graphene barrier. A recently report from Yang Chai's group showed that a single layer Graphene would not be a perfect barrier since Cu atom would pass an 8 atom vacancy defect on Graphene. Single layer Graphene showed excellent diffusion barrier performance though it fade out at high temperature after long time operation, but still, the result predicted a possible method to effectively block metal atom diffusion while maintaining good conductivity.

2.3.2 Diffusion and efficiency test for Ni/G/PbTe and Ni/PbTe

EDAX result for transferred single layer Graphene on PbTe device is shown in Figure 2.10, Ni diffused into PbTe after annealing at 500C for 12hrs for both Ni/PbTe and Ni/G/PbTe devices, but single layer Graphene barrier has slowed down the Ni diffusion rate significantly, lead to a less than 10wt% of Ni in the PbTe compare to device without Graphene has about 40wt% Ni diffused into PbTe. This result is not as good as that for Ni/Cu metal structure which is not surprising, since the single layer Graphene barrier was transferred onto the wafer which could cause fracture and introduce more defects.

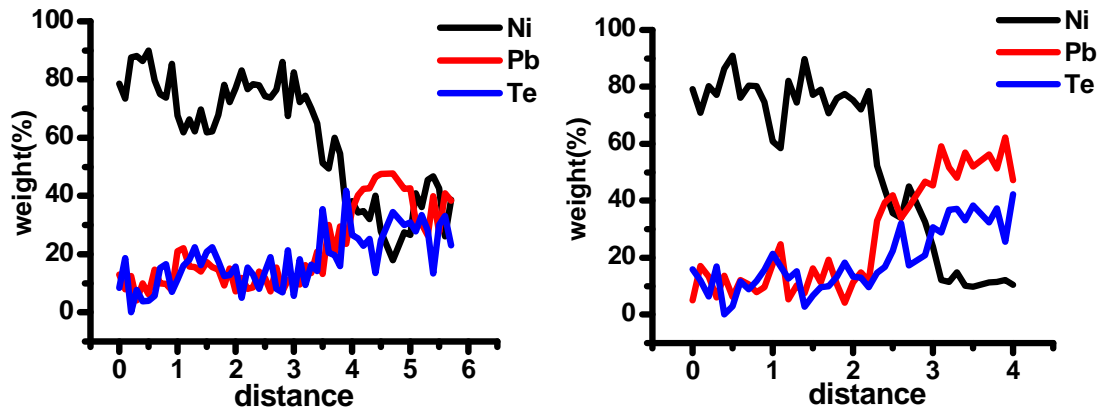


Figure 2.10 EDAX of Ni/PbTe and Ni/G/PbTe after annealing at 500C for 12hrs.

The efficiency test data was plotted in Figure 2.11, during the first cycle, Ni/G/PbTe device and Ni/PbTe device showed identical power output, as both devices are made from the same piece of PbTe wafer. Start with second cycle, device without Graphene barrier shows a decrease of power output at high temperature range (>320C), this decrease became more severe in the 4th cycle, a

large power output difference could be observed between device with Graphene and without Graphene (marked with black cycle in Figure 2.11). These preliminary results confirmed Graphene could be a good diffusion barrier material for high temperature thermoelectric devices.

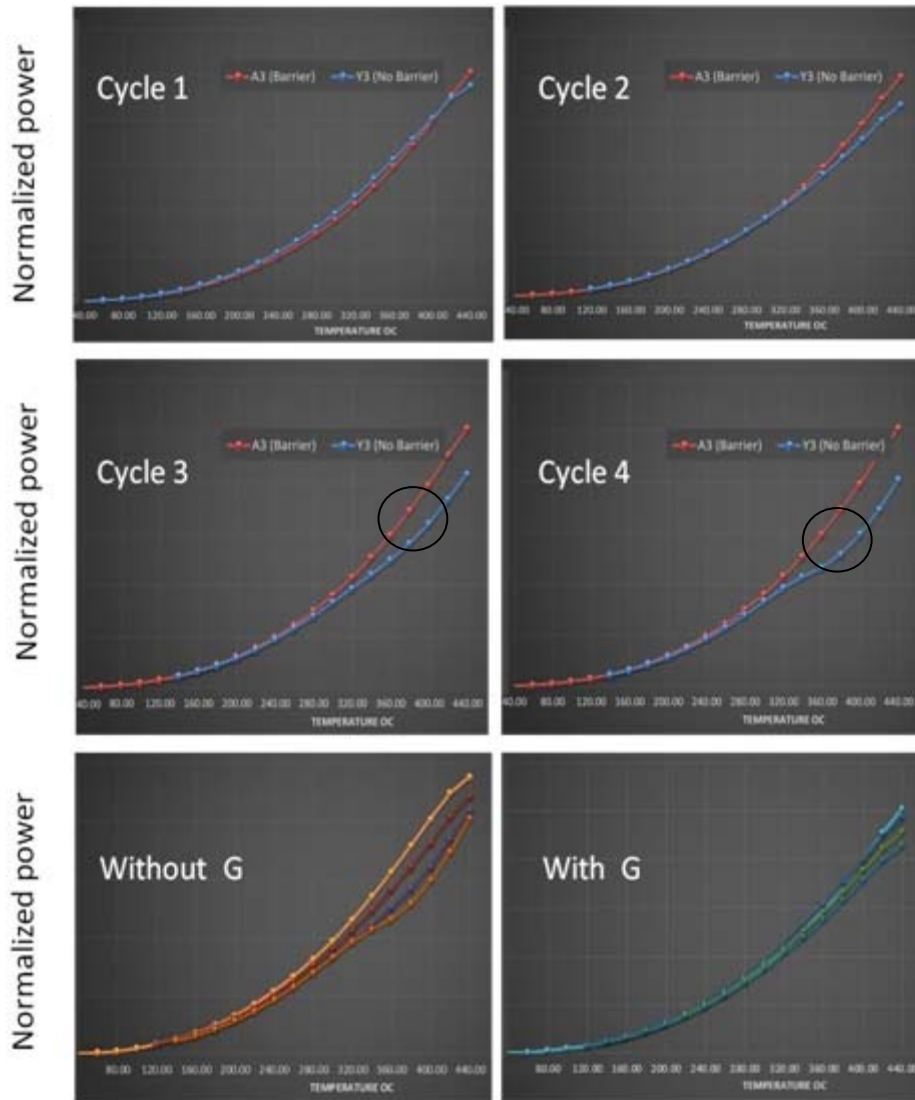


Figure 2.11 Top, Normalized output power efficiency of Ni/G/PbTe (red) and Ni/PbTe (blue), the black cycles are fading out of device without Graphene

at high temperature; bottom, normalized efficiency of first 4 cycles for Ni/G/PbTe (left) and Ni/ PbTe (right).

2.3.3 Diffusion test for InTe/mG/PbTe and InTe/PbTe

Multilayer graphene is used as barrier layer to enhance the block performance of graphene barrier, Ni is a metal with very high inner residue stress, Ni layer deposit on multilayer graphene peels off easily, makes it an ineffective solder with multilayer graphene.

To meet more practical requirements in the industry, we used In as solder instead of Ni to test the performance of transferred multilayer polycrystalline Graphene diffusion barrier. In has been used as a buffer layer for many electro solder and it could form uniform solder layer on multilayer graphene through electroplating method, but In has an extremely high diffusion rate in PbTe. Single layer Graphene grown on Cu was transferred to PbTe wafer on both sides for 4 times to enhance the barrier performance. InTe was then electroplated on top of the wafer.

EDAX mapping for InTe/mG/PbTe before anneal is shown in Figure 2.12, upper left is the backscattered SEM image. Due to the atomic number (Z) differences between Lead and Indium, we can see a dark region of InTe (In, atomic number 49) and the bright region for PbTe (Pb, atomic number 82). As expected, a clear boundary between InTe and PbTe domains is observed. The slightly brighter blue color for Te is because the percentage of Te in InTe (~53%) is higher than that in PbTe (~46%).

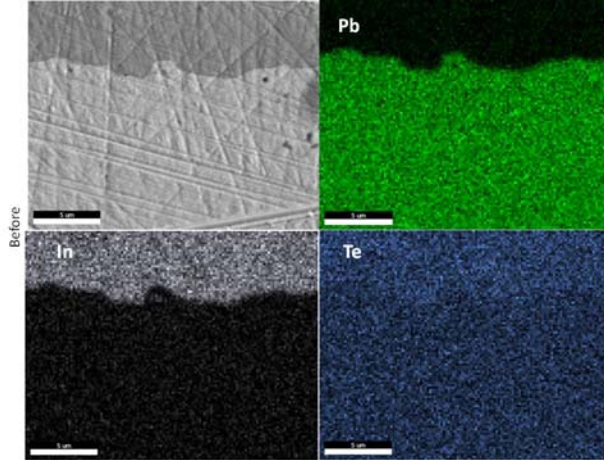


Figure 2.12 EDAX image of device before anneal (Red, lead; Silver, Indium; Green, Tellurium).

Line EDAX results for InTe/PbTe and InTe/mG/PbTe device after anneal at 500C for 3hr is shown in Figure 2.13. Indium and Lead had diffused into each other for sample without Graphene barrier while less than 10wt% of In was observed in PbTe and about 10% Pb was observed in InTe for device with four layers Graphene barrier after annealing at 500C for 3hr.

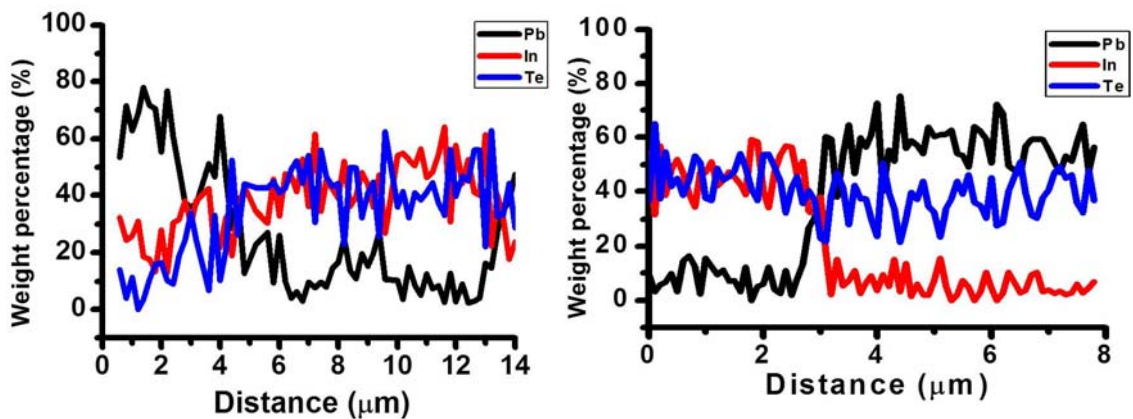


Figure 2.13 Line EDS for InTe/PbTe (left) and InTe/mG/PbTe (right) after annealing at 500C for 3hr.

EDAX mapping data for devices annealed at 500C for 3hrs, 8hrs, 13hrs, 15hrs, 24hrs and 36 hrs are shown in Figure 2.14-19, for chips with 4 layers Graphene as barrier they each has a clear boundary between Indium and Lead. But with increasing anneal time (at 36hr) some Indium component diffused into PbTe, same for Pb diffused into InTe. This may due to defects on Graphene layers formed by Cu etchant. For chips without Graphene, InPb compound was observed (region lack of Te) as increase annealing time to 36hrs, since Indium and Lead diffused into each other and formed the compound. The separating of Te/Pb signal and spreading of In signal gave us a hint on how the InTe/PbTe diffused into each other for device without Graphene and transmitted into InPb or InTe compounds from its PbTe structure. Moreover, 3 out of 4 chips without Graphene cracked after annealing at 500C for 36hrs.

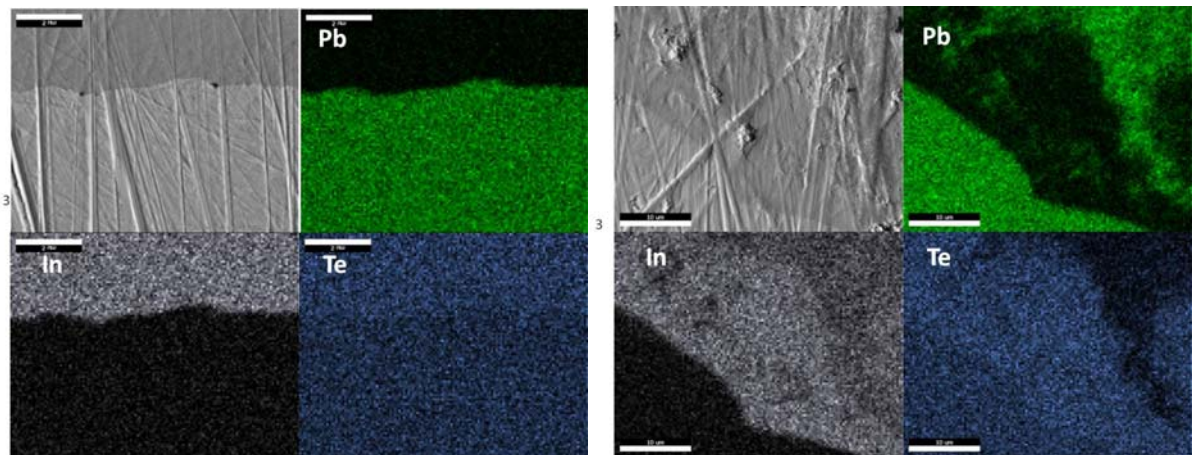


Figure 2.14 Device with (left, scale bar 10 μm) and without (right, scale bar 10 μm) Graphene barrier after annealing at 500C for 3hrs (Green, lead; Silver, Indium; Blue, Tellurium), Te in the circle was replaced by Pb.

After annealing at 500C for 3hrs, InTe/PbTe maintained sharp boundary of Indium and Lead, even the little higher Te content (slighter bright blue) still can be seen for device with Graphene barrier. Very little inter-diffusion could be observed for device with Graphene barrier. On the contrary, Lead was detected in the InTe region as circled, trying to replace Te in InTe, formed InPb compound, and a blur boundary of Pb and Te can be seen.

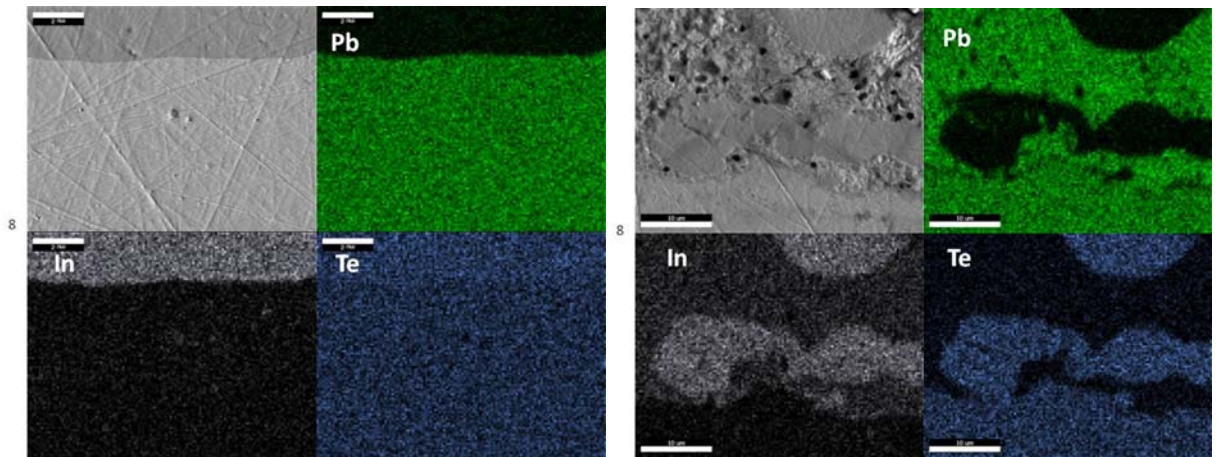


Figure 2.15 Device with (left, scale bar 5 μm) and without (right, scale bar 10 μm)

Graphene barrier after annealing at 500C for 8hrs (Green, lead; Silver, Indium; Blue, Tellurium).

After annealing at 500C for 8 hrs, not much difference can be observed for device with Graphene barrier. Sharp boundary still remains and homogenous Te distribution is maintained with slightly higher Te content in InTe layer as before anneal. Several Indium spots were observed also, as tiny Indium diffused into the PbTe region. While for device without Graphene barrier, Lead replaced Te in InTe formed large size InPb compound.

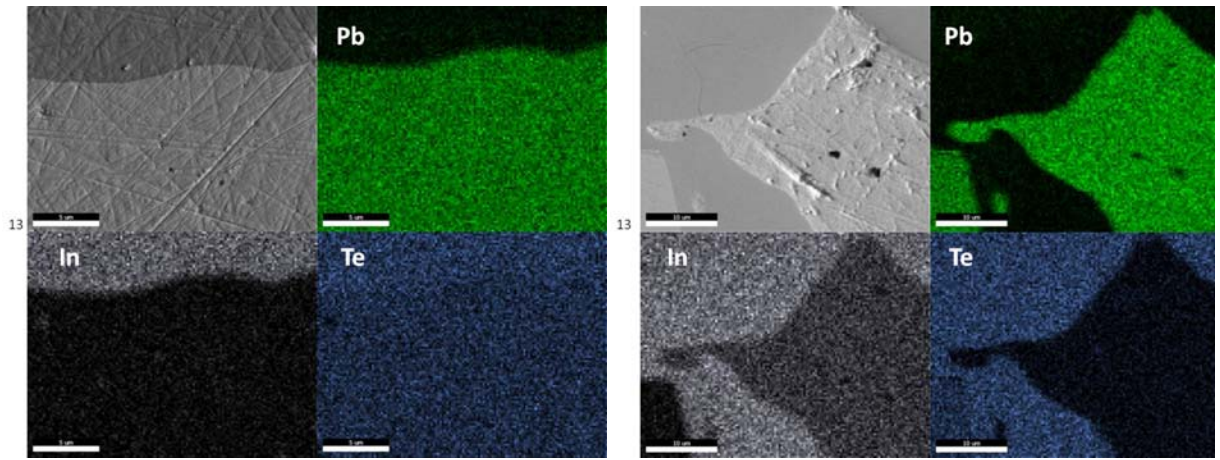


Figure 2.16 Device with (left, scale bar 5 μm) and without (right, scale bar 10 μm) Graphene barrier after annealing at 500C for 13hrs (Green, lead; Silver, Indium; Blue, Tellurium).

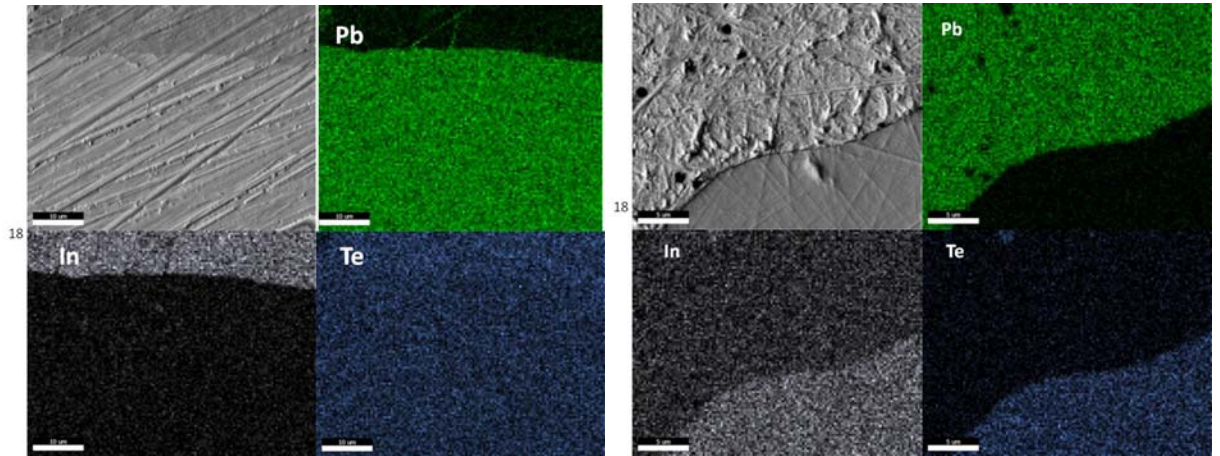


Figure 2.17 Device with (left, scale bar 5 μm) and without (right, scale bar 5 μm) Graphene barrier after annealing at 500C for 18hrs (Green, lead; Silver, Indium; Blue, Tellurium) .

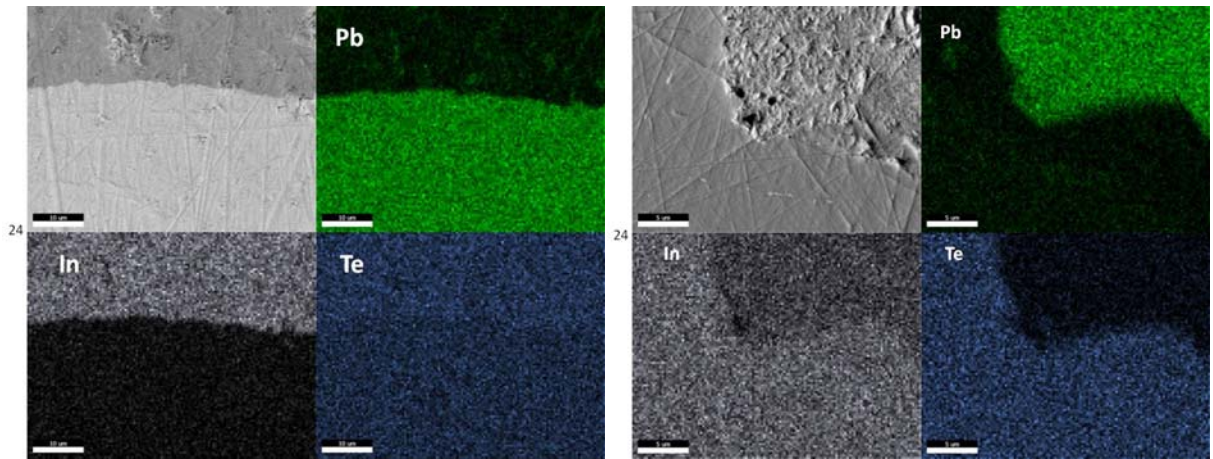


Figure 2.18 Device with (left, scale bar 10 μm) and without (right, scale bar 5 μm) Graphene barrier after annealing at 500C for 24hrs (Green, lead; Silver, Indium; Blue, Tellurium).

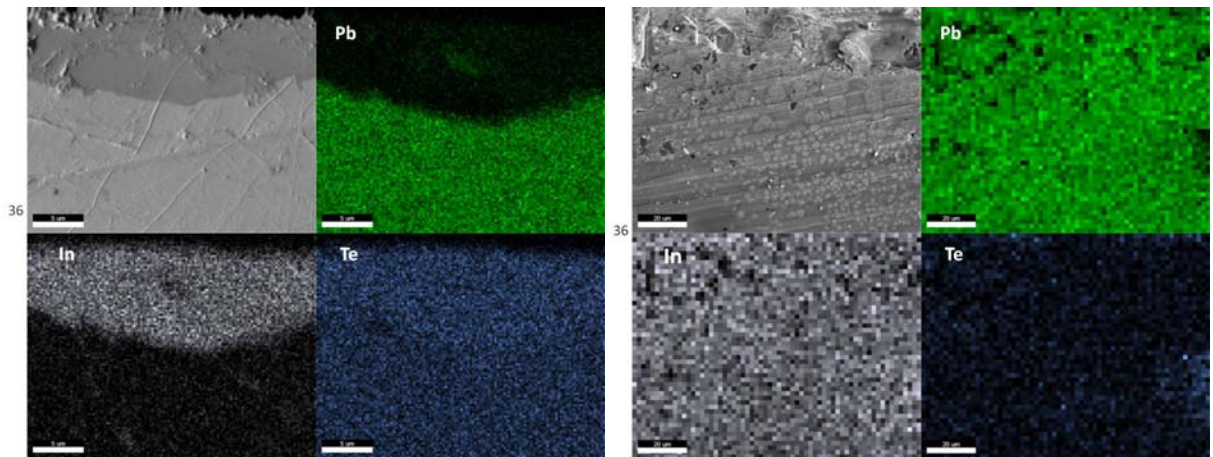


Figure 2.19 Device with (left, scale bar 5 μm) and without (right, scale bar 20 μm) Graphene barrier after annealing at 500C for 36hrs (Green, lead; Silver, Indium; Blue, Tellurium), nearly no Te was detected in a large portion of area for device without Graphene.

Increasing anneal time to 36hrs (Figure 2.19), EDS image for device with multilayer graphene has a blurred boundary between In and Pb, as the inter

diffusion between solder layer and thermoelectric device just accumulated to a detectable level. Lead dots are found inside InTe layer and In strip was found in PbTe device region. For device without graphene barrier, in a large area (scare bar increase to 20 μ m), only InPb compound can be found.

2.3.4 Power conversion efficiency test for InTe/mG/PbTe and InTe/PbTe

Power output result at highest ΔT (420C) is shown in Figure 2.20, devices with and without Graphene was tested after annealing at 500C for 3, 13, 18, 24 and 36hrs. For as made device with Graphene barrier, power output is about 23.6, 35% higher than that without Graphene barrier which is 16.8. After initial drop (13hrs, 17.3 for device with Graphene barrier and 11.2 for device without Graphene barrier), PbTe thermoelectrical devices maintained relative stable power output as increasing annealing time (~13 for device with Graphene barrier and ~11 for device without Graphene barrier). Overall performance of devices with Graphene barrier showed a 20-30% higher power output than devices without Graphene barrier after long time anneal (>13hrs).

Device with Graphene has a merit of $zT = 0.30$ after annealed at 500C for 36hrs while device without Graphene only had a $zT = 0.20$, a 50% improvement achieved. Also, after annealing at 500C for 36hrs, InTe/PbTe has a relative efficiency of 6.3% while device with Graphene barrier maintained efficiency of 8.9%. That is a 41.2% increase. The normalized current density increased from 182 to 252 (A*mm/cm²) for device with Graphene barrier indicated device with Graphene degraded slower than device without Graphene barrier. Normalized

output power density for InTe/mG/PbTe device is 14.05w/cm^2 compare to device without Graphen 9.90w/cm^2 (a 41.9% improvement).

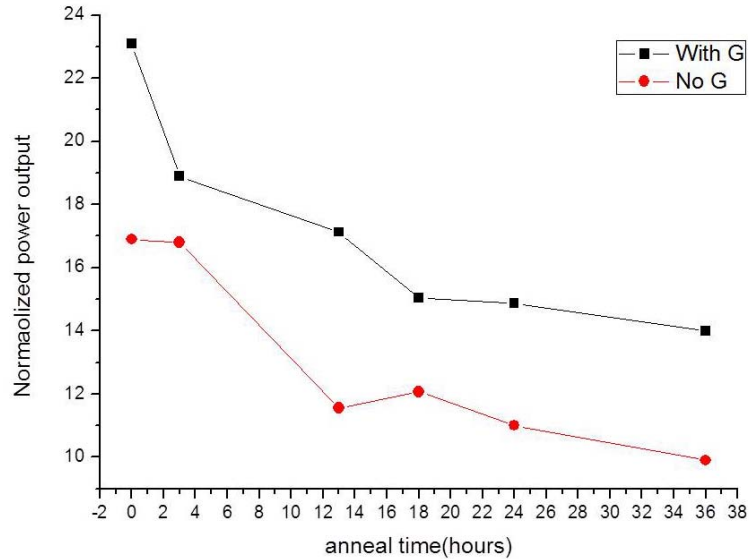


Figure 2.20 Normalized power output at $\Delta T = 420\text{C}$ for InTe/mG/PbTe and InTe/PbTe after annealing at 500C for 0, 3, 13, 18, 24 and 36hrs.

Normalized power output vs Δ temperature is plotted in Figure 2.21. Since thermoelectric materials are not only work at peak temperature, a high output through wide temperature range is preferred (covered area). For as made (0hr) samples, power output for both devices with and without graphene are identical below $\Delta T = 300\text{C}$, at higher temperature, where diffusion rate increased dramatically, power output of device without graphene became lower than device with graphene. For all pre-annealed samples, device with graphene barrier started generate more power than device without graphene from low $\Delta T = 150\text{C}$ to high working temperature $\Delta T = 420\text{C}$ (45% more power in average).

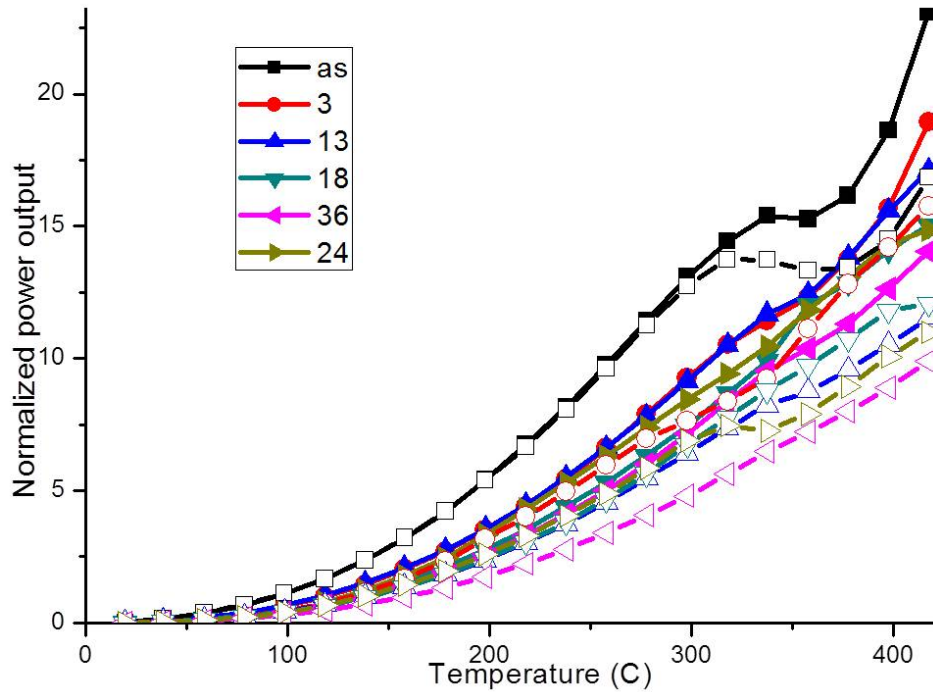


Figure 2.21 Normalized power output of devices with (solid) and without (hollow) graphene after annealing at 500C for different times.

2.4 Conclusion

Single layer graphene has been used as diffusion barrier for Ni/Cu and Ni/PbTe interface. With graphene barrier, Cu and Ni metal layers remained separate after annealing at 500C for 4hrs while Ni coated Cu film became Ni/Cu alloy after annealing at 500C for 30mins. Though after annealing at 500C for 4hrs, the Ni/G/Cu raised a narrow transition region composed by Ni/Cu alloy, single layer graphene directly used on Cu substrate still showed reliable performance as diffusion barrier. Randomly formed defects and abundant grain boundaries would allow atoms to pass through.

For transferred graphene barrier, more defects formed during the procedure and reduced the block performance significantly. That is why graphene transferred on PbTe device showed limited block performance, certain amount Ni diffused into PbTe device with transferred single layer graphene barrier after annealing at 500C for 12hrs, but the Ni content (~10%) penetrated through graphene into Cu is still much lower than that for device without graphene barrier (~40%).

To prolong device life time and maintain high power conversion efficiency of thermoelectric materials, 4 layers graphene barrier was used to block inter-diffuse of materials in solder and thermoelectric device. EDS results indicated that with an increasing annealing time from 0hrs to 36hrs, device with 4 layers graphene barrier maintained its InTe/mG/PbTe structure while device without graphene barrier formed new compound InPb. As expected, power output of devices with 4 layers graphene barrier shows an average of 40% higher power output compare to devices without graphene barrier since graphene barrier helped to maintain device structure from degradation. After 36hrs annealing at 500C under Ar, the InTe/mG/PbTe device generate more than 40 wt% power than InTe/PbTe as In and lead have diffused thoroughly into each other .

As there is no special bonding required for Graphene barrier, we consider Graphene could be used as a good diffusion barrier preventing thermoelectric material degradation to increase device life time and power conversion efficiency.

APPENDIX SECTION

Raw data for Figure 1.24.

	Wave number	Wave number	average	¹³ C %
0	2671.8	2669	2669	0.03994
1	2671.4	2669.1	2669.1	0.038915
2	2670.7	2668.5	2668.5	0.045068
3	2670.6	2668.8	2668.8	0.041991
4	2672	2670.4	2670.4	0.025599
5	2671.8	2671.1	2671.1	0.018437
6	2673.8	2670.9	2670.9	0.020483
7	2673.5	2669.7	2669.7	0.032767
8	2646.8	2670.1	2670.1	0.028671
9	2631.1	2669.3	2669.3	0.036865
10	2629.3	2645.3	2645.3	0.286179
11	2627.1	2634.3	2634.3	0.402732
12	2625.3	2628.2	2628.2	0.467997
13	2622.3	2625.7	2625.7	0.494877
14	2619.3	2625.9	2625.9	0.492724
15	2618.9	2624.6	2624.6	0.506728
16	2616	2623.5	2623.5	0.518595
17	2613.4	2623	2623	0.523993
18	2611.4	2621.5	2621.5	0.540208
19	2612.2	2616.7	2616.7	0.592282
20	2610.6	2611.8	2611.8	0.645738
21	2603.5	2611.8	2612.2	0.641363
22	2603.4	2607.4	2610.6	0.658875
23	2604.9	2604.2	2603.5	0.736975
24	2603.5	2600.2	2603.4	0.73808
25	2602.2	2599.3	2604.9	0.721525
26	2601.2	2600.6	2603.5	0.736975
27	2600	2600.4	2602.2	0.751345
28	2597.6	2600.1	2601.2	0.762413
29	2595.3	2598.9	2600	0.775711
30	2592.8	2597.4	2597.6	0.802363
31	2590	2597	2595.3	0.827974
32	2591.5	2595.4	2592.8	0.855889
33	2593.5	2593.6	2590	0.887251
34	2617.6	2591.8	2591.5	0.870437

35	2628.3	2588	2593.5	0.848065
36	2634.2	2584.4	2617.6	0.582497
37	2638.5	2587	2628.3	0.466924
38	2640.5	2614.5	2634.2	0.403798
39	2643.6	2630	2638.5	0.358058
40	2645.6	2635	2640.5	0.336859
41	2644.6	2635.3	2643.6	0.304097
42	2645.1	2638.5	2645.6	0.283021
43	2647.3	2640.7	2644.6	0.293553
44	2649.5	2643	2645.1	0.288285
45	2652.7	2643.4	2647.3	0.265144
46	2654.9	2648.1	2649.5	0.24206
47	2653.9	2651.7	2652.7	0.208585
48	2652.8	2652	2654.9	0.185642
49	2652.1	2653.3	2653.9	0.196064
50	2653.8	2652.6	2652.8	0.207541
51	2653.6	2651.3	2652.1	0.214853
52	2657.7	2652.2	2653.8	0.197107
53		2651.6	2653.6	0.199193
54		2653.7	2657.7	0.156524
55		2655.3	2659.3	0.139926
56		2657.1	2659.4	0.13889
57		2659.3	2660	0.132674
58		2660.4	2661	0.122324

Table 1 Power output raw data: as made InTe/mG/PbTe.

ΔT	E,mV	I,A	Normali zed Current Density, J (A*mm/ cm2)	Normali zed Power Density , P _n (W/cm 2)	Normaliz ed Match ed Power, P _m (W/cm2)	Chip Match ed Power , P _c (W)	Chip Therma l Flux, q _c (W)	Normali zed Therma l Flux, q _n (W/cm 2)	Chip Absolute Efficiency y _{ab} =P _c /q _c	Normaliz ed Absolute Efficiency y _{ab} =P _m / q _n	Carnot Efficie ncy %	Chip Relativ e Efficie ncy %	Zt	Seebeck Coeff $\Delta V/\Delta T$ ($\mu V/K$)
58.62	5.02	1.52	70.19	0.35	0.09	0.00	0.21	9.47	0.01	0.01	0.17	0.06	0.23	93.14
78.40	7.18	2.05	94.26	0.68	0.17	0.01	0.27	12.66	0.01	0.01	0.21	0.06	0.26	109.17
98.53	9.31	2.59	119.16	1.11	0.28	0.01	0.35	15.91	0.02	0.02	0.25	0.07	0.28	106.14
118.33	11.66	3.07	141.43	1.65	0.41	0.02	0.41	19.11	0.02	0.02	0.29	0.08	0.30	118.57
138.41	14.30	3.58	164.76	2.36	0.59	0.03	0.49	22.35	0.03	0.03	0.32	0.08	0.33	131.64
158.23	17.00	4.08	188.08	3.20	0.80	0.03	0.55	25.55	0.03	0.03	0.35	0.09	0.35	136.02
178.01	19.85	4.59	211.71	4.20	1.05	0.04	0.62	28.75	0.04	0.04	0.38	0.10	0.38	144.15
198.23	23.10	5.09	234.55	5.42	1.35	0.06	0.69	32.01	0.04	0.04	0.40	0.11	0.41	160.54
218.38	26.36	5.55	255.94	6.75	1.69	0.07	0.77	35.27	0.05	0.05	0.42	0.11	0.44	161.86
237.90	29.63	5.98	275.63	8.17	2.04	0.09	0.83	38.42	0.05	0.05	0.45	0.12	0.47	167.67
257.82	33.03	6.42	295.69	9.77	2.44	0.10	0.90	41.64	0.06	0.06	0.47	0.13	0.49	170.53
277.56	36.53	6.80	313.33	11.44	2.86	0.12	0.97	44.83	0.06	0.06	0.48	0.13	0.51	177.18
297.44	40.18	7.07	325.91	13.10	3.27	0.14	1.04	48.04	0.07	0.07	0.50	0.14	0.53	184.04
316.93	43.71	7.17	330.34	14.44	3.61	0.15	1.11	51.18	0.07	0.07	0.52	0.14	0.52	180.94
337.34	47.53	7.03	324.01	15.40	3.85	0.16	1.18	54.48	0.07	0.07	0.53	0.13	0.50	186.93
356.52	51.06	6.50	299.35	15.28	3.82	0.16	1.25	57.58	0.07	0.07	0.55	0.12	0.44	184.26
376.43	54.95	6.39	294.31	16.17	4.04	0.17	1.32	60.79	0.07	0.07	0.56	0.12	0.43	195.26
396.01	58.44	6.92	318.82	18.63	4.66	0.20	1.39	63.96	0.07	0.07	0.57	0.13	0.46	178.60
415.31	61.43	8.16	376.05	23.10	5.77	0.25	1.46	67.07	0.09	0.09	0.58	0.15	0.55	154.42

Table 2 Power output raw data: as made InTe /PbTe.

ΔT	E,mV	I,A	Normalized Current Density, J (A*mm/cm ²)	Normalized Power Density, P _n (W/cm ²)	Normalized Matched Power, P _m (W/cm ²)	Chip Matched Power, P _c (W)	Chip Thermal Flux, q _c (W)	Normalized Thermal Flux, q _n (W/cm ²)	Chip Absolute Efficiency $\eta_{ab}=P_c/q_c$	Normalized Absolute Efficiency $\eta_{ab}=P_m/q_n$	Carnot Efficiency %	Chip Relative Efficiency %	Zt	Seebeck Coeff $\Delta V/\Delta T$ ($\mu V/K$)
58.87	4.98	1.75	72.29	0.36	0.09	0.00	0.23	9.51	0.01	0.01	0.17	0.06	0.23	94.88
78.87	7.08	2.40	98.96	0.70	0.18	0.01	0.31	12.74	0.01	0.01	0.21	0.07	0.27	105.06
98.52	9.14	2.97	122.34	1.12	0.28	0.01	0.39	15.91	0.02	0.02	0.25	0.07	0.28	104.86
118.32	11.41	3.55	146.20	1.67	0.42	0.02	0.46	19.11	0.02	0.02	0.29	0.08	0.30	114.83
138.27	13.94	4.12	169.87	2.37	0.59	0.02	0.54	22.33	0.03	0.03	0.32	0.08	0.33	126.76
157.99	16.67	4.69	193.31	3.22	0.81	0.03	0.62	25.52	0.03	0.03	0.35	0.09	0.36	138.13
178.24	19.51	5.25	216.70	4.23	1.06	0.04	0.70	28.79	0.04	0.04	0.38	0.10	0.38	140.33
197.99	22.56	5.80	239.21	5.40	1.35	0.05	0.78	31.97	0.04	0.04	0.40	0.11	0.41	154.64
217.90	25.64	6.30	259.69	6.66	1.66	0.07	0.85	35.19	0.05	0.05	0.42	0.11	0.44	154.64
238.11	28.97	6.76	278.70	8.07	2.02	0.08	0.93	38.46	0.05	0.05	0.45	0.12	0.46	164.65
257.91	32.42	7.20	296.91	9.63	2.41	0.10	1.01	41.65	0.06	0.06	0.47	0.12	0.48	174.24
277.85	35.92	7.60	313.44	11.26	2.81	0.11	1.09	44.87	0.06	0.06	0.48	0.13	0.50	175.63
297.15	39.36	7.85	323.83	12.75	3.19	0.13	1.16	47.99	0.07	0.07	0.50	0.13	0.51	178.35
317.12	42.95	7.76	320.15	13.75	3.44	0.14	1.24	51.21	0.07	0.07	0.52	0.13	0.49	179.52
337.17	46.54	7.15	295.06	13.73	3.43	0.14	1.32	54.45	0.06	0.06	0.53	0.12	0.43	179.19
356.68	50.08	6.45	266.09	13.33	3.33	0.13	1.40	57.60	0.06	0.06	0.55	0.11	0.37	181.57
376.44	53.77	6.06	250.13	13.45	3.36	0.14	1.47	60.80	0.06	0.06	0.56	0.10	0.34	186.51
396.08	57.48	6.11	252.10	14.49	3.62	0.15	1.55	63.97	0.06	0.06	0.57	0.10	0.34	188.80
415.41	60.45	6.76	278.95	16.86	4.22	0.17	1.63	67.09	0.06	0.06	0.58	0.11	0.37	153.85

Table 1 Power output raw data: as made InTe/mG/PbTe.

ΔT	E,mV	I,A	Normali zed Current Density, J (A*mm/ cm2)	Normali zed Power Density , P _n (W/cm 2)	Normaliz ed Match ed Power, P _m (W/cm2)	Chip Match ed Power , P _c (W)	Chip Therma l Flux, q _c (W)	Normali zed Therma l Flux, q _n (W/cm 2)	Chip Absolute Efficiency y _{ab} =P _c /q _c	Normaliz ed Absolute Efficiency y _{ab} =P _m / q _n	Carnot Efficie ncy %	Chip Relativ e Efficie ncy %	Zt	Seebeck Coeff $\Delta V/\Delta T$ ($\mu V/K$)
58.62	5.02	1.52	70.19	0.35	0.09	0.00	0.21	9.47	0.01	0.01	0.17	0.06	0.23	93.14
78.40	7.18	2.05	94.26	0.68	0.17	0.01	0.27	12.66	0.01	0.01	0.21	0.06	0.26	109.17
98.53	9.31	2.59	119.16	1.11	0.28	0.01	0.35	15.91	0.02	0.02	0.25	0.07	0.28	106.14
118.33	11.66	3.07	141.43	1.65	0.41	0.02	0.41	19.11	0.02	0.02	0.29	0.08	0.30	118.57
138.41	14.30	3.58	164.76	2.36	0.59	0.03	0.49	22.35	0.03	0.03	0.32	0.08	0.33	131.64
158.23	17.00	4.08	188.08	3.20	0.80	0.03	0.55	25.55	0.03	0.03	0.35	0.09	0.35	136.02
178.01	19.85	4.59	211.71	4.20	1.05	0.04	0.62	28.75	0.04	0.04	0.38	0.10	0.38	144.15
198.23	23.10	5.09	234.55	5.42	1.35	0.06	0.69	32.01	0.04	0.04	0.40	0.11	0.41	160.54
218.38	26.36	5.55	255.94	6.75	1.69	0.07	0.77	35.27	0.05	0.05	0.42	0.11	0.44	161.86
237.90	29.63	5.98	275.63	8.17	2.04	0.09	0.83	38.42	0.05	0.05	0.45	0.12	0.47	167.67
257.82	33.03	6.42	295.69	9.77	2.44	0.10	0.90	41.64	0.06	0.06	0.47	0.13	0.49	170.53
277.56	36.53	6.80	313.33	11.44	2.86	0.12	0.97	44.83	0.06	0.06	0.48	0.13	0.51	177.18
297.44	40.18	7.07	325.91	13.10	3.27	0.14	1.04	48.04	0.07	0.07	0.50	0.14	0.53	184.04
316.93	43.71	7.17	330.34	14.44	3.61	0.15	1.11	51.18	0.07	0.07	0.52	0.14	0.52	180.94
337.34	47.53	7.03	324.01	15.40	3.85	0.16	1.18	54.48	0.07	0.07	0.53	0.13	0.50	186.93
356.52	51.06	6.50	299.35	15.28	3.82	0.16	1.25	57.58	0.07	0.07	0.55	0.12	0.44	184.26
376.43	54.95	6.39	294.31	16.17	4.04	0.17	1.32	60.79	0.07	0.07	0.56	0.12	0.43	195.26
396.01	58.44	6.92	318.82	18.63	4.66	0.20	1.39	63.96	0.07	0.07	0.57	0.13	0.46	178.60
415.31	61.43	8.16	376.05	23.10	5.77	0.25	1.46	67.07	0.09	0.09	0.58	0.15	0.55	154.42

Table 2 Power output raw data: as made InTe /PbTe.

ΔT	E,mV	I,A	Normalized Current Density, J (A*mm/cm ²)	Normalized Power Density, P _n (W/cm ²)	Normalized Matched Power, P _m (W/cm ²)	Chip Matched Power, P _c (W)	Chip Thermal Flux, q _c (W)	Normalized Thermal Flux, q _n (W/cm ²)	Chip Absolute Efficiency $\eta_{ab}=P_c/q_c$	Normalized Absolute Efficiency $\eta_{ab}=P_m/q_n$	Carnot Efficiency %	Chip Relative Efficiency %	Zt	Seebeck Coeff $\Delta V/\Delta T$ ($\mu V/K$)
58.87	4.98	1.75	72.29	0.36	0.09	0.00	0.23	9.51	0.01	0.01	0.17	0.06	0.23	94.88
78.87	7.08	2.40	98.96	0.70	0.18	0.01	0.31	12.74	0.01	0.01	0.21	0.07	0.27	105.06
98.52	9.14	2.97	122.34	1.12	0.28	0.01	0.39	15.91	0.02	0.02	0.25	0.07	0.28	104.86
118.32	11.41	3.55	146.20	1.67	0.42	0.02	0.46	19.11	0.02	0.02	0.29	0.08	0.30	114.83
138.27	13.94	4.12	169.87	2.37	0.59	0.02	0.54	22.33	0.03	0.03	0.32	0.08	0.33	126.76
157.99	16.67	4.69	193.31	3.22	0.81	0.03	0.62	25.52	0.03	0.03	0.35	0.09	0.36	138.13
178.24	19.51	5.25	216.70	4.23	1.06	0.04	0.70	28.79	0.04	0.04	0.38	0.10	0.38	140.33
197.99	22.56	5.80	239.21	5.40	1.35	0.05	0.78	31.97	0.04	0.04	0.40	0.11	0.41	154.64
217.90	25.64	6.30	259.69	6.66	1.66	0.07	0.85	35.19	0.05	0.05	0.42	0.11	0.44	154.64
238.11	28.97	6.76	278.70	8.07	2.02	0.08	0.93	38.46	0.05	0.05	0.45	0.12	0.46	164.65
257.91	32.42	7.20	296.91	9.63	2.41	0.10	1.01	41.65	0.06	0.06	0.47	0.12	0.48	174.24
277.85	35.92	7.60	313.44	11.26	2.81	0.11	1.09	44.87	0.06	0.06	0.48	0.13	0.50	175.63
297.15	39.36	7.85	323.83	12.75	3.19	0.13	1.16	47.99	0.07	0.07	0.50	0.13	0.51	178.35
317.12	42.95	7.76	320.15	13.75	3.44	0.14	1.24	51.21	0.07	0.07	0.52	0.13	0.49	179.52
337.17	46.54	7.15	295.06	13.73	3.43	0.14	1.32	54.45	0.06	0.06	0.53	0.12	0.43	179.19
356.68	50.08	6.45	266.09	13.33	3.33	0.13	1.40	57.60	0.06	0.06	0.55	0.11	0.37	181.57
376.44	53.77	6.06	250.13	13.45	3.36	0.14	1.47	60.80	0.06	0.06	0.56	0.10	0.34	186.51
396.08	57.48	6.11	252.10	14.49	3.62	0.15	1.55	63.97	0.06	0.06	0.57	0.10	0.34	188.80
415.41	60.45	6.76	278.95	16.86	4.22	0.17	1.63	67.09	0.06	0.06	0.58	0.11	0.37	153.85

Table 3 Power output raw data: 3hrs InTe/mG/PbTe.

ΔT	E,mV	I,A	Normalized Current Density, J (A*mm/cm ²)	Normalized Power Density, P _n (W/cm ²)	Normalized Matched Power, P _m (W/cm ²)	Chip Matched Power, P _c (W)	Chip Thermal Flux, q _c (W)	Normalized Thermal Flux, q _n (W/cm ²)	Chip Absolute Efficiency $\eta_{ab}=P_c/q_c$	Normalized Absolute Efficiency $\eta_{yab}=P_m/q_n$	Carnot Efficiency %	Chip Relative Efficiency %	Zt	Seebeck Coeff $\Delta V/\Delta T$ ($\mu V/K$)
58.64	5.13	0.83	38.47	0.20	0.05	0.00	0.20	9.47	0.01	0.01	0.17	0.03	0.12	92.07
78.19	7.16	1.14	52.72	0.38	0.09	0.01	0.27	12.63	0.01	0.01	0.21	0.04	0.14	103.90
98.30	9.25	1.48	68.34	0.63	0.16	0.01	0.34	15.88	0.01	0.01	0.25	0.04	0.15	104.10
118.20	11.61	1.84	84.97	0.99	0.25	0.02	0.41	19.09	0.01	0.01	0.29	0.05	0.17	118.52
137.93	14.02	2.23	103.44	1.45	0.36	0.03	0.48	22.28	0.02	0.02	0.32	0.05	0.19	121.93
158.00	16.75	2.62	121.17	2.03	0.51	0.04	0.55	25.52	0.02	0.02	0.35	0.06	0.21	136.24
177.83	19.53	2.99	138.56	2.71	0.68	0.05	0.62	28.72	0.02	0.02	0.38	0.06	0.23	139.84
198.02	22.57	3.38	156.49	3.53	0.88	0.07	0.69	31.98	0.03	0.03	0.40	0.07	0.25	150.90
217.72	25.65	3.73	172.74	4.43	1.11	0.08	0.76	35.16	0.03	0.03	0.42	0.07	0.27	156.42
237.68	28.87	4.08	189.01	5.46	1.36	0.10	0.83	38.39	0.04	0.04	0.45	0.08	0.29	160.95
257.31	32.26	4.43	205.13	6.62	1.65	0.13	0.90	41.56	0.04	0.04	0.46	0.09	0.31	173.00
277.25	35.70	4.78	221.39	7.90	1.98	0.15	0.97	44.78	0.04	0.04	0.48	0.09	0.33	172.59
297.24	39.27	5.10	235.91	9.26	2.32	0.18	1.04	48.00	0.05	0.05	0.50	0.10	0.35	178.49
316.80	42.93	5.30	245.31	10.53	2.63	0.20	1.11	51.16	0.05	0.05	0.52	0.10	0.35	187.24
336.81	46.63	5.30	245.35	11.44	2.86	0.22	1.18	54.39	0.05	0.05	0.53	0.10	0.35	184.75
356.69	50.43	5.28	244.36	12.32	3.08	0.23	1.24	57.60	0.05	0.05	0.55	0.10	0.34	191.03
376.40	54.19	5.48	253.78	13.75	3.44	0.26	1.31	60.79	0.06	0.06	0.56	0.10	0.35	191.11
396.05	57.64	5.88	271.96	15.68	3.92	0.30	1.38	63.96	0.06	0.06	0.57	0.11	0.37	175.35
415.26	60.35	6.43	297.51	17.96	4.49	0.34	1.45	67.06	0.07	0.07	0.58	0.11	0.40	141.28

Table 4 Power output raw data: 3hrs InTe /PbTe.

ΔT	E,mv	I,A	Normalized Current Density, J (A*mm/cm ²)	Normalized Power Density, P _n (W/cm ²)	Normalized Matched Power, P _m (W/cm ²)	Chip Matched Power, P _c (W)	Chip Thermal Flux, q _c (W)	Normalized Thermal Flux, q _n (W/cm ²)	Chip Absolute Efficiency $\eta_{ab}=P_c/q_c$	Normalized Absolute Efficiency $\eta_{ab}=P_m/q_n$	Carnot Efficiency %	Chip Relative Efficiency %	Zt	Seebeck Coeff $\Delta V/\Delta T$ ($\mu V/K$)
58.67	4.63	0.57	26.50	0.12	0.03	0.00	0.20	9.48	0.00	0.00	0.17	0.02	0.07	95.05
78.64	6.36	0.84	39.20	0.25	0.06	0.01	0.27	12.70	0.00	0.00	0.21	0.02	0.09	86.83
98.32	8.47	1.14	52.92	0.45	0.11	0.01	0.34	15.88	0.01	0.01	0.25	0.03	0.10	107.16
118.34	10.61	1.50	69.72	0.74	0.18	0.02	0.41	19.11	0.01	0.01	0.29	0.03	0.12	107.09
138.53	13.08	1.91	88.79	1.16	0.29	0.03	0.48	22.37	0.01	0.01	0.32	0.04	0.15	122.37
157.98	15.52	2.31	107.55	1.67	0.42	0.04	0.55	25.51	0.02	0.02	0.35	0.05	0.17	125.03
178.23	18.31	2.76	128.47	2.35	0.59	0.06	0.62	28.78	0.02	0.02	0.38	0.05	0.20	137.97
198.38	21.26	3.20	148.89	3.17	0.79	0.08	0.69	32.04	0.02	0.02	0.40	0.06	0.22	146.41
217.87	24.23	3.57	166.10	4.02	1.01	0.10	0.76	35.19	0.03	0.03	0.42	0.07	0.24	152.21
238.11	27.42	3.90	181.42	4.97	1.24	0.13	0.83	38.45	0.03	0.03	0.45	0.07	0.26	157.82
257.59	30.44	4.22	196.44	5.98	1.49	0.15	0.89	41.60	0.04	0.04	0.47	0.08	0.27	154.83
277.34	33.74	4.44	206.33	6.96	1.74	0.18	0.96	44.79	0.04	0.04	0.48	0.08	0.28	167.21
297.24	37.59	4.37	203.34	7.64	1.91	0.19	1.03	48.00	0.04	0.04	0.50	0.08	0.28	193.56
317.23	41.70	4.33	201.40	8.40	2.10	0.21	1.10	51.23	0.04	0.04	0.52	0.08	0.27	205.38
336.76	45.42	4.37	203.32	9.23	2.31	0.24	1.17	54.39	0.04	0.04	0.53	0.08	0.27	190.53
355.85	49.23	4.86	226.22	11.14	2.78	0.28	1.24	57.47	0.05	0.05	0.55	0.09	0.30	199.83
376.60	52.94	5.20	241.98	12.81	3.20	0.33	1.31	60.82	0.05	0.05	0.56	0.09	0.32	178.86
396.19	56.39	5.41	251.65	14.19	3.55	0.36	1.38	63.99	0.06	0.06	0.57	0.10	0.33	176.01
415.39	59.79	5.67	263.51	15.75	3.94	0.40	1.44	67.09	0.06	0.06	0.58	0.10	0.34	176.80

Table 5 Power output raw data: 13hrs InTe/mG/PbTe.

ΔT	E,mv	I,A	Normalized Current Density, J (A*mm/cm ²)	Normalized Power Density, P _n (W/cm ²)	Normalized Matched Power, P _m (W/cm ²)	Chip Matched Power, P _c (W)	Chip Thermal Flux, q _c (W)	Normalized Thermal Flux, q _n (W/cm ²)	Chip Absolute Efficiency $\eta_{ab}=P_c/q_c$	Normalized Absolute Efficiency $\eta_{ab}=P_m/q_n$	Carnot Efficiency %	Chip Relative Efficiency %	Zt	Seebeck Coeff $\Delta V/\Delta T$ ($\mu V/K$)
60.17	5.17	0.85	39.73	0.21	0.05	0.00	0.21	9.72	0.01	0.01	0.17	0.03	0.12	91.02
79.76	7.11	1.18	54.76	0.39	0.10	0.01	0.28	12.88	0.01	0.01	0.21	0.04	0.14	98.88
99.92	9.16	1.55	72.03	0.66	0.16	0.01	0.35	16.14	0.01	0.01	0.25	0.04	0.15	101.85
119.60	11.36	1.96	91.21	1.04	0.26	0.02	0.42	19.32	0.01	0.01	0.29	0.05	0.17	111.52
139.35	13.59	2.39	111.17	1.51	0.38	0.03	0.48	22.50	0.02	0.02	0.32	0.05	0.19	113.29
159.19	16.04	2.78	129.42	2.08	0.52	0.04	0.55	25.71	0.02	0.02	0.35	0.06	0.21	123.16
179.35	18.60	3.19	148.20	2.76	0.69	0.05	0.62	28.96	0.02	0.02	0.38	0.06	0.23	127.39
199.40	21.34	3.58	166.51	3.55	0.89	0.06	0.69	32.20	0.03	0.03	0.40	0.07	0.25	136.44
218.93	24.14	3.96	184.38	4.45	1.11	0.08	0.76	35.36	0.03	0.03	0.43	0.07	0.27	143.42
238.86	27.12	4.36	202.99	5.50	1.38	0.10	0.83	38.58	0.04	0.04	0.45	0.08	0.29	149.36
258.93	30.10	4.73	220.14	6.63	1.66	0.12	0.90	41.82	0.04	0.04	0.47	0.08	0.30	148.63
278.71	33.11	5.07	235.95	7.81	1.95	0.14	0.97	45.01	0.04	0.04	0.48	0.09	0.32	151.95
298.44	36.26	5.42	252.13	9.14	2.29	0.17	1.04	48.20	0.05	0.05	0.50	0.09	0.34	159.88
318.04	39.44	5.72	266.20	10.50	2.62	0.19	1.10	51.36	0.05	0.05	0.52	0.10	0.35	162.34
338.09	42.80	5.87	272.88	11.68	2.92	0.21	1.17	54.60	0.05	0.05	0.53	0.10	0.35	167.24
357.76	46.13	5.79	269.54	12.43	3.11	0.23	1.24	57.78	0.05	0.05	0.55	0.10	0.34	169.44
377.48	49.49	6.01	279.75	13.84	3.46	0.25	1.31	60.96	0.06	0.06	0.56	0.10	0.35	170.32
396.98	52.94	6.33	294.33	15.58	3.90	0.28	1.38	64.11	0.06	0.06	0.57	0.11	0.37	176.90
416.06	55.87	6.59	306.59	17.13	4.28	0.31	1.44	67.19	0.06	0.06	0.58	0.11	0.38	153.61

Table 6 Power output raw data: 13hrs InTe/PbTe.

ΔT	E,mV	I,A	Normalized Current Density, J (A*mm/cm ²)	Normalized Power Density, P _n (W/cm ²)	Normalized Matched Power, P _m (W/cm ²)	Chip Matched Power, P _c (W)	Chip Thermal Flux, q _c (W)	Normalized Thermal Flux, q _n (W/cm ²)	Chip Absolute Efficiency $\eta_{ab}=P_c/q_c$	Normalized Absolute Efficiency $\eta_{ab}=P_m/q_n$	Carnot Efficiency %	Chip Relative Efficiency %	Zt	Seebeck Coeff $\Delta V/\Delta T$ ($\mu V/K$)
58.31	4.33	0.62	28.73	0.12	0.03	0.00	0.20	9.42	0.00	0.00	0.16	0.02	0.08	92.21
78.29	6.29	0.85	39.49	0.25	0.06	0.01	0.27	12.64	0.00	0.00	0.21	0.02	0.09	98.31
98.10	8.25	1.08	50.34	0.42	0.10	0.01	0.34	15.84	0.01	0.01	0.25	0.03	0.10	98.63
118.18	10.38	1.35	62.81	0.65	0.16	0.02	0.41	19.09	0.01	0.01	0.29	0.03	0.11	106.27
138.12	12.71	1.62	75.34	0.96	0.24	0.02	0.48	22.31	0.01	0.01	0.32	0.03	0.12	116.65
158.12	15.25	1.91	88.70	1.35	0.34	0.03	0.55	25.54	0.01	0.01	0.35	0.04	0.13	127.32
177.85	17.89	2.20	102.25	1.83	0.46	0.05	0.62	28.72	0.02	0.02	0.38	0.04	0.15	133.92
197.90	20.60	2.52	117.05	2.41	0.60	0.06	0.69	31.96	0.02	0.02	0.40	0.05	0.16	135.13
217.91	23.47	2.80	130.43	3.06	0.77	0.08	0.76	35.19	0.02	0.02	0.42	0.05	0.18	143.09
237.98	26.47	3.10	144.16	3.82	0.95	0.10	0.83	38.43	0.02	0.02	0.45	0.06	0.19	149.48
257.84	29.52	3.41	158.57	4.68	1.17	0.12	0.90	41.64	0.03	0.03	0.47	0.06	0.21	153.68
277.78	32.72	3.70	172.26	5.64	1.41	0.14	0.96	44.86	0.03	0.03	0.48	0.06	0.22	160.51
297.72	35.99	4.01	186.70	6.72	1.68	0.17	1.03	48.08	0.03	0.03	0.50	0.07	0.24	164.10
317.74	39.39	4.24	197.26	7.77	1.94	0.20	1.10	51.31	0.04	0.04	0.52	0.07	0.25	169.84
337.64	42.80	4.42	205.46	8.79	2.20	0.22	1.17	54.53	0.04	0.04	0.53	0.08	0.25	171.20
357.40	46.26	4.52	210.28	9.73	2.43	0.25	1.24	57.72	0.04	0.04	0.55	0.08	0.26	174.97
377.55	49.88	4.63	215.28	10.74	2.68	0.27	1.31	60.97	0.04	0.04	0.56	0.08	0.26	179.91
397.40	53.37	4.76	221.35	11.81	2.95	0.30	1.38	64.18	0.05	0.05	0.57	0.08	0.26	175.83
417.12	56.79	4.94	230.00	13.06	3.27	0.33	1.45	67.37	0.05	0.05	0.58	0.08	0.27	173.39

Table 7 Power output raw data: 18hrs InTe/mG/PbTe.

ΔT	E,mV	I,A	Normalized Current Density, J (A*mm/cm ²)	Normalized Power Density, P _n (W/cm ²)	Normalized Matched Power, P _m (W/cm ²)	Chip Matched Power, P _c (W)	Chip Thermal Flux, q _c (W)	Normalized Thermal Flux, q _n (W/cm ²)	Chip Absolute Efficiency $\eta_{ab} = P_c / q_c$	Normalized Absolute Efficiency $\eta_{yab} = P_m / q_n$	Carnot Efficiency %	Chip Relative Efficiency %	Zt	Seebeck Coeff $\Delta V / \Delta T$ ($\mu V / K$)
59.83	4.69	0.54	24.83	0.12	0.03	0.00	0.21	9.66	0.00	0.00	0.17	0.02	0.07	85.47
80.09	6.60	0.78	35.87	0.24	0.06	0.01	0.28	12.94	0.00	0.00	0.21	0.02	0.08	94.02
99.48	8.64	1.05	48.32	0.42	0.10	0.01	0.35	16.07	0.01	0.01	0.25	0.03	0.09	105.53
119.83	10.74	1.37	62.80	0.67	0.17	0.02	0.42	19.35	0.01	0.01	0.29	0.03	0.11	103.25
139.31	13.01	1.76	80.68	1.05	0.26	0.03	0.49	22.50	0.01	0.01	0.32	0.04	0.13	116.40
159.26	15.33	2.16	99.19	1.52	0.38	0.04	0.56	25.72	0.01	0.01	0.35	0.04	0.15	116.43
179.54	18.01	2.54	116.74	2.10	0.53	0.06	0.63	29.00	0.02	0.02	0.38	0.05	0.17	132.23
198.95	20.65	2.92	134.01	2.77	0.69	0.08	0.70	32.13	0.02	0.02	0.40	0.05	0.19	135.64
219.27	23.50	3.28	150.47	3.54	0.88	0.10	0.77	35.41	0.02	0.02	0.43	0.06	0.21	140.37
239.16	26.27	3.65	167.37	4.40	1.10	0.12	0.84	38.62	0.03	0.03	0.45	0.06	0.22	139.19
258.64	29.03	4.00	183.40	5.33	1.33	0.15	0.91	41.77	0.03	0.03	0.47	0.07	0.24	141.98
278.74	32.08	4.30	197.36	6.33	1.58	0.18	0.98	45.02	0.04	0.04	0.48	0.07	0.25	151.28
298.65	35.21	4.62	211.83	7.46	1.86	0.21	1.05	48.23	0.04	0.04	0.50	0.08	0.27	157.33
318.18	38.40	4.93	226.02	8.68	2.17	0.24	1.12	51.39	0.04	0.04	0.52	0.08	0.28	163.33
337.99	41.71	5.18	237.76	9.92	2.48	0.28	1.19	54.58	0.05	0.05	0.53	0.09	0.29	167.39
358.02	45.01	5.82	267.15	12.03	3.01	0.34	1.26	57.82	0.05	0.05	0.55	0.10	0.33	164.77
377.55	48.65	5.76	264.29	12.86	3.21	0.36	1.33	60.97	0.05	0.05	0.56	0.09	0.32	186.27
397.14	52.05	5.90	270.78	14.09	3.52	0.39	1.40	64.14	0.05	0.05	0.57	0.10	0.33	173.21
415.97	54.93	5.97	273.98	15.05	3.76	0.42	1.46	67.18	0.06	0.06	0.58	0.10	0.32	152.97

Table 8 Power output raw data: 18hrs InTe/PbTe.

ΔT	E,mv	I,A	Normalized Current Density, J (A*mm/cm ²)	Normalized Power Density, P _n (W/cm ²)	Normalized Matched Power, P _m (W/cm ²)	Chip Matched Power, P _c (W)	Chip Thermal Flux, q _c (W)	Normalized Thermal Flux, q _n (W/cm ²)	Chip Absolute Efficiency $\eta_{ab}=P_c/q_c$	Normalized Absolute Efficiency $\eta_{ab}=P_m/q_n$	Carnot Efficiency %	Chip Relative Efficiency %	Zt	Seebeck Coeff $\Delta V/\Delta T$ ($\mu V/K$)
60.13	4.72	0.61	28.02	0.13	0.03	0.00	0.21	9.71	0.00	0.00	0.17	0.02	0.08	92.54
79.75	6.58	0.83	38.34	0.25	0.06	0.01	0.28	12.88	0.00	0.00	0.21	0.02	0.09	94.66
99.50	8.60	1.08	50.12	0.43	0.11	0.01	0.35	16.07	0.01	0.01	0.25	0.03	0.10	102.04
119.53	10.77	1.36	63.06	0.68	0.17	0.02	0.42	19.30	0.01	0.01	0.29	0.03	0.11	108.55
139.61	13.03	1.65	76.61	1.00	0.25	0.03	0.49	22.55	0.01	0.01	0.32	0.03	0.12	112.39
159.32	15.34	1.93	89.38	1.37	0.34	0.04	0.56	25.73	0.01	0.01	0.35	0.04	0.13	117.47
179.05	17.87	2.20	102.06	1.82	0.46	0.05	0.62	28.92	0.02	0.02	0.38	0.04	0.15	128.22
199.44	20.65	2.49	115.30	2.38	0.60	0.06	0.70	32.21	0.02	0.02	0.40	0.05	0.16	136.04
219.16	23.49	2.80	129.52	3.04	0.76	0.08	0.76	35.39	0.02	0.02	0.43	0.05	0.17	144.14
238.66	26.31	3.08	142.71	3.75	0.94	0.10	0.83	38.54	0.02	0.02	0.45	0.05	0.19	144.69
258.57	29.41	3.35	155.28	4.57	1.14	0.12	0.90	41.76	0.03	0.03	0.47	0.06	0.20	155.41
278.71	32.61	3.63	168.13	5.48	1.37	0.14	0.97	45.01	0.03	0.03	0.48	0.06	0.21	159.38
298.75	35.71	3.87	179.39	6.41	1.60	0.17	1.04	48.25	0.03	0.03	0.50	0.07	0.22	154.55
318.33	38.92	4.09	189.31	7.37	1.84	0.19	1.11	51.41	0.04	0.04	0.52	0.07	0.23	164.00
337.93	42.23	4.21	194.76	8.23	2.06	0.21	1.18	54.57	0.04	0.04	0.53	0.07	0.24	168.98
357.88	45.60	4.16	192.43	8.77	2.19	0.23	1.25	57.80	0.04	0.04	0.55	0.07	0.23	168.60
377.72	49.15	4.21	194.84	9.58	2.39	0.25	1.32	61.00	0.04	0.04	0.56	0.07	0.23	178.99
397.20	52.60	4.33	200.29	10.54	2.63	0.27	1.39	64.15	0.04	0.04	0.57	0.07	0.23	177.10
416.05	55.70	4.48	207.39	11.55	2.89	0.30	1.45	67.19	0.04	0.04	0.58	0.07	0.24	164.41

Table 9 Power output raw data: 24hrs InTe/mG/PbTe.

ΔT	E,mv	I,A	Normalized Current Density, J (A*mm/cm ²)	Normalized Power Density, P _n (W/cm ²)	Normalized Matched Power, P _m (W/cm ²)	Chip Matched Power, P _c (W)	Chip Thermal Flux, q _c (W)	Normalized Thermal Flux, q _n (W/cm ²)	Chip Absolute Efficiency $\eta_{ab}=P_c/q_c$	Normalized Absolute Efficiency $\eta_{ab}=P_m/q_n$	Carnot Efficiency %	Chip Relative Efficiency %	Zt	Seebeck Coeff $\Delta V/\Delta T$ ($\mu V/K$)
119.64	10.32	1.65	75.51	0.78	0.19	0.00	0.42	19.32	0.01	0.01	0.29	0.04	0.13	
139.89	12.64	2.08	95.14	1.20	0.30	0.01	0.50	22.59	0.01	0.01	0.32	0.04	0.15	114.59
159.39	15.12	2.56	116.89	1.77	0.44	0.01	0.56	25.74	0.02	0.02	0.35	0.05	0.18	126.84
179.34	17.80	3.03	138.08	2.46	0.61	0.01	0.63	28.96	0.02	0.02	0.38	0.06	0.20	134.41
199.35	20.67	3.53	160.98	3.33	0.83	0.02	0.71	32.20	0.03	0.03	0.40	0.06	0.23	143.38
219.04	23.59	3.99	181.98	4.29	1.07	0.02	0.78	35.37	0.03	0.03	0.43	0.07	0.26	148.35
238.91	26.47	4.39	200.12	5.30	1.32	0.03	0.85	38.58	0.03	0.03	0.45	0.08	0.28	145.17
258.73	29.24	4.73	216.05	6.32	1.58	0.03	0.92	41.78	0.04	0.04	0.47	0.08	0.29	139.59
278.92	32.30	5.02	229.00	7.40	1.85	0.04	0.99	45.05	0.04	0.04	0.49	0.08	0.30	151.49
298.76	35.59	5.20	237.09	8.44	2.11	0.05	1.06	48.25	0.04	0.04	0.50	0.09	0.31	166.06
318.42	38.94	5.31	242.28	9.43	2.36	0.05	1.13	51.42	0.05	0.05	0.52	0.09	0.31	170.11
338.02	42.37	5.40	246.61	10.45	2.61	0.06	1.20	54.59	0.05	0.05	0.53	0.09	0.31	174.93
358.08	45.86	5.64	257.58	11.81	2.95	0.06	1.27	57.83	0.05	0.05	0.55	0.09	0.32	174.31
377.84	49.14	5.83	266.12	13.08	3.27	0.07	1.34	61.02	0.05	0.05	0.56	0.10	0.33	165.89
397.14	52.40	5.99	273.48	14.33	3.58	0.08	1.41	64.14	0.06	0.06	0.57	0.10	0.33	168.64
415.75	55.51	5.87	267.92	14.87	3.72	0.08	1.47	67.14	0.06	0.06	0.58	0.09	0.32	167.36

Table 10 Power output raw data: 24hrs InTe/PbTe.

ΔT	E,mv	I,A	Normalized Current Density, J (A*mm/cm ²)	Normalized Power Density, P _n (W/cm ²)	Normalized Matched Power, P _m (W/cm ²)	Chip Matched Power, P _c (W)	Chip Thermal Flux, q _c (W)	Normalized Thermal Flux, q _n (W/cm ²)	Chip Absolute Efficiency $\eta_{ab} = P_c / q_c$	Normalized Absolute Efficiency $\eta_{ab} = P_m / q_n$	Carnot Efficiency %	Chip Relative Efficiency %	Zt	Seebeck Coeff $\Delta V / \Delta T$ ($\mu V / K$)
58.53	4.13	0.51	25.20	0.10	0.03	0.00	0.19	9.45	0.00	0.00	0.17	0.02	0.06	86.48
78.11	5.94	0.71	35.24	0.21	0.05	0.01	0.25	12.62	0.00	0.00	0.21	0.02	0.07	92.49
98.20	8.09	0.98	48.36	0.39	0.10	0.01	0.32	15.86	0.01	0.01	0.25	0.02	0.09	107.21
117.92	10.21	1.29	63.95	0.65	0.16	0.02	0.38	19.04	0.01	0.01	0.28	0.03	0.11	107.64
138.20	12.38	1.65	82.05	1.02	0.25	0.03	0.45	22.32	0.01	0.01	0.32	0.04	0.13	106.95
158.00	14.76	1.96	97.42	1.44	0.36	0.04	0.51	25.52	0.01	0.01	0.35	0.04	0.14	120.08
178.08	17.29	2.28	113.14	1.96	0.49	0.06	0.58	28.76	0.02	0.02	0.38	0.05	0.16	126.01
198.13	20.10	2.60	128.95	2.59	0.65	0.07	0.65	32.00	0.02	0.02	0.40	0.05	0.18	140.33
217.95	22.82	2.90	143.78	3.28	0.82	0.09	0.71	35.20	0.02	0.02	0.42	0.05	0.19	137.25
237.74	25.64	3.19	158.12	4.05	1.01	0.12	0.77	38.39	0.03	0.03	0.45	0.06	0.21	142.50
257.73	28.62	3.45	171.31	4.90	1.23	0.14	0.84	41.62	0.03	0.03	0.47	0.06	0.22	148.67
277.77	31.66	3.73	185.20	5.86	1.47	0.17	0.90	44.86	0.03	0.03	0.48	0.07	0.23	152.18
297.73	34.89	3.99	197.64	6.90	1.72	0.20	0.97	48.08	0.04	0.04	0.50	0.07	0.24	161.76
317.77	38.12	3.95	195.96	7.47	1.87	0.21	1.03	51.32	0.04	0.04	0.52	0.07	0.24	161.11
337.46	41.15	3.57	176.81	7.28	1.82	0.21	1.10	54.50	0.03	0.03	0.53	0.06	0.21	153.99
357.47	44.65	3.57	177.00	7.90	1.98	0.22	1.16	57.73	0.03	0.03	0.55	0.06	0.20	174.59
377.36	48.15	3.75	185.90	8.95	2.24	0.25	1.23	60.94	0.04	0.04	0.56	0.07	0.21	175.96
397.38	51.73	3.93	194.72	10.07	2.52	0.29	1.29	64.18	0.04	0.04	0.57	0.07	0.22	178.88
417.00	55.13	4.02	199.45	11.00	2.75	0.31	1.36	67.35	0.04	0.04	0.58	0.07	0.22	173.30

Table 11 Power output raw data: 36hrs InTe/mG/PbTe.

ΔT	E,mV	I,A	Normalized Current Density, J (A*mm/cm ²)	Normalized Power Density, P _n (W/cm ²)	Normalized Matched Power, P _m (W/cm ²)	Chip Matched Power, P _c (W)	Chip Thermal Flux, q _c (W)	Normalized Thermal Flux, q _n (W/cm ²)	Chip Absolute Efficiency $\eta_{ab}=P_c/q_c$	Normalized Absolute Efficiency $\eta_{ab}=P_m/q_n$	Carnot Efficiency %	Chip Relative Efficiency %	Zt	Seebeck Coeff $\Delta V/\Delta T$ ($\mu V/K$)
58.61	4.16	0.65	29.09	0.12	0.03	0.00	0.21	9.47	0.00	0.00	0.17	0.02	0.07	88.85
78.42	5.93	0.87	39.31	0.23	0.06	0.01	0.28	12.67	0.00	0.00	0.21	0.02	0.08	89.22
98.33	7.99	1.14	51.55	0.41	0.10	0.01	0.35	15.88	0.01	0.01	0.25	0.03	0.10	103.50
118.33	10.12	1.43	64.62	0.65	0.16	0.02	0.42	19.11	0.01	0.01	0.29	0.03	0.11	106.65
138.19	12.36	1.80	81.02	1.00	0.25	0.03	0.50	22.32	0.01	0.01	0.32	0.04	0.13	112.46
157.98	14.72	2.14	96.46	1.42	0.36	0.04	0.57	25.51	0.01	0.01	0.35	0.04	0.14	119.65
178.07	17.30	2.52	113.66	1.97	0.49	0.05	0.64	28.76	0.02	0.02	0.38	0.05	0.16	128.22
197.84	20.06	2.87	129.37	2.60	0.65	0.07	0.71	31.95	0.02	0.02	0.40	0.05	0.18	139.87
217.98	22.82	3.20	144.25	3.29	0.82	0.08	0.78	35.20	0.02	0.02	0.42	0.06	0.19	136.67
237.99	25.75	3.54	159.39	4.11	1.03	0.10	0.85	38.44	0.03	0.03	0.45	0.06	0.21	146.79
257.72	28.74	3.86	173.87	5.00	1.25	0.13	0.92	41.62	0.03	0.03	0.47	0.06	0.22	151.51
277.75	31.91	4.18	188.40	6.01	1.50	0.15	1.00	44.86	0.03	0.03	0.48	0.07	0.24	158.19
297.76	35.10	4.53	203.87	7.16	1.79	0.18	1.07	48.09	0.04	0.04	0.50	0.07	0.25	159.35
317.78	38.51	4.82	217.29	8.37	2.09	0.21	1.14	51.32	0.04	0.04	0.52	0.08	0.27	170.43
337.54	41.85	5.06	227.86	9.54	2.38	0.24	1.21	54.51	0.04	0.04	0.53	0.08	0.28	168.78
357.65	45.24	5.10	229.53	10.39	2.60	0.26	1.28	57.76	0.04	0.04	0.55	0.08	0.28	168.94
377.44	48.79	5.14	231.62	11.30	2.82	0.29	1.35	60.96	0.05	0.05	0.56	0.08	0.28	178.86
397.51	52.29	5.37	241.74	12.64	3.16	0.32	1.43	64.20	0.05	0.05	0.57	0.09	0.29	174.58
417.34	55.61	5.61	252.68	14.05	3.51	0.36	1.50	67.40	0.05	0.05	0.58	0.09	0.30	167.36

Table 12 Power output raw data: 36hrs InTe/PbTe.

ΔT	E,mV	I,A	Normalized Current Density, J (A*mm/cm ²)	Normalized Power Density, P _n (W/cm ²)	Normalized Matched Power, P _m (W/cm ²)	Chip Matched Power, P _c (W)	Chip Thermal Flux, q _c (W)	Normalized Thermal Flux, q _n (W/cm ²)	Chip Absolute Efficiency $\eta_{ab}=P_c/q_c$	Normalized Absolute Efficiency $\eta_{ab}=P_m/q_n$	Carnot Efficiency %	Chip Relative Efficiency %	Zt	Seebeck Coeff $\Delta V/\Delta T$ ($\mu V/K$)
58.24	3.94	0.45	20.64	0.08	0.02	0.00	0.21	9.41	0.00	0.00	0.16	0.01	0.05	79.61
78.20	5.82	0.62	28.33	0.16	0.04	0.01	0.28	12.63	0.00	0.00	0.21	0.02	0.06	94.14
98.22	7.81	0.80	36.59	0.29	0.07	0.01	0.35	15.86	0.00	0.00	0.25	0.02	0.07	99.36
118.02	9.79	1.03	46.84	0.46	0.11	0.02	0.42	19.06	0.01	0.01	0.28	0.02	0.08	99.82
137.98	12.03	1.26	57.59	0.69	0.17	0.02	0.49	22.28	0.01	0.01	0.32	0.02	0.09	112.18
157.99	14.36	1.49	68.25	0.98	0.24	0.03	0.56	25.51	0.01	0.01	0.35	0.03	0.10	116.59
177.87	16.86	1.71	78.25	1.32	0.33	0.05	0.63	28.73	0.01	0.01	0.38	0.03	0.11	125.91
197.85	19.51	1.96	89.52	1.75	0.44	0.06	0.70	31.95	0.01	0.01	0.40	0.03	0.12	132.70
218.11	22.33	2.19	100.18	2.24	0.56	0.08	0.77	35.22	0.02	0.02	0.42	0.04	0.13	139.25
237.76	25.21	2.42	110.34	2.78	0.70	0.10	0.84	38.40	0.02	0.02	0.45	0.04	0.14	146.47
257.77	28.15	2.65	121.01	3.41	0.85	0.12	0.91	41.63	0.02	0.02	0.47	0.04	0.15	146.88
277.74	31.11	2.86	130.47	4.06	1.01	0.14	0.98	44.86	0.02	0.02	0.48	0.05	0.15	148.06
297.76	34.24	3.07	140.22	4.80	1.20	0.17	1.05	48.09	0.02	0.02	0.50	0.05	0.16	156.64
317.81	37.53	3.29	149.99	5.63	1.41	0.20	1.12	51.33	0.03	0.03	0.52	0.05	0.17	163.92
337.74	40.85	3.47	158.48	6.47	1.62	0.23	1.19	54.54	0.03	0.03	0.53	0.06	0.18	166.42
357.60	44.09	3.59	163.77	7.22	1.81	0.25	1.27	57.75	0.03	0.03	0.55	0.06	0.18	163.36
377.36	47.51	3.69	168.60	8.01	2.00	0.28	1.33	60.94	0.03	0.03	0.56	0.06	0.19	173.18
397.39	50.99	3.81	174.14	8.88	2.22	0.31	1.41	64.18	0.03	0.03	0.57	0.06	0.19	173.53
417.37	54.31	3.99	182.29	9.90	2.48	0.35	1.48	67.41	0.04	0.04	0.58	0.06	0.20	166.32

REFERENCES

1. (a) Geim, A. K.; Novoselov, K. S., The rise of graphene. *Nat Mater* **2007**, *6* (3), 183-191; (b) Allen, M. J.; Tung, V. C.; Kaner, R. B., Honeycomb carbon: a review of graphene. *Chemical reviews* **2009**, *110* (1), 132-145.
2. Ghosh, S.; Calizo, I.; Teweldebrhan, D.; Pokatilov, E.; Nika, D.; Balandin, A.; Bao, W.; Miao, F.; Lau, C., Extremely high thermal conductivity of graphene: Prospects for thermal management applications in nanoelectronic circuits. *Applied Physics Letters* **2008**, *92* (15), 151911.
3. Balandin, A. A.; Ghosh, S.; Bao, W.; Calizo, I.; Teweldebrhan, D.; Miao, F.; Lau, C. N., Superior thermal conductivity of single-layer graphene. *Nano letters* **2008**, *8* (3), 902-907.
4. Novoselov, K. S.; Fal, V.; Colombo, L.; Gellert, P.; Schwab, M.; Kim, K., A roadmap for graphene. *Nature* **2012**, *490* (7419), 192-200.
5. (a) Kim, K. S.; Zhao, Y.; Jang, H.; Lee, S. Y.; Kim, J. M.; Kim, K. S.; Ahn, J.-H.; Kim, P.; Choi, J.-Y.; Hong, B. H., Large-scale pattern growth of graphene films for stretchable transparent electrodes. *Nature* **2009**, *457* (7230), 706-710; (b) Choi, W.; Lahiri, I.; Seelaboyina, R.; Kang, Y. S., Synthesis of graphene and its applications: a review. *Critical Reviews in Solid State and Materials Sciences* **2010**, *35* (1).
6. Kim, H.; Miura, Y.; Macosko, C. W., Graphene/polyurethane nanocomposites for improved gas barrier and electrical conductivity. *Chemistry of Materials* **2010**, *22* (11), 3441-3450.
7. Loh, K. P.; Bao, Q.; Ang, P. K.; Yang, J., The chemistry of graphene. *Journal of Materials Chemistry* **2010**, *20* (12), 2277-2289.
8. Dai, B.; Fu, L.; Zou, Z.; Wang, M.; Xu, H.; Wang, S.; Liu, Z., Rational design of a binary metal alloy for chemical vapour deposition growth of uniform single-layer graphene. *Nat Commun* **2011**, *2*, 522.
9. Yu, Q.; Lian, J.; Siriponglert, S.; Li, H.; Chen, Y. P.; Pei, S.-S., Graphene segregated on Ni surfaces and transferred to insulators. *Applied Physics Letters* **2008**, *93* (11), 113103.
10. Li, X.; Cai, W.; An, J.; Kim, S.; Nah, J.; Yang, D.; Piner, R.; Velamakanni, A.; Jung, I.; Tutuc, E., Large-area synthesis of high-quality and uniform graphene films on copper foils. *Science* **2009**, *324* (5932), 1312-1314.
11. Dreyer, D. R.; Park, S.; Bielawski, C. W.; Ruoff, R. S., The chemistry of graphene oxide. *Chemical Society Reviews* **2010**, *39* (1), 228-240.
12. Norimatsu, W.; Kusunoki, M., Epitaxial graphene on SiC {0001}: advances and perspectives. *Physical Chemistry Chemical Physics* **2014**, *16* (8), 3501-3511.
13. Li, X.; Zhang, G.; Bai, X.; Sun, X.; Wang, X.; Wang, E.; Dai, H., Highly conducting graphene sheets and Langmuir-Blodgett films. *Nat Nano* **2008**, *3* (9), 538-542.
14. Blake, P.; Brimicombe, P. D.; Nair, R. R.; Booth, T. J.; Jiang, D.; Schedin, F.; Ponomarenko, L. A.; Morozov, S. V.; Gleeson, H. F.; Hill, E. W.; Geim, A. K.; Novoselov, K. S., Graphene-Based Liquid Crystal Device. *Nano letters* **2008**, *8* (6), 1704-1708.
15. Liu, N.; Luo, F.; Wu, H.; Liu, Y.; Zhang, C.; Chen, J., One-Step Ionic-Liquid-Assisted Electrochemical Synthesis of Ionic-Liquid-Functionalized Graphene Sheets Directly from Graphite. *Advanced Functional Materials* **2008**, *18* (10), 1518-1525.
16. Brodie, B. C., On the atomic weight of graphite. *Philosophical Transactions of the Royal Society of London* **1859**, *149*, 249-259.

17. Hummers, W. S.; Offeman, R. E., Preparation of Graphitic Oxide. *Journal of the American Chemical Society* **1958**, *80* (6), 1339-1339.
18. Niyogi, S.; Bekyarova, E.; Itkis, M. E.; McWilliams, J. L.; Hamon, M. A.; Haddon, R. C., Solution Properties of Graphite and Graphene. *Journal of the American Chemical Society* **2006**, *128* (24), 7720-7721.
19. Eigler, S.; Enzelberger-Heim, M.; Grimm, S.; Hofmann, P.; Kroener, W.; Geworski, A.; Dotzer, C.; Röckert, M.; Xiao, J.; Papp, C.; Lytken, O.; Steinrück, H.-P.; Müller, P.; Hirsch, A., Wet Chemical Synthesis of Graphene. *Advanced Materials* **2013**, *25* (26), 3583-3587.
20. Badami, D. V., X-Ray studies of graphite formed by decomposing silicon carbide. *Carbon* **1965**, *3* (1), 53-57.
21. Van Bommel, A. J.; Crombeen, J. E.; Van Tooren, A., LEED and Auger electron observations of the SiC(0001) surface. *Surface Science* **1975**, *48* (2), 463-472.
22. Mattevi, C.; Kim, H.; Chhowalla, M., A review of chemical vapour deposition of graphene on copper. *Journal of Materials Chemistry* **2011**, *21* (10), 3324-3334.
23. Tuinstra, F.; Koenig, J. L., Raman spectrum of graphite. *The Journal of Chemical Physics* **1970**, *53* (3), 1126-1130.
24. Tsen, A. W.; Brown, L.; Levendorf, M. P.; Ghahari, F.; Huang, P. Y.; Havener, R. W.; Ruiz-Vargas, C. S.; Muller, D. A.; Kim, P.; Park, J., Tailoring electrical transport across grain boundaries in polycrystalline graphene. *Science* **2012**, *336* (6085), 1143-1146.
25. Ma, T.; Ren, W.; Zhang, X.; Liu, Z.; Gao, Y.; Yin, L.-C.; Ma, X.-L.; Ding, F.; Cheng, H.-M., Edge-controlled growth and kinetics of single-crystal graphene domains by chemical vapor deposition. *Proceedings of the National Academy of Sciences* **2013**, *110* (51), 20386-20391.
26. Li, J.; Wang, X.-Y.; Liu, X.-R.; Jin, Z.; Wang, D.; Wan, L.-J., Facile growth of centimeter-sized single-crystal graphene on copper foil at atmospheric pressure. *Journal of Materials Chemistry C* **2015**, *3* (15), 3530-3535.
27. Hao, Y.; Bharathi, M.; Wang, L.; Liu, Y.; Chen, H.; Nie, S.; Wang, X.; Chou, H.; Tan, C.; Fallahzad, B., The role of surface oxygen in the growth of large single-crystal graphene on copper. *Science* **2013**, *342* (6159), 720-723.
28. Miseikis, V.; Convertino, D.; Mishra, N.; Gemmi, M.; Mashoff, T.; Heun, S.; Haghighian, N.; Bisio, F.; Canepa, M.; Piazza, V., Rapid CVD growth of millimetre-sized single crystal graphene using a cold-wall reactor. *2D Materials* **2015**, *2* (1), 014006.
29. Liu, X.; Fu, L.; Liu, N.; Gao, T.; Zhang, Y.; Liao, L.; Liu, Z., Segregation growth of graphene on Cu-Ni alloy for precise layer control. *The Journal of Physical Chemistry C* **2011**, *115* (24), 11976-11982.
30. Gupta, A.; Chen, G.; Joshi, P.; Tadigadapa, S.; Eklund, P., Raman scattering from high-frequency phonons in supported n-graphene layer films. *Nano letters* **2006**, *6* (12), 2667-2673.
31. Ferrari, A. C.; Basko, D. M., Raman spectroscopy as a versatile tool for studying the properties of graphene. *Nature nanotechnology* **2013**, *8* (4), 235-246.
32. Mapelli, C.; Castiglioni, C.; Zerbi, G.; Müllen, K., Common force field for graphite and polycyclic aromatic hydrocarbons. *Physical Review B* **1999**, *60* (18), 12710-12725.
33. Castiglioni, C.; Tommasini, M.; Zerbi, G., Raman spectroscopy of polyconjugated molecules and materials: confinement effect in one and two dimensions. *Philosophical Transactions of the Royal Society of London A: Mathematical, Physical and Engineering Sciences* **2004**, *362* (1824), 2425-2459.
34. Wada, N.; Solin, S., Raman efficiency measurements of graphite. *Physica B + C* **1981**, *105* (1), 353-356.

35. Vidano, R.; Fischbach, D. B., New Lines in the Raman Spectra of Carbons and Graphite. *Journal of the American Ceramic Society* **1978**, *61* (1-2), 13-17.
36. Nemanich, R. J.; Solin, S. A., First- and second-order Raman scattering from finite-size crystals of graphite. *Physical Review B* **1979**, *20* (2), 392-401.
37. Vidano, R. P.; Fischbach, D. B.; Willis, L. J.; Loehr, T. M., Observation of Raman band shifting with excitation wavelength for carbons and graphites. *Solid State Communications* **1981**, *39* (2), 341-344.
38. Ferrari, A.; Meyer, J.; Scardaci, V.; Casiraghi, C.; Lazzeri, M.; Mauri, F.; Piscanec, S.; Jiang, D.; Novoselov, K.; Roth, S., Raman spectrum of graphene and graphene layers. *Physical review letters* **2006**, *97* (18), 187401.
39. Margolin, H., Constitution of Binary Alloys. *Journal of the American Chemical Society* **1959**, *81* (10), 2600-2600.
40. Lander, J. J.; Kern, H. E.; Beach, A. L., Solubility and Diffusion Coefficient of Carbon in Nickel: Reaction Rates of Nickel - Carbon Alloys with Barium Oxide. *Journal of Applied Physics* **1952**, *23* (12), 1305-1309.
41. Heremans, J. P.; Thrush, C. M.; Morelli, D. T., Thermopower enhancement in PbTe with Pb precipitates. *Journal of Applied Physics* **2005**, *98* (6), 063703.
42. LaLonde, A. D.; Pei, Y.; Wang, H.; Snyder, G. J., Lead telluride alloy thermoelectrics. *Materials today* **2011**, *14* (11), 526-532.
43. Barako, M. T.; Park, W.; Marconnet, A. M.; Asheghi, M.; Goodson, K. E., Thermal Cycling, Mechanical Degradation, and the Effective Figure of Merit of a Thermoelectric Module. *Journal of electronic materials* **2013**, *42* (3), 372-381.
44. Snyder, G. J.; Toberer, E. S., Complex thermoelectric materials. *Nature materials* **2008**, *7* (2), 105-114.
45. Mahan, G.; Sales, B.; Sharp, J., Thermoelectric materials: New approaches to an old problem. *Physics Today* **2008**, *50* (3), 42-47.
46. Xia, H.; Drymiotis, F.; Chen, C.-L.; Wu, A.; Snyder, G. J., Bonding and interfacial reaction between Ni foil and n-type PbTe thermoelectric materials for thermoelectric module applications. *Journal of Materials Science* **2014**, *49* (4), 1716-1723.
47. Ajay, S.; Bhattacharya, S.; Thinaharan, C.; Aswal, D. K.; Gupta, S. K.; Yakhmi, J. V.; Bhanumurthy, K., Development of low resistance electrical contacts for thermoelectric devices based on n-type PbTe and p-type TAGS-85 ((AgSbTe)₂ 0.15 (GeTe)_{0.85}). *Journal of Physics D: Applied Physics* **2009**, *42* (1), 015502.
48. Kim, D.-H.; Park, J.-S.; Seong, T.-Y., Graphene diffusion barrier for forming ohmic contact on N-polar n-type GaN for high-power vertical-geometry light-emitting diodes. *Applied Physics Express* **2014**, *7* (4), 046501.
49. Roy, S. S.; Arnold, M. S., Improving graphene diffusion barriers via stacking multiple layers and grain size engineering. *Advanced Functional Materials* **2013**, *23* (29), 3638-3644.
50. Berry, V., Impermeability of graphene and its applications. *Carbon* **2013**, *62*, 1-10.
51. Li, J.-F.; Liu, W.-S.; Zhao, L.-D.; Zhou, M., High-performance nanostructured thermoelectric materials. *NPG Asia Materials* **2010**, *2* (4), 152-158.